ELECTROCHEMISTRY OF FORMIC ACID AND CARBON DIOXIDE ON METAL ELECTRODES WITH APPLICATIONS TO FUEL CELLS AND CARBON DIOXIDE CONVERSION DEVICES

BY

JOHN LEONARD HAAN

DISSERTATION

Submitted in partial fulfillment of the requirements
for the degree of Doctor of Philosophy in Chemistry
in the Graduate College of the
University of Illinois at Urbana-Champaign, 2010

Urbana, Illinois

Doctoral Committee

Professor Richard I. Masel, Chair
Professor Andrew Gewirth
Professor Alexander Scheeline
Professor Andrzej Wieckowski

Abstract

There is a growing awareness of the need for basic and applied energy research due to the environmental impact of energy use and limitations in the supply of energy sources. In this work, electrochemical research is reported for fuel cells and carbon dioxide reduction, with the aim of reducing the environmental footprint of global energy use.

In studies of the formic acid fuel cell, it is reported here that an increase in the formic acid fuel pH increases the rate of formic acid oxidation on palladium and platinum. It is also shown that an increase in fuel pH decreases the potential at which the catalyst poison is removed from the electrode surface. This poison is detrimental to fuel cell operation. This work reports the first such studies in an electrochemical cell on high surface area platinum and palladium nanoparticles.

New catalyst formulations were developed via electrochemical surface modification in attempt to eliminate the catalyst poisoning and improve performance of the formic acid fuel cell. Electrochemical studies showed substantial improvement to the rate of formic acid oxidation by a combination of high surface area palladium with tin, antimony, or lead, due to steric and electronic effects. A membrane electrode assembly was developed and reported here that enables fuel cell testing of such electrochemically modified catalysts. Tests in an operating fuel cell demonstrated less performance gains compared with the electrochemical cell, although some gains were shown.

Finally, the reduction of carbon dioxide in the ionic liquid, EMIM BF_4, was shown to occur at a more positive potential that in previous aprotic solvents such as acetonitrile. The conversion of carbon dioxide to its charged intermediate was shown to occur as the rate limiting step in the complete conversion of carbon dioxide to adsorbed carbon monoxide. This work is part of the initial stages of an effort to convert carbon dioxide to a usable fuel such as formic acid or some other larger hydrocarbon fuel.

Dedicated to Joanna, Abby, Rachel, Danny, and Jimmy

Acknowledgments

I first want to thank my very supportive and understanding wife Joanna for helping me through the long road of graduate school. Her support and love was critical to my time at the University of Illinois, and I look forward to continuing with her through all the adventures of life.

I also want to thank my children who always welcomed me home with smiles even after long, frustrating days in the lab. Abby has been with me through two graduate degrees and Rachel for the bulk of this one. The boys, Danny and Jimmy, came along in duplicate just in time to make the last year very interesting.

I also owe gratitude to my advisor, Dr. Rich Masel, who taught me about energy chemistry and provided advice, ideas, equipment, supplies, and financial support for me to pursue interests in that field. I enjoyed working with students and post-docs in the Masel group. Zach Dunbar was my mentor in the group. He showed me the ropes at my first conference; he introduced me to fuel cells and answered numerous questions about their operation; and, most importantly, he demonstrated for me the wonders of Luer. I had interesting collaborations and discussions with Rob Morgan, who also made Hulu an important part of the front office. Discussions with Kevin Lin about the new found "success" of Rutgers sports were also a welcome diversion from the rigors of graduate research. Supervising several undergraduates was an enjoyable experience for me, and in particular, Kristin Stafford's reliable work over my last year of school was invaluable to

helping me finish my research. I also had many worthwhile conversations with other Masel group members past and present, too many to be named individually, but none left out intentionally.

I also owe thanks to the members of my thesis committee and their research groups. I am honored that each committee member played such a strong role in my education; I feel that each went above the call of duty for my sake. I had many valuable conversations with Dr. Andrzej Wieckowski about my dissertation research. I enjoyed going to his group meetings as often as I could, felt as if I was an honorary group member, and enjoyed valuable discussions with his group members, including Rachel Behrens, Hung Duong, and Jacob Spendelow. I also had many valuable conversations about my research with Dr. Andrew Gewirth, and really appreciated his willingness to collaborate with me on an EC-STM project. Although we did not get the information we had hoped for, it was a valuable learning experience, both about STM and electrochemistry. I am especially thankful to Jeremy Hatch for his dedication to that project while we tried to make it work. I also appreciated the academic advising and support I received from Dr. Alexander Scheeline. While I worked in an engineering group, he was always available to provide guidance and help to be sure I stayed on track and successfully fulfilled my requirements in the chemistry program.

I would also like to thank Dr. Dana Dlott for providing access to his BB-SFG instrument to study carbon dioxide reduction in ionic liquids. My collaboration with Drs.

Prabuddha Mukherjee and Bjoern Braunschweig was very profitable; their excitement and dedication to this project, both present and future, are invaluable to its success.

The facilities at the University of Illinois are outstanding. I thank the staff who helped me with services at UIUC, only some of whom I can name here: MRL (Drs. Richard Haasch, Mike Marshall, Jim Mabon), glass shop (Donnie O'Brien), machine shop (Bill Knight), electronics shop (Ron Edmison), libraries (Tina Chrzastowski), and XRD lab (Dr. Scott Wilson). I also thank Kay Busboom and Julie Sides for their reliable support with all kinds of help related to the Masel group and analytical chemistry, respectively.

The funding for this work came from both the US Army Research Office (ARO), and the Defense Advance Research Project Agency (DARPA). I would like to thank both for their generosity. The opinions in this work are those of the author and do not reflect those of the ARO or DARPA

Table of Contents

Chapter 1: Introduction

In recent years, there has been a growing awareness of the need for basic and applied energy research due to (1) the impact of energy use on the environment and (2) the limited supply of popular sources of energy. The issues discussed in this work include electrochemical research in both fuel cells and carbon dioxide reduction, with the aim of reducing the environmental footprint of global energy use. Such issues invite strong collaborations between chemists and engineers in order to bring a multidisciplinary approach; the entirety of this work involves such collaboration.

Energy and the Environment. The atmosphere of the earth maintains a global temperature that is warm enough to sustain life by trapping incoming radiation via gases such as carbon dioxide and water vapor; this is called the greenhouse effect. However, the industrial revolution brought about significant increases in the amount of carbon dioxide present in the atmosphere, as shown in Figure 1.1. Discussions about the effects of rapidly increasing atmospheric concentrations of carbon dioxide began in the late 1800s and continue today. [1] Gradual increases in global temperature have been correlated with this increase in carbon dioxide, as shown in Figure 1.2. In January in the Midwest, many people wish for global warming. However, the broader impacts of a warmer climate include a substantial rise in sea levels (as much as a few feet), and a shift in regions suitable for agriculture (including a shift away from some regions already in or near famine). These impacts would clearly have a catastrophic impact on many cultures in a rapidly growing world where political and economic instabilities would lead to resource wars.

Although some debate continues on the correlation between carbon dioxide concentrations and global temperature rise, the scientific community generally agrees that there is some anthropogenic contribution to a warming climate due to release of carbon dioxide. [2, 3] Fossil fuels such as coal, oil, and natural gas, were the most commonly used fuels over the past century, and the quantities used by developed nations have drastically increased over that time. Even if developed nations decrease their reliance on fossil fuels over the next century, developing countries will likely continue to increase their use of fossil fuels, and the trend of increasing carbon dioxide emission will then continue into the foreseeable future. China, still considered a developing country, already uses nearly as much energy as the United States, and emits more carbon dioxide into the atmosphere. [4] It is not economically feasible for developing countries to rely solely on renewable energies such as wind and solar, so they will continue to depend heavily on fossil fuels.

The other issue brought about by intense use of fossil fuels is that, as primary energy sources, their availability is not limitless; they are not naturally replaced at a rate that would make them available indefinitely. Advanced technologies make discovery of new deposits of fuels possible, but there is little debate that the supply will eventually run out. Therefore, it is imperative that, along with conservation efforts, research is done to discover or create energy which is either renewable or carbon-neutral.

The Fuel Cell. The fuel cell has been discussed recently as an alternative or even renewable energy option. The first demonstration of what is known today as a fuel cell was made by William Grove in 1839 when he demonstrated a flow of current during reverse electrolysis: the recombination of hydrogen and oxygen to form water. The reaction:

$$H_2 + ½\ O_2 \rightarrow H_2O \qquad (1.1)$$

involves the transfer of 2 electrons per hydrogen molecule. Although all fuel cell reactions discussed in this work involve the reaction of a fuel with oxygen, the energy produced from these reactions is electrical rather than thermal. In a polymer electrolyte membrane (PEM) fuel cell with an acid membrane, which is the most common membrane to date, the half reactions in a hydrogen fuel cell are:

$$H_2 \rightarrow 2\ H^+ + 2\ e^- \qquad (1.2)$$

$$½\ O_2 + 2\ H^+ + 2\ e^- \rightarrow H_2O \qquad (1.3)$$

which combine to the overall reaction in Equation 1.1. This is the simplest PEM fuel cell design, in which both hydrogen and oxygen are in their gaseous form, and the oxygen can be fed in the form of air, since nitrogen is inert to these reactions.

Other fuels, which are characterized as hydrogen carriers, can also be used in place of hydrogen in direct liquid fuel cells. The direct methanol fuel cell (DMFC) and the direct formic acid fuel cell (DFAFC) will be discussed in this work. In each of these, the liquid fuel is fed to the anode in the place of gaseous hydrogen. Figure 1.3 shows a diagram of a direct liquid fuel cell, in which the byproducts are carbon dioxide and water. The anode oxidation reactions for methanol and formic acid, respectively:

$$CH_3OH + H_2O \rightarrow 6\ H^+ + 6\ e^- + CO_2 \quad (1.4)$$

$$HCOOH \rightarrow 2\ H^+ + 2\ e^- + CO_2 \quad (1.5)$$

both produce protons as in Equation 1.2.

While DMFCs and DFAFCs each have the unfortunate byproduct of carbon dioxide, it is important to carefully consider the impacts of this anode waste stream. Direct liquid fuel cells with small organic molecules do not directly reduce emissions of carbon dioxide. Therefore, they would not reduce anthropogenic impacts on global warming unless they came from a renewable energy source. However, it is critical for this discussion to understand that hydrogen, although its fuel cell has an apparently clean waste stream, is not always produced from clean sources. Hydrogen from natural gas, coal, and biomass, for example, involves the release of carbon dioxide in its production. Therefore, a hydrogen fuel cell should only be considered carbon neutral if the hydrogen is produced from a non-fossil fuel source, which might involve solar, wind, or nuclear, to split water.

Carbon Dioxide to Fuel. If one could find a means to efficiently convert fossil fuel waste (i.e., carbon dioxide) into usable fossil fuels (such as formic acid or a larger hydrocarbon fuel), this would constitute a major breakthrough in energy science. Studies are already being performed to develop technologies that would remove carbon dioxide from the atmosphere or capture carbon dioxide emissions in a waste stream prior to its release into the atmosphere. One example is the capture of carbon dioxide in the waste streams of fossil fuel power plants. The carbon dioxide could then be sequestered in

underground storage to prevent further release into the atmosphere. However, this process itself is very energy intensive and would significantly increase the cost of power to the consumer. [5] As already discussed, another method of accomplishing these goals would be a dramatic switch to renewable energy. Such a switch would be catastrophic to the economies of developing countries, but would also be quite difficult economically for developed countries. It is clear that renewable energies such as wind, solar, and biomass, will have a significant role in the next century in both developed and developing countries. However, continued global population growth, economic growth, and Westernization of politics and culture, will drive energy demands higher over the next century. Fossil fuels will continue to be a primary source of energy to meet these demands.

A very powerful method to accomplish the goals of reducing carbon dioxide emissions and dependence on fossil fuels is to convert captured carbon dioxide into a usable hydrocarbon fuel rather than to sequester it. [6] It has been suggested that this recycling method could be powered by solar energy. [2] The focus of this work is to study the electrochemistry of carbon dioxide reduction as an initial stage of a project aimed at development of a carbon dioxide capture method that is less energy intensive than existing methods. Concurrent work involves the direct conversion of carbon dioxide into hydrocarbon fuels.

1.1 Figures

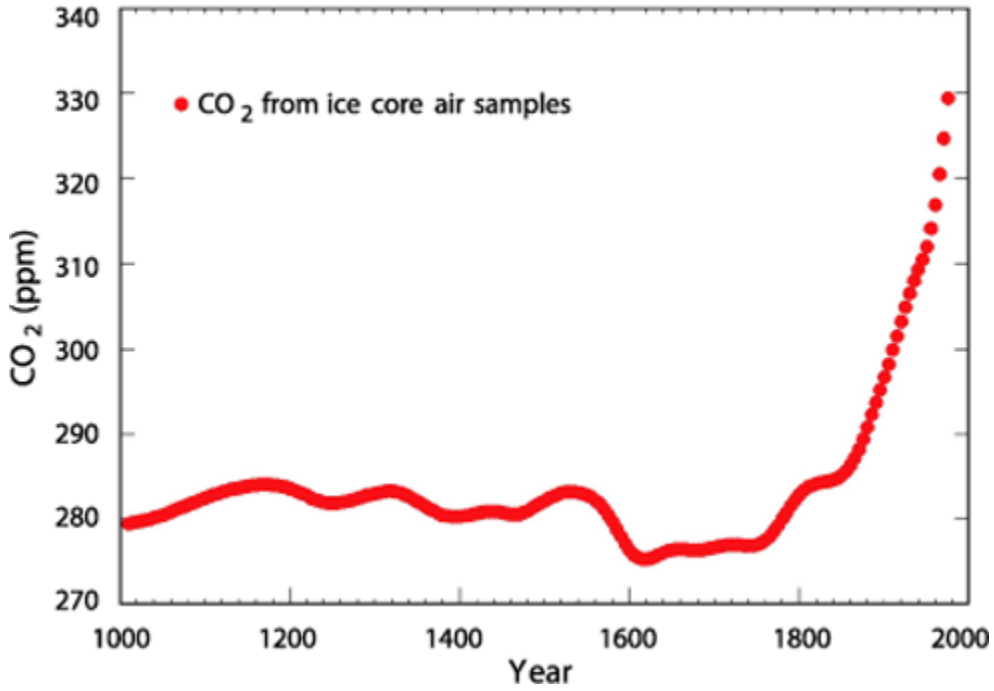

Figure 1.1. Carbon dioxide concentration in the atmosphere for the past millennium as measured from core ice samples. A significant increase is observed in conjunction with the industrial revolution. [7]

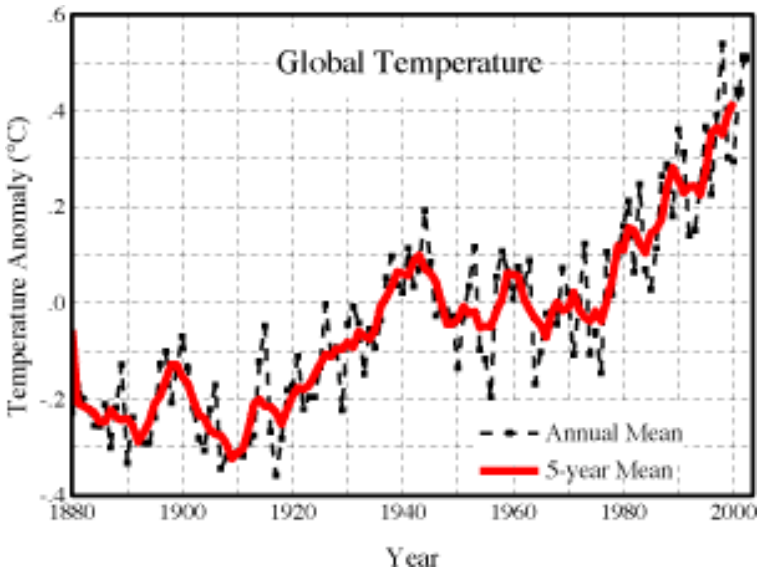

Figure 1.2. A trend toward an increase in global temperatures is shown, and the trend has been particularly strong in the past three decades. [8]

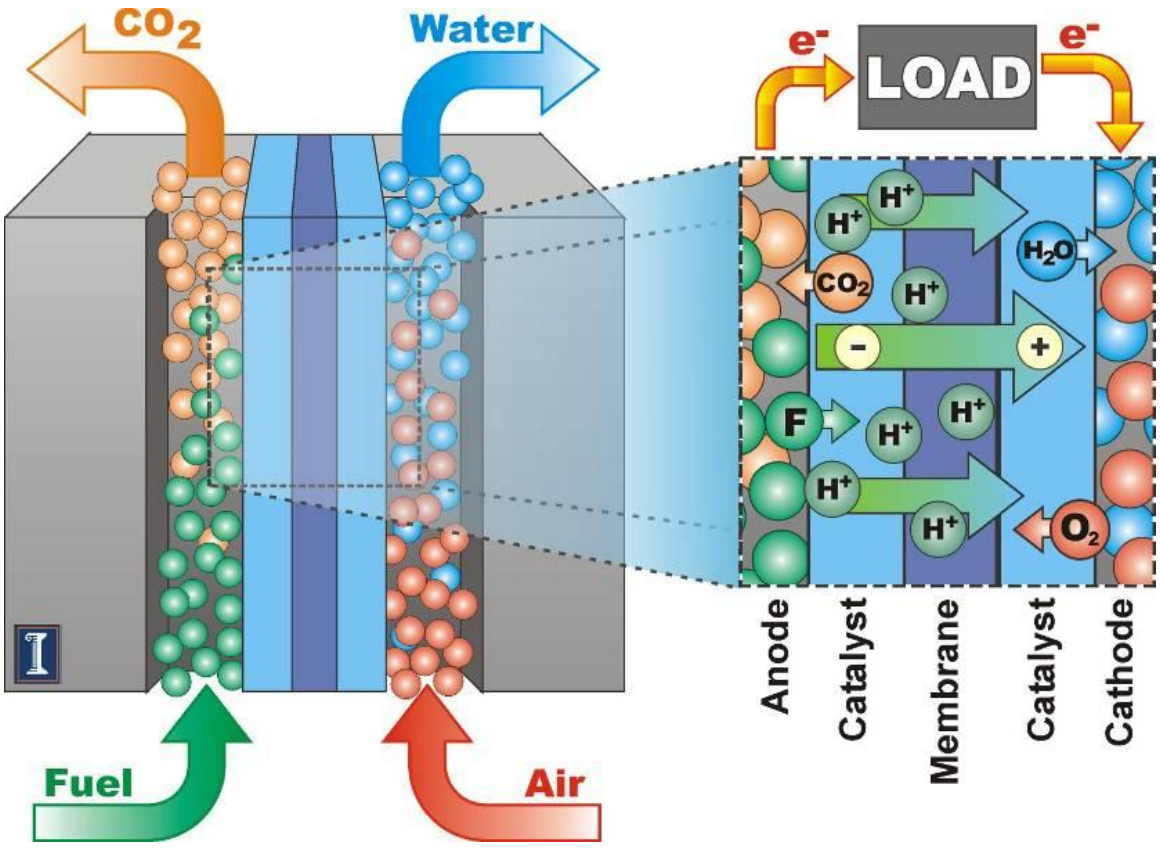

Figure 1.3. Diagram of a direct liquid fuel cell. The liquid fuel is fed to the anode, while air is fed to the cathode. The combination of hydrogen, passed through the membrane, and oxygen produces water in the cathode waste stream. The oxidation of the fuel leaves behind carbon dioxide in the anode waste stream.

Chapter 2: Literature Review

2.1 Fuel Cell Electrochemistry and Operation

Fuel Cell Thermodynamics and Efficiencies. The total amount of electrical work theoretically possible in a fuel cell is simply the change in the Gibbs free energy for the overall fuel cell reaction. In the case of the hydrogen fuel cell, ΔG^o, is -237.2 kJ mol^{-1} for Equation 1, and the Gibbs free energy is related to the standard potential, E^o, for the reaction:

$$\Delta G^o = -nFE^o_{cell} \quad (2.1)$$

where n is the number of electrons transferred and F is the Faraday constant, 96485 C mol^{-1}. Therefore, the standard potential for the hydrogen fuel cell, in which two electrons are transferred per hydrogen molecule reacted, is 1.23 V.

The standard potentials for the half reactions in Equations 1.2 and 1.3 can also be calculated using Equation 2.1. The hydrogen oxidation reaction occurs at 0.00 V (versus the standard hydrogen electrode (SHE), by definition) and the oxygen reduction reaction occurs at 1.23 V vs. SHE. The overall theoretical cell voltage is the difference between these two reactions:

$$\Delta E_{cell} = E_{cathode} - E_{anode} \quad (2.2)$$

However, since the activities of each reactant and product are not necessarily equal to unity in practice, Equation 2.1 does not hold, and the actual open circuit voltage of the fuel cell is lower than 1.23 V. In addition, there are other losses, such as kinetic activation barriers, resistances in the fuel cell, and mass transport limitations, which reduce the voltage of the fuel cell far from 1.23 V in practice.

Since fuel cells do not produce their energy from heat (although in practice some heat is released), they are not limited by Carnot efficiencies:

$$Carnot\ limit = \frac{T_1 - T_2}{T_1} \tag{2.3}$$

where T_1 is the temperature of the hot reservoir and T_2 is the temperature of the cold reservoir. Rather, fuel cells have been modeled for efficiency based on a thermodynamic efficiency:

$$Thermodynamic\ limit = \frac{\Delta G_f^o}{\Delta H_f^o} \tag{2.4}$$

where ΔH^o is the standard enthalpy of formation. For the hydrogen fuel cell, this thermodynamic efficiency limit at STP is 83%. [9]

Performance Losses and Tests to Monitor Losses. In practice, an operating fuel cell has voltage losses that increase as more current is drawn from the cell as shown in the fuel cell polarization curve in Figure 2.1. At low current, *activation polarization*, the energy required to overcome kinetic reaction barriers, severely reduces the cell voltage. The difference between the theoretical and actual cell voltages is called the overpotential, η, and is given by one form of the Tafel equation:

$$\eta = A \ln\left(\frac{i}{i_o}\right) \tag{2.5}$$

where i is the current, i_o is the exchange current, and A is the slope of the Tafel plot and is defined by:

$$A = \frac{RT}{n\alpha F} \tag{2.6}$$

where R is the gas constant, T is the temperature, and α is the electron transfer coefficient.

The value of the exchange current, which is the current at equilibrium, can vary by several orders of magnitude and have a significant impact on the activation overpotential. For example, the use of platinum as a hydrogen oxidation catalyst results in an exchange current two orders of magnitude larger than that for nickel, which results in a lower overpotential (Equation 2.5). [9] In a hydrogen fuel cell, the significant kinetics losses occur at the cathode, where the exchange current is five orders of magnitude lower than at the anode. However, in direct liquid fuel cells, kinetic losses occur at both electrodes, with the anode kinetics being more sluggish. [9] Development of more efficient, high surface area catalysts is key to increasing the exchange current, since catalysts are able to reduce the kinetic activation barriers.

In the Ohmic region of Figure 2.2, losses occur due to the *cell resistance*, and the losses grow linearly in accordance with Ohm's Law:

$$V = IR \tag{2.7}$$

A major component of the fuel cell that contributes resistance is the membrane. Current PEM fuel cell technology uses a Nafion® membrane which contains sulfonic acid groups that conduct protons from the anode to the cathode without leaking electrical current. The protons are drawn through the membrane either via a hydrogen bonding network of static water molecules or via bonding to mobile water molecules which escort the proton through the membrane. [10-14] Clearly, this resistance will be strongly dependent on the amount of current passed as well as the membrane thickness. Another component that contributes to resistance is charge transfer through the conductive components of the fuel

cell such as each catalyst layer, diffusion layer, and current collector. These are typically less significant than the membrane resistance, but they still contribute. [15]

The third region shown in Figure 2.1 exhibits losses due to *mass transport* of the fuels to the catalyst. As high current is drawn through the cell, the reactions at the catalyst surfaces occur faster than the reactants can be replenished by diffusion. This region represents the practical limit of fuel cell operation without advanced fuel delivery methods or catalyst layer design.

Another source of losses that is partially demonstrated by an open circuit voltage lower than theoretical is fuel crossover. Although crossover does occur in hydrogen fuel cells, it is a more important consideration in direct liquid fuel cells, especially DMFCs. Since methanol mixes well with water, it is easy to understand how it could be dragged through the membrane at the same time that protons are crossing during fuel cell operation. [16, 17] When the methanol reaches the cathode, it oxidizes readily on the platinum that is already used to reduce the oxygen. This dual reaction creates a mixed potential, which drags the cathode potential lower than it would be if only oxygen were reacting. In addition, the loss of methanol from the anode catalyst surface reduces its efficiency per unit volume of methanol that is fed into the fuel cell. Crossover can be reduced by use of highly active anode catalysts, reduced fuel concentration, and thicker membranes. Although cost is the only concern for the first solution, the latter two solutions have obvious drawbacks in terms of overall fuel cell efficiency.

The PEM Fuel Cell. The PEM fuel cell uses a polymer electrolyte membrane to pass protons, and in its most common configuration hydrogen is the anode fuel and oxygen in air is the cathode fuel. The hydrogen/air fuel cell is efficient and exhibits minimal long-term performance losses; it has been touted for applications ranging from transportation to miniature military devices with a volume of one cubic millimeter. [18] Such fuel cells can be operated at room temperature, but are often operated between 60 and 100 °C for improved performance. For large scale applications such as transportation, there are significant drawbacks to using hydrogen/air fuel cells. The first problem is with the hydrogen fuel. Many hydrogen sources, such as natural gas, are not carbon neutral and would not appreciably reduce pollution. In order for sufficient amounts of hydrogen to be stored in a vehicle, the hydrogen is compressed at a significant energy cost. The second problem is the cost; technologies for catalysts and membranes are very costly and underdeveloped. The final problem is that it is not economically feasible for the transportation infrastructure to move to hydrogen fuel. However, the focus of this work is the direct liquid PEM fuel cell, which is a promising energy source for portable electronic devices.

The Direct Methanol Fuel Cell. Although the DMFC is not the focus of this work, it merits a brief discussion because of its parallel comparison to the DFAFC. In the DMFC, the anode reaction (Equation 1.4) occurs at a standard potential of 0.02 V. Therefore, a methanol/oxygen fuel cell has a theoretical open circuit voltage of 1.21 V, comparable with that of a hydrogen/oxygen fuel cell. [19] The DMFC has been the most commonly studied direct liquid fuel cell for portable devices in recent years. Methanol

fuel cells are particularly suited for applications in which high power density is not needed, but rather a sustained energy density. Such a fuel cell could be used to power portable electronic devices such as wireless phones, laptops, and two-way pagers.

However, DMFCs have some serious deficiencies that have driven research into other forms of direct liquid fuel cells. First, the toxicity of methanol makes it dangerous if it escapes its packaging in a fuel cell. Second, it is strongly susceptible to fuel crossover, limiting the maximum concentration of methanol and therefore its energy density. Finally, the oxidation mechanism for methanol on platinum has various pathways, several of which lead to a strongly bound CO intermediate. This intermediate can only be removed by oxidation via adsorbed water, which is drawn to the surface using a bifunctional catalyst such as Pt-Ru. [20-23] A steady state is reached, whereby the methanol and CO are both oxidized simultaneously by raising the anode potential. This results in stable fuel cell operation, but the high potential at which this occurs results in low overall fuel cell voltage.

The Direct Formic Acid Fuel Cell. The merits of a DFAFC are similar to that of a DMFC, but there are several advantages which make it a more practical fuel cell. First, the anode oxidation reaction (Equation 1.5) occurs at -0.22 V, resulting in a theoretical cell voltage of 1.45 V, which is significantly higher than that of methanol. [24] Since the activation polarization losses are approximately 0.5 V for both the DFAFC and the DMFC, the actual open circuit potential is approximately 0.95 V for the DFAFC and 0.70 V for the DMFC. [19, 25] Second, formic acid is a safer fuel to use than methanol; it has

been used in production of food packaging materials and is non-toxic and inflammable even at high concentrations. [26, 27] The third advantage of the DFAFC is that fuel crossover is much less than in a DMFC due to the anionic nature of the formic acid molecule. Much higher fuel concentrations can be used in the DFAFC without significant crossover; even though fewer electrons are transferred during fuel oxidation, a higher energy density can be attained due to the increased concentration. [28-31] Finally, anode catalysts have been developed that reduce the impact of catalyst poisoning and permit operation at high voltages, as compared with DMFCs.

Typical formic acid fuel cells are operated at high formic acid concentrations (50-88 vol%), and can be run in a passive mode with oxygen from ambient air diffusing to the cathode. The anode kinetics are rather sluggish, especially in comparison to the cathode kinetics, and the most significant losses are found at the anode. Therefore, this work is dedicated to minimization of such losses at the anode. Most recent literature related to the DFAFC concerns the anode catalyst, which is generally palladium-based. However, much of the literature does not take a holistic approach such as that taken in this work: a discussion of the electrochemical merits of particular catalysts as well as their implementation in an operating fuel cell.

2.2 Half Cell Electrochemistry

Electrochemical methods. A standard three electrode electrochemical cell can be used to study the oxidation or reduction half reactions that occur in a fuel cell. In such an electrochemical cell it is possible to isolate the oxidation and reduction half reactions

to study the catalyst/solution interface and the associated mechanisms and kinetics. For hydrogen fuel cells, the focus of this type of research is on the cathode half reaction, the reduction of oxygen. [32] However, for small organic molecule fuel cells, the focus of half cell research is typically the anode half reaction. [33, 34] One notable exception to this trend is the study of cathode catalysts that are tolerant to methanol crossover: catalysts which do not create a mixed potential between methanol oxidation and oxygen reduction. [35] A three electrode cell employs a *working* electrode, where the reaction of interest occurs, a *counter* electrode, through which the current flows to or from the working electrode, and a *reference* electrode, through which the potential is controlled without passing current. This configuration and the choice of electrode materials will be discussed later in greater detail.

Since electrochemistry is an interfacial science, it permits characterization of the catalyst surface and its interaction with the fuel and the electrolyte. One method of characterization of the surface is cyclic voltammetry, where the potential is scanned linearly in one direction, and then scanned in the opposite direction to create a current loop, as shown in Figure 2.3. Cyclic voltammetry is used in half cell electrochemistry to determine the cleanliness of an electrode surface, the electrochemical surface area (ECSA), and the potential dependence of the fuel oxidation or reduction reaction. The palladium electrode scanned in 0.1 M sulfuric acid is shown in Figure 2.4. In the hydrogen region, protons interact with the catalyst surface, adsorbing to the surface in the cathodic scan and desorbing in the anodic scan. In the oxygen region, hydroxide ions oxidize the surface in the anodic scan and are reduced from the surface in the cathodic

scan. Between these regions is the double layer region, in which only double layer charging occurs. The increased surface area from nanoparticles (as compared with smooth polycrystalline electrodes or single crystals) results in a higher double current magnitude in this region.

A cyclic voltammogram can also be used to determine the ECSA of a high surface area fuel cell catalyst. Figure 2.5 shows the voltammogram of a palladium catalyst which has been saturated with carbon monoxide. In the first cycle, no hydrogen activity is observed because the surface is poisoned by the CO. As the potential reaches ~0.9 V, the CO is oxidized from the surface, and the surface oxidation and reduction activities resume. In the second cycle, with a clean palladium surface, the hydrogen surface interactions also resume. Integration of either the hydrogen peaks or the CO stripping peak can be used to calculate the charge passed for the one or two electron process, respectively. It is widely accepted that both platinum and palladium can be characterized in this manner, where the surface area from the hydrogen peaks is determined from the relationship of 210 $\mu C\ cm^{-2}$ and from the CO peaks by the relationship of 420 $\mu C\ cm^{-2}$. [36-41]

Cyclic voltammetry can also be used to determine the transient fuel oxidation or reduction activity of the catalyst. Figure 2.6 shows an example of how transient oxidation currents can be used to characterize a half reaction of interest to fuel cells. In this case, a clean palladium black catalyst is compared to a palladium black catalyst after lead was adsorbed in 40 mM Pb^{2+} for 10 minutes at 0.45 V vs RHE. It is quite apparent

that the presence of lead enhances the transient formic acid oxidation current of the palladium catalyst. However, this figure says nothing of the long-term effects of the presence of lead. For this reason, it is preferable to also study the steady state current, which demonstrates the longer term stability of the catalyst for oxidation of the fuel.

In the half cell, steady state data on formic acid oxidation can be obtained by stepping the potential from open circuit potential (OCP) to a potential at which the oxidation reaction proceeds. When the reaction is under diffusion control, the Cottrell equation shows a relationship between the current and the time duration of the experiment:

$$i(t) = \frac{nFAD_o^{1/2}C_o^*}{\pi^{1/2}t^{1/2}} \qquad (2.8)$$

where A is the area of the electrode, D_o is the diffusion coefficient of the oxidized species, and C_o^* is the bulk concentration of the oxidized species. In order to directly characterize the electrode kinetics, hydrodynamic methods can be employed.

In hydrodynamic methods, steady state is achieved rapidly and mass transfer of reactants to the electrode is faster than it is for simple diffusion so that the electrode reaction is limited by kinetics rather than mass transport. A rotating disk electrode (RDE) is a commonly used hydrodynamic method in which the current is proportional to the RDE rotation speed, $\omega^{1/2}$. The Koutecky-Levich equation, which relates the current and rotation rate for an irreversible, one step, one electron reaction, is:

$$\frac{1}{i} = \frac{1}{i_K} + \frac{1}{0.62nFAD_o^{2/3}\omega^{1/2}\nu^{-1/6}C_o^*} \qquad (2.9)$$

where i_K is the current in the absence of mass transport effects, and must be large, and v is the scan rate. The plot of i^{-1} vs. $\omega^{-1/2}$, the Koutecky-Levich plot, has a linear region where mass transport is controlled by the RDE, and the extrapolated intercept of this region at $\omega^{-1/2} = 0$ gives i_K^{-1}. Comparison of i_K at different reaction potentials can provide kinetic information about the reaction. When employing an RDE, the rotation speed is chosen within this linear region of the plot, which is typically not beyond the practical bounds of 100 and 10,000 rpm. At sufficiently low rotation rate, the hydrodynamic boundary layer (the thickness of solution near the electrode surface that is affected by the RDE) becomes larger than the electrode and approximations leading to Equation 2.9 break down. At sufficiently high rotation rate, turbulent flow to the electrode surface complicates kinetic analysis.

The current-overpotential equation relates the change in potential with the change in measured current:

$$i = i_o \left[\frac{C_O(0,t)}{C_O^*} e^{-\alpha F \eta} - \frac{C_R(0,t)}{C_R^*} e^{(1-\alpha)F\eta} \right] \qquad (2.10)$$

where the subscripts O and R refer to the species oxidized or reduced, respectively, α represents the reaction symmetry, and the overpotential, η, is $E - E_{eq}$, the difference between the applied potential and the equilibrium potential, and i_o, the exchange current, is directly proportional to the rate constant, k^o, according to:

$$i_o = FAk^o C_O^{*(1-\alpha)} C_R^{*\alpha} \qquad (2.11)$$

When mass transfer effects are eliminated, as is the case when an RDE is appropriately employed, Equation 2.10 reduces to the Butler-Volmer equation:

$$i = i_o \left[e^{-\alpha F \eta} - e^{(1-\alpha)F\eta} \right] \qquad (2.12)$$

For smaller exchange current a larger overpotential must be applied, which is known as the activation overpotential. Conversely, a lesser overpotential is required for a reaction with a larger exchange current. At small overpotentials, Equation 2.12 further reduces to an equation that demonstrates the linearity of the current-potential relationship under these conditions:

$$i = -i_o F\eta \tag{2.13}$$

At large overpotentials, Tafel behavior is observed whereby the current-potential relationship is logarithmic, according to the following relationship:

$$i = -i_o e^{-\alpha F\eta} \tag{2.14}$$

When the equation is rearranged and the log of the current is plotted versus the overpotential:

$$\eta = a + b \log(i) \tag{2.15}$$

the linear region of this plot identifies the Tafel slope, from which kinetic parameters can be obtained. For example, the exchange current is found at the intercept of no overpotential (the equilibrium potential). The equations and concepts from this section come from *Electrochemical Methods*, and can be explored in much greater detail in that text. [16]

Formic acid oxidation. In the direct formic acid fuel cell, which is a major focus of this work, the performance limitation is the sluggish anode kinetics on platinum and palladium at ambient temperature. Many studies related to formic acid oxidation on smooth platinum and palladium electrodes were performed in the 1970s and 1980s. It was discovered that the kinetics of formic acid oxidation on platinum were interesting

and followed a dual-pathway mechanism. [42-53] In the first pathway, formic acid is directly oxidized via a weakly-bound intermediate:

$$HCOOH + Pt^0 \rightarrow X \rightarrow CO_2 + 2\ H^+ + 2\ e^- + Pt^0 \qquad (2.16)$$

However, the second pathway involves oxidation via a strongly-bound intermediate that is now understood to be CO:

$$HCOOH + Pt^0 \rightarrow Pt\text{-}CO + H_2O \qquad (2.17)$$

$$H_2O + Pt^0 \rightarrow Pt\text{-}OH + H^+ + e^- \qquad (2.18)$$

$$Pt\text{-}CO + Pt\text{-}OH \rightarrow CO_2 + 2\ Pt^0 + H^+ + e^- \qquad (2.19)$$

The second reaction, adsorption of hydroxyls on the electrode surface is slow, resulting in significant and rapid buildup of CO on the catalyst surface, blocking reaction sites. [54, 55] The first DFAFCs were developed with platinum and platinum-ruthenium anode catalysts. [54] The platinum-ruthenium catalysts work via a bi-functional mechanism, whereby the ruthenium adsorbs hydroxyls at the surface more readily than platinum does (at 0.3 V vs SHE on ruthenium vs. 0.6 V on platinum). [51] The hydroxyls then migrate to the strongly-bound CO and permit its oxidation and removal from the surface at potentials closer to that found in an operating fuel cell: [20-22, 56, 57]

$$Ru^0 + H_2O \rightarrow Ru\text{-}OH + H^+ + e^- \qquad (2.20)$$

$$Pt\text{-}CO + Ru\text{-}OH \rightarrow Pt^0 + Ru^0 + CO_2 + H^+ + e^- \qquad (2.21)$$

It was later discovered that the addition of palladium to a platinum electrode helped enhance the oxidation current and reduce the effects of CO poisoning. [37, 58] A third pathway has also been discovered for platinum, whereby formate is adsorbed at the surface, but this occurs at a potential that is much greater than potentials used for fuel cell studies. [59]

Since rapid poisoning was a serious concern for platinum-based catalysts, a more significant breakthrough occurred when it was discovered that high surface area palladium catalysts primarily follow the first pathway, direct oxidation via an active, weakly bound intermediate as in Equation 2.16, with very little, if any, contribution from the second pathway, the indirect route. [45, 49, 60-62] Indeed, palladium outperforms platinum in the DFAFC. Although the indirect oxidation route is not significant on palladium as compared with platinum, it has been discovered that the palladium surface still poisons over the course of several hours, necessitating a regeneration step for the DFAFC; following regeneration, full fuel cell performance is regained. [25, 31, 63-65] The reason for CO buildup is not clear, but it is most apparent in a fuel cell environment, in which the catalyst ink contains Nafion® binder and the anode catalyst is also in contact with a Nafion® membrane. One possible reason for CO formation in the fuel cell might be that the presence of Nafion® enhances the electrooxidation of formic acid via a CO intermediate. Gates, et al., previously found that polystyrene sulfonic acid catalyzes the dehydration of formic acid to yield carbon monoxide and water. [66] The carbon monoxide could slowly adsorb on the palladium. Alternatively, the acid in the Nafion® could cause steps to form on the palladium surface. [67, 68] Such steps could be active for C-O bond scission on palladium leading to CO formation. [69-71] Another source of CO buildup on the catalyst is the impurities found in formic acid; studies have shown the purification of formic acid reduces the rate of poisoning but does not eliminate it. [25, 31, 63-65, 72]

Palladium catalyst modifications. One of the emphases of this work is modifications to the palladium anode catalyst for formic acid oxidation as an attempt to reduce the amount of CO poisoning that occurs during fuel cell operation. Over the past forty years, catalyst adatom modifications have been studied for both platinum and palladium catalysts for formic acid oxidation. Initial studies of formic acid oxidation on platinum and palladium showed substantial increases (several orders of magnitude on platinum) in transient oxidation current when adatoms such as lead, tin, cadmium, and others, were added to the platinum surface via underpotential deposition (UPD). [73-77] Irreversible adsorption occurs when the catalyst is held at an underpotential for a period of time, typically minutes, and the adatoms are irreversibly adsorbed to the surface [78, 79]. Such adatoms do not strip off the surface during anodic potential scans as do atoms that are reversible adsorbed during UPD. Recently, lead was shown to completely eliminate CO buildup on platinum electrodes. [80] There have been several studies of modified platinum anode catalysts in the DFAFC, but these fuel cells are inferior to palladium-based fuel cells even with the improvements to the platinum anode catalyst. [81-83] This work is the first reported study of adatom-modified palladium-based anode catalysts for the DFAFC.

Catalysts modified with adatoms via UPD or irreversible adsorption are known to enhance the oxidation of formic acid via any or all of three possible routes. First, the coverage of less than one monolayer of catalyst with an adatom that is inert to formic acid isolates individual catalyst sites and reduces the amount of CO poison that can build up on the surface, particularly CO that is multiply bonded to the surface [42, 73, 74, 84-

89]. This is known as the "steric effect" and is strongly supported by empirical evidence in which an adatom such as lead is shown to completely block CO buildup on platinum during formic acid oxidation [80]. Second, the adatom can create a bi-functional catalyst, in which the inert adatom may still be inert to formic acid, but performs some other role [90-92]. For example, ruthenium readily adsorbs water, which is necessary for removal of CO from a platinum surface during formic acid oxidation, as shown in Equations 2.20 and 2.21, although ruthenium itself will not oxidize formic acid [54]. Third, the adatom may shift the core level binding energy of the catalyst, changing the adsorption characteristics of formic acid and CO on the catalyst surface [45, 93, 94]. This is known as the "electronic effect", and will be discussed further in this work.

Literature for formic acid fuel cells. Due to interest in the DFAFC, much literature has been written describing catalysts that are supposed to be superior to palladium black for formic acid oxidation. Although many of these papers contain "in a formic acid fuel cell" in their titles, they quite often describe catalysts that have never been studied "in a formic acid fuel cell." [95-99] Without reporting fuel cell tests, many of these catalyst are shown to exhibit superior performance for only one hour in an electrochemical cell at potentials that are often much higher than applied in an operating fuel cell. Some experiments only show transient voltammetry measurements, demonstrating little proof that the developed catalysts would operate well in a real fuel cell. In this work, we have used the electrochemical cell to develop and study catalysts of interest, while using the operating direct formic acid fuel cell to demonstrate the behavior of the catalysts in an actual fuel cell environment. We found that the extent of

performance superiority observed in an electrochemical cell is, not surprisingly, much greater than the superiority observed in an operating fuel cell. Thus, literature reports of catalysts that have been characterized only in an electrochemical cell need to be stated as such: catalysts with stronger activity for formic acid oxidation in an electrochemical half cell environment.

2.3 The Electronic Effect in Formic Acid Oxidation

The electronic effect. One of the aforementioned effects that an adatom catalyst modification can have on the original catalyst is called the "electronic effect." An electronic effect indicates that a change in catalytic activity occurs when the catalyst metal d-band center changes, which correlates with a shift in core level binding energy (BE). [100-104] These shifts in d-band center (and thus BE) have been shown to alter the bond strength of molecules adsorbed to the electrode surface, with a lowering of the d-band center decreasing the adsorbate bond strength. [105] Formic acid oxidation on palladium is very particle size dependent; it has been shown that decreasing the particle size results in a lower d-band center and increased core level BE, promoting the reaction by binding surface adsorbates more loosely and favoring the direct oxidation pathway. [105] Recently, others have confirmed this result and found that alloy modifications to the palladium catalyst cause an upshift in BE. [106, 107] However, this recent work was done with carbon supported palladium, which is an inferior catalyst for the DFAFC; unsupported palladium performs much better. [25]

Measuring the electronic effect. Shifts in the core level binding energy (and therefore, the presence of an electronic effect) can be measured by x-ray photoelectron spectroscopy (XPS). In XPS, high energy x-rays irradiate the sample and cause the ejection of core electrons that are detected from the top 1-10 nm of the substrate. The number of electrons ejected and their associated kinetic energies are measured; from this the core level electron BEs can be determined:

$$E_{BE} = E_{photon} - E_{KE} - \Phi \qquad (2.22)$$

where E_{BE} is the binding energy of the ejected electron, E_{photon} is the energy of the irradiating x-ray, E_{KE} is the kinetic energy of the ejected electron, and Φ is the work function of the instrument. Changes in the binding energy of an atom indicate changes in its electronic environment.

However, the electronic environment of an atom is sensitive not only to the "adatom" (in the application of this work), but also to other contaminants at the surface. Specifically, oxygen binds readily to a surface of platinum or palladium, and other carbon-based contaminants are difficult to eliminate in practice. In our work, we have made very strong efforts to prevent contamination by air and organic matter and will be discussed in greater detail. Such efforts are not often mentioned in fuel cell catalyst literature. However, without a completely enclosed system that combines electrochemistry and XPS with no air exposure between steps, we do not make our XPS measurements the centerpiece of our work; we simply refer to our data as information that supports our theory that an electronic effect plays some role in the increased formic acid oxidation of our catalysts. [105]

2.4 Carbon Dioxide Reduction

Electro-reduction of carbon dioxide. A method of carbon dioxide capture that would work well with a solar energy source is the electrochemical reduction of carbon dioxide and subsequent conversion to hydrocarbon products; this has been studied on a variety of electrodes in a variety of aqueous and non-aqueous environments. [108-157] When this reduction takes place in aqueous solutions, the presence of protons aids in carbon dioxide reduction and produces a variety of products at pH 7: [158]

$$CO_2 + 2\ H^+ + 2\ e^- \rightarrow HCOOH \qquad (E^o = -0.61\ V) \qquad (2.23)$$

$$CO_2 + 2\ H^+ + 2\ e^- \rightarrow CO + H_2O \qquad (E^o = -0.52\ V) \qquad (2.24)$$

$$CO_2 + 4\ H^+ + 4\ e^- \rightarrow HCHO + H_2O \qquad (E^o = -0.48\ V) \qquad (2.25)$$

$$CO_2 + 6\ H^+ + 6\ e^- \rightarrow CH_3OH + H_2O \qquad (E^o = -0.38\ V) \qquad (2.26)$$

$$CO_2 + 8\ H^+ + 8\ e^- \rightarrow CH_4 + 2\ H_2O \qquad (E^o = -0.24\ V) \qquad (2.27)$$

However, one disadvantage of using aqueous solutions is that the hydrogen evolution reaction (HER) begins at 0.000 V vs SHE (approximately -0.42 V in a solution of pH 7). The competition between the two reductions decreases the Faradaic efficiency of carbon dioxide reduction. [109, 119, 120, 159, 160]. Even Equation 2.27, which occurs above HER theoretically, would compete with HER if any overpotential was required. Another complication with aqueous solutions is the low solubility of carbon dioxide. One method that would make direct carbon dioxide reduction to practical fuels in aqueous solutions more efficient is being studied in our lab: by suppression of hydrogen formation via tetra-alkyl ammonium salts, we expect to increase the efficiency of the conversion.

When carbon dioxide is electrochemically reduced in organic solvents, the preferred products are carbon monoxide and oxalic acid: [158, 161]

$$2\ CO_2 + 2\ e^- \rightarrow CO + CO_3^{2-} \qquad (E^o = -0.64\ V) \qquad (2.28)$$

Although the reaction is not thermodynamically favorable compared with aqueous solutions, the absence of HER allows for a more efficient reduction to CO. However, carbon dioxide still is not very soluble in aprotic organic solvents. The mechanism which has been proposed in non-aqueous, aprotic solvents on several different metal electrodes shows carbon dioxide conversion via a charged, radical intermediate as the rate determining step (rds): [109 , 158, 162-167]

$$CO_2 + e^- \rightarrow {\cdot}CO_2^- \qquad \text{(rds)} \qquad (2.29)$$

$$2\ {\cdot}CO_2^- \rightarrow C_2O_4^{2-} \qquad (2.30)$$

$$C_2O_4^{2-} \rightarrow CO + CO_3^{2-} \qquad (2.31)$$

In acetonitrile, a strong correlation was found between the choice of electrode and the overpotential necessary to drive the reduction, indicating that the rds involves an adsorbed species. [166, 167] Platinum electrodes, on which CO readily adsorbs, favors production of CO, while other electrodes favor oxalate production. On platinum, which is studied in this work, one Tafel slope of nearly 700 mV decade^{-1} was observed and corresponds to Equation 2.29, electron capture by carbon dioxide to produce the ${\cdot}CO_2^-$ intermediate.

In this work, we demonstrate that the ${\cdot}CO_2^-$ intermediate can be stabilized via an ionic liquid, whereby the reduction potential needed to convert carbon dioxide is reduced by 0.5 V. It has been shown that the ${\cdot}O_2^-$ intermediate formed during oxygen reduction in

1-butyl-3-methyl-imidazolium bis(trifluoromethylsulfonyl)imide (BMIM NTf_2) forms a complex between the intermediate and the $BMIM^+$ cation. [168, 169] This intermediate causes a positive shift in the reduction potential by 0.65 V. Therefore, we expected that we also could use ionic liquids to lower the reduction potential required to form the $\cdot CO_2^-$ radical intermediate, which could significantly reduce the amount of energy needed to produce carbon monoxide from carbon dioxide reduction. In addition, CO_2 forms a weak complex with some imidazolium cations, which suggests that the charged $\cdot CO_2^-$ would also form such a complex. [170-172] Finally, we take advantage of the benefit that carbon dioxide is more soluble in ionic liquid than it is in other aprotic, non-aqueous solvents. [170, 173-177]

2.5 Ionic Liquid Chemistry

Electrochemistry of ionic liquids. The unique characteristics of room temperature ionic liquids (RTILs) are of interest to this work. By definition, an RTIL is entirely composed of ions and is a liquid at room temperature. Such RTILs were originally studied for the purpose of electrochemistry, for which they exhibit a large potential window as compared with water (as much as 4 V, compared with ~1 V). [178, 179] However, initial RTILs were plagued with excessive sensitivities to atmospheric conditions until anions such as tetrafluoroborate, which is used in this work, were found to be much less sensitive. [180] We have found that, although RTILs made with these anions absorb water, the absorption rate is slow enough to permit electrochemical experiments in an inert environment. A few common ions are shown in Figure 2.7, and cations such as the C_nMIM have the advantage that changes to the carbon chain length

result in slight changes to their characteristics, which allows one to tailor the RTIL to a specific application.

There are several additional considerations to make when choosing an RTIL for a specific electrochemical application: conductivity, diffusion, potential window, and reference electrode. Conductivity of ionic liquids is generally lower than that of aqueous solutions containing a supporting electrolyte because of the bulky ions, but we found that the conductivity of the imidazolium-based RTILs is generally sufficient for electrochemistry. Conductivity can also be enhanced if necessary by the inclusion of tetraalkylammonium salts. Diffusion is generally slower in RTILs because of the increased viscosity. The diffusion coefficient for carbon dioxide in BMIM BF_4 is approximately $5x10^{-7}$ cm^2 s^{-1}, while in water, the value is approximately double. [181] However, we have found that the RDE is able to overcome the slower diffusion so that kinetic studies can be performed in an electrochemical cell. Due to the absence of water in the RTIL, such a liquid is not bound by the potential limits of hydrogen and oxygen evolution as in aqueous solutions. The much larger potential window is bounded, instead, by reduction of the ionic liquid cation and oxidation of the ionic liquid anion. In order to maintain a constant reference over such a large potential window, it is recommended that one use a silver-silver wire reference electrode that has been calibrated to a well-known metallocene redox couple such as ferrocene; a quasi-reference electrode is not sufficiently reliable. [182-184]

Surface chemistry of ionic liquids. When an ionic liquid with an alkyl-methylimidazolium cation interacts with a metal surface such as platinum, its interaction can be simplified to that of a Helmholtz double layer, in which no solvation occurs (due to the lack of solvating molecules), and the charged ions shield the charged surface from the bulk liquid. [185] The imidazolium ring has its charge centered on the aromatic ring, although the charge density slightly favors the carbon bonded to both nitrogens. In the case of BMIM BF_4 adsorbed on a platinum surface, the ring lies approximately 30° from parallel with the surface when the surface is held at a potential negative of its point of zero charge (PZC) so that the positive charge on the ring can shield the negatively charged electrode surface from the bulk. [185] When the potential is scanned positive of the PZC, the ring tilts to 45° from the surface to allow the anion better access to the surface to balance the charge. Similar behavior is observed on other surfaces and is predicted from molecular simulations. [186-188] It also has been shown that a smaller alkyl chain (e.g., the ethyl chain used in our work) should further favor a parallel orientation at low potentials. [189] The PZC for EMIM BF_4 has been reported as -0.25 V vs SHE, which suggests that the ionic liquid used in our experiments should be oriented less than 45° to the platinum surface within the potential window in which our carbon dioxide reduction takes place. [190]

2.6 Broad-Band Sum-Frequency Generation

Sum frequency generation spectroscopy as a surface probe. In this work, broad-band sum frequency generation (BB-SFG) was used to study the mechanism of carbon dioxide reduction on platinum in ionic liquid in order to compare the ionic liquid

solvent with previous studies in aprotic organic solvents. Specifically, we wanted to demonstrate formation of carbon monoxide, which could be used to produce hydrocarbons, essentially recycling the carbon dioxide into usable fuel.

Sum-frequency generation (SFG) is a second order non-linear spectroscopic technique that adds (Figure 2.8) the frequencies of a visible and an infrared beam at a surface to produce a single outgoing beam: [191]

$$\omega_{SFG} = \omega_{vis} + \omega_{IR} \tag{2.32}$$

As a second order non-linear process, SFG signal intensity, I_{SFG}, is related to the SFG polarization, P_{SFG}: [192]

$$I_{SFG} \propto |P_{SFG}|^2 \propto \left|\chi_{NR}^{(2)} + \sum_v \left|\chi_{Rv}^{(2)} e^{i\gamma v}\right|^2 I_{vis} I_{IR}\right| \tag{2.33}$$

where $\chi_{NR}^{(2)}$ and $\chi_R^{(2)}$ represent the non-resonant and resonant components, respectively, of $\chi_S^{(2)}$, the effective surface non-linear susceptibility, and γ_v is the relative phase of the v^{th} vibrational mode. SFG is not allowed in centrosymmetric media because of its dependence on $\chi_S^{(2)}$; in an isotropic medium, such as water or an ionic liquid, there is no net dipole, which causes P_{SFG}, and thus the SFG signal, to disappear. The signal is only generated where the symmetry is broken, such as at a solid-liquid interface; this makes SFG sensitive to a surface in an electrochemistry experiment, which necessarily has an electrode surface and an electrolyte media. [193] The incoming visible beam is typically held constant, while the wavelength of the incoming infrared beam can be changed to probe a desired spectral window. A picosecond infrared pulse is used to permit scanning over a specific spectral window, or a femtosecond pulse (as in BB-SFG) is used with a broad spectral window and faster acquisition time. In our experiments, we sacrificed a

small spectral window for fast acquisition times, which permit good potential resolution for simultaneous cyclic voltammetry. [194-196]

Sum frequency generation spectroscopy combined with electrochemistry. Over the past several years, collaborations between the research groups of Drs. Dana Dlott and Andrzej Wieckowski, have demonstrated the effectiveness of combined SFG and electrochemistry using thin-layer electrochemistry (TLE) to probe electrode surfaces relevant to fuel cell catalysts. [194-196] In this research, they determined appropriate parameters for cell thickness, scan rate, and synchronization to confirm that the electrochemistry and the spectroscopy occur simultaneously during oxidation of formic acid and measurement of oxidation intermediates. They were able to study the adsorption of CO molecules on platinum polycrystalline and single crystal electrode surfaces, with an ability to differentiate between singly- and multiply-bonded CO molecules. [194] CO stripping experiments demonstrated that the electrochemistry in the TLE correlates directly with the presence, then disappearance, of CO signal in the SFG spectra during an anodic potential scan.

Platinum strongly promotes the formation of CO from carbon dioxide reduction in aprotic solvents, and the CO adsorbs strongly to platinum, giving a strong vibrational signal. Therefore, in this work, we initiated collaboration with the aforementioned groups in which we observed a strong CO signal from SFG on platinum in ionic liquids, as well as other interesting signals.

2.7 Figures

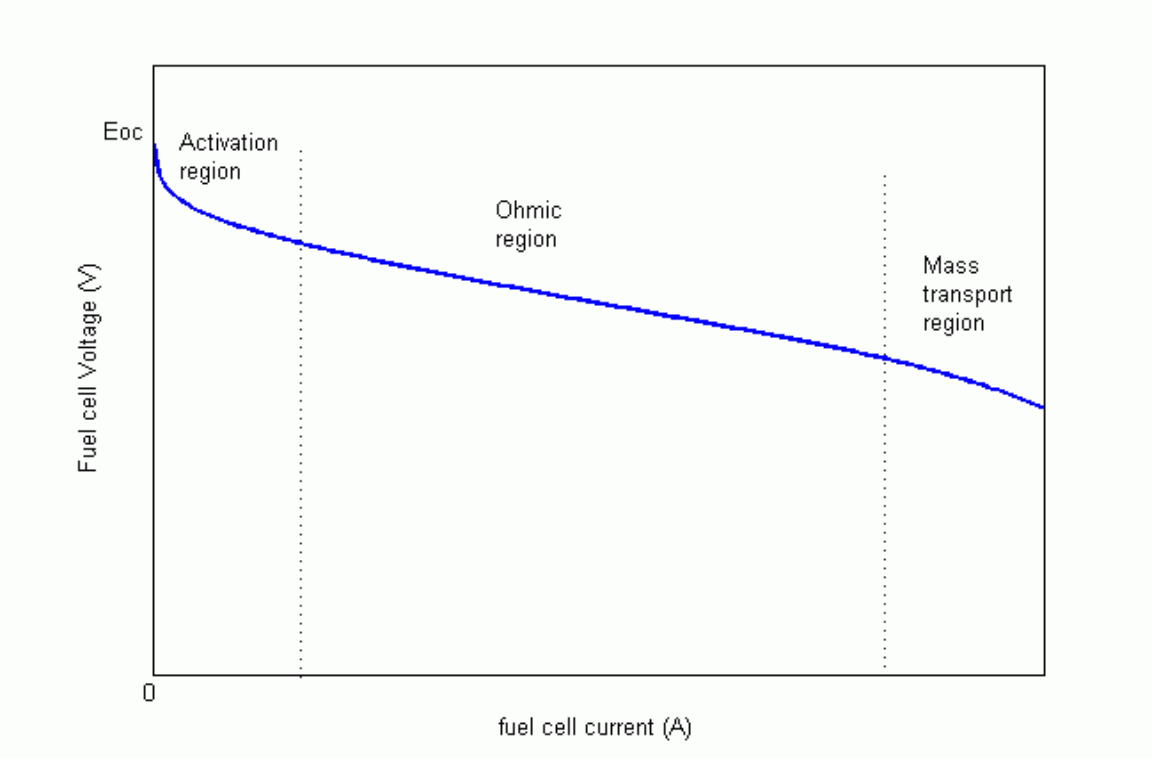

Figure 2.1. A sample fuel cell polarization curve. [197] Three regions of losses are shown here as the value of the current increases: kinetic, Ohmic, and mass transport.

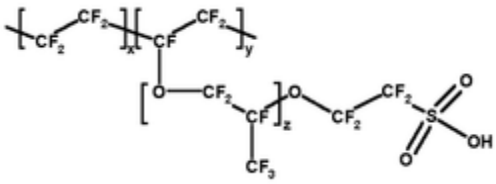

Figure 2.2. The Nafion polymer that is used as an acid membrane in most PEM fuel cell applications. [198] Protons are transferred via the sulfonic acid side groups.

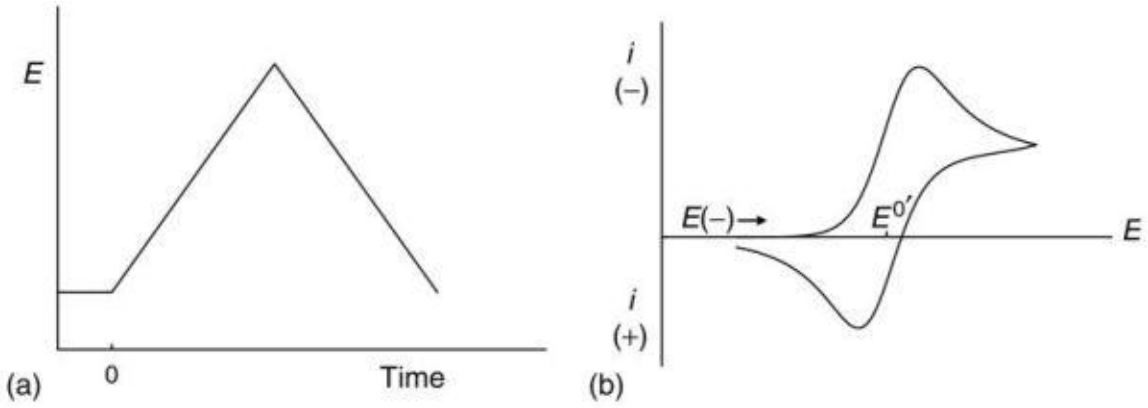

Figure 2.3. The cyclic voltammetric waveform, in which potential is scanned to *E* and returned to the original potential in a linear fashion (a). The resulting current-potential scan demonstrating a cathodic current in the forward scan and an anodic current in the back scan. [197]

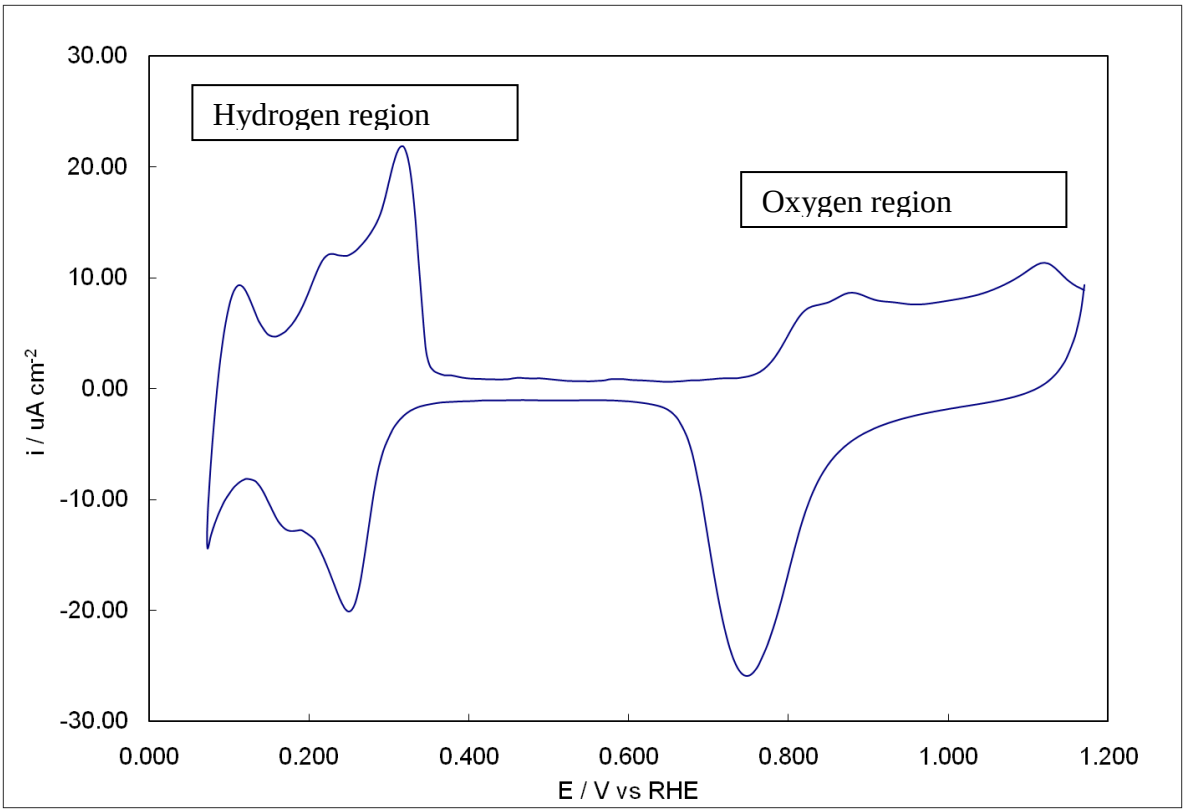

Figure 2.4. A cyclic voltammogram of palladium black high surface area catalyst in 0.1 M sulfuric acid: scan rate 10 mV s^{-1}. In the hydrogen region, protons interact with the catalyst surface, adsorbing in the negative sweep and desorbing in the positive sweep. In the oxygen region, hydroxide ions oxidize the surface in the positive sweep and are reduced from the surface in the negative sweep.

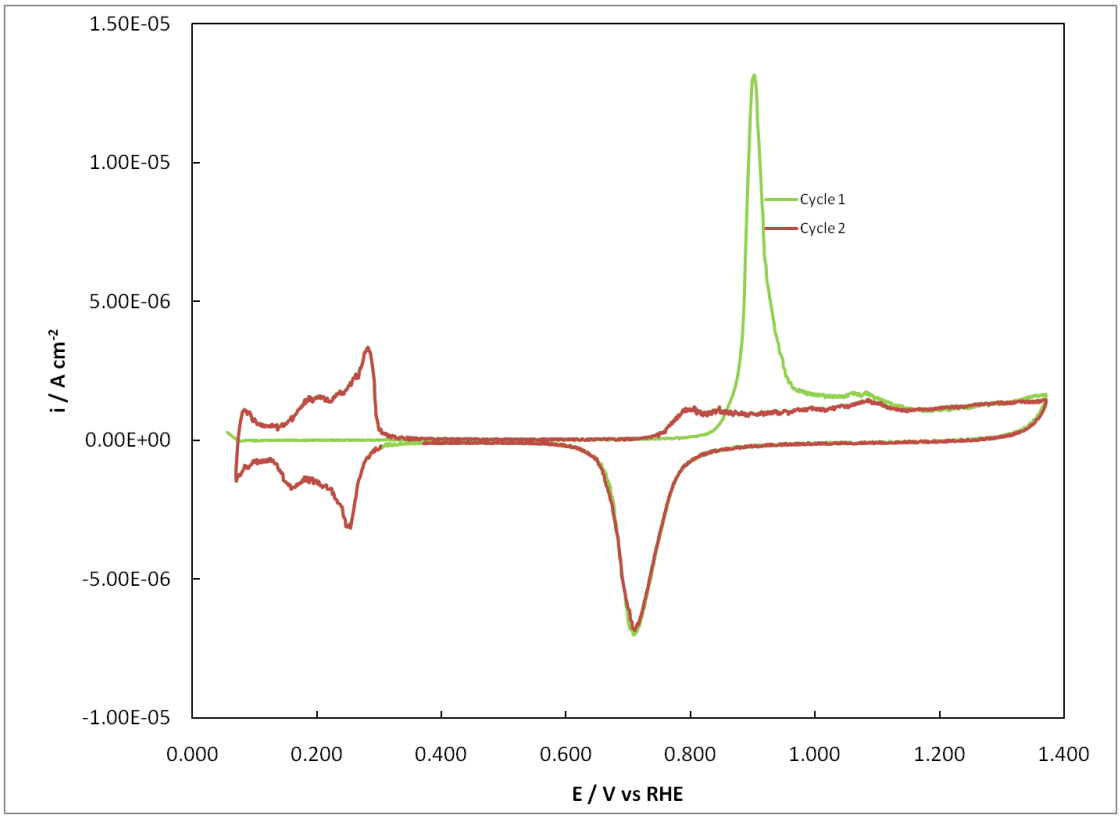

Figure 2.5. A cyclic voltammogram of high surface palladium in sulfuric acid following surface saturation of CO. During the first cycle, the CO is stripped from the surface at ~0.9 V vs RHE. In the second cycle, the normal hydrogen and oxygen surface interactions are restored. Scan rate: 10 mV s^{-1}.

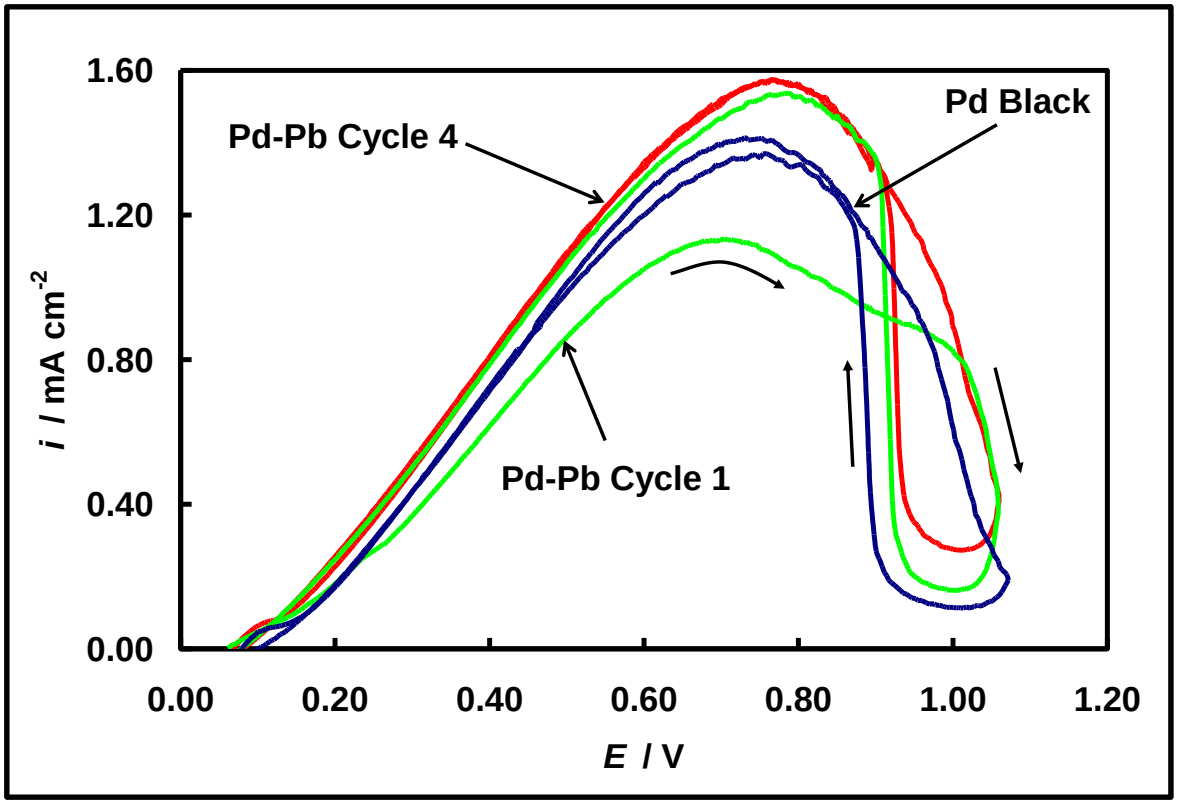

Figure 2.6. Cyclic voltammogram of formic acid oxidation on palladium black in 0.1 M formic acid + 0.5 M perchloric acid shown with and without lead adsorbed on surface. Cycle 1 after lead adsorption shows a suppression of formic acid oxidation in the anodic sweep. Cycle 4 after lead adsorption shows a 20% enhancement in current at 0.3 V and a 12% enhancement in peak current over clean palladium black after four cycles.

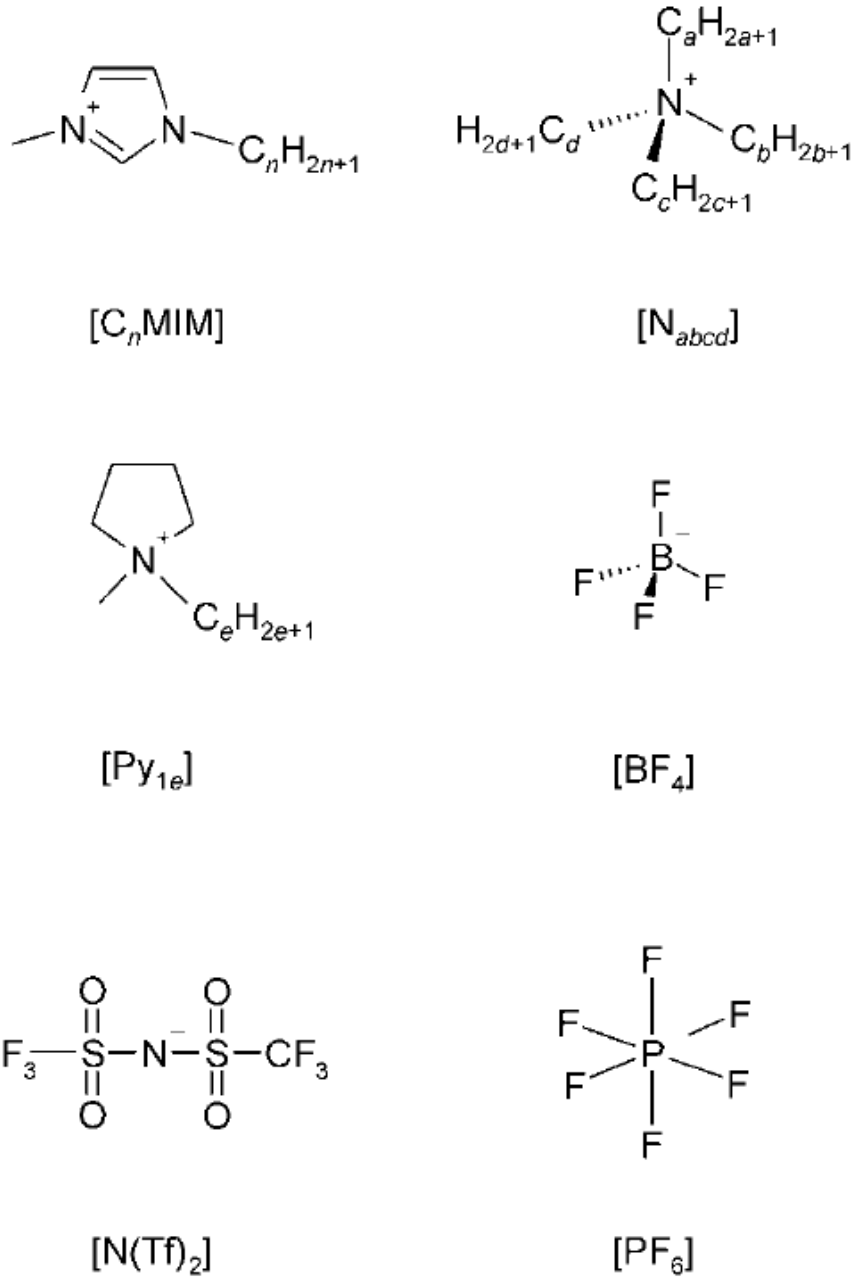

Figure 2.7. Anions and cations used for various RTILs. The ionic liquid studied in this work was 1-ethyl-3methyl-imidazolium tetrafluoroborate (EMIM BF_4). Image is from [179], Copyright Wiley-VCH Verlag GmbH & Co. KGaA; reproduced with permission.

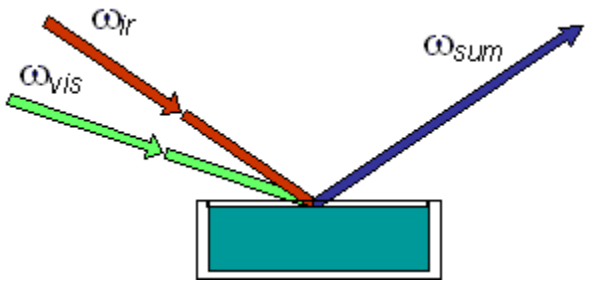

Figure 2.8. Incoming visible and infrared beams are overlapped at the surface to form an outgoing beam that is the sum of the incoming frequencies. This method is sensitive to the broken symmetry at an interface. [199]

Chapter 3: Statement of Purpose

The research performed for this work involves the electrochemistry of applied energy technologies: the direct formic acid fuel cell (DFAFC) and carbon dioxide conversion devices.

The DFAFC was developed in the research group of the author's advisor, Dr. Richard Masel, at the University of Illinois. Once an operating fuel cell was developed, it quickly became apparent that the anode reaction, oxidation of formic acid, would be the limiting factor in the DFAFC. Anode catalyst improvements were made, particularly when the catalyst was switched from platinum to palladium black. However, the palladium catalyst still suffers from poisoning when the fuel cell is operated for several hours.

In order to address the poisoning of the palladium catalyst, two approaches were taken in this work. First, adjustments were made to the formic acid fuel pH, which shifted the oxidation potential for catalyst poison removal to lower potentials versus the standard hydrogen electrode. Both platinum and palladium catalysts were studied (since the main problem with platinum catalysts is rapid poisoning), and it was confirmed that the formic acid oxidation reaction was promoted at higher pH. However, the current acid membranes, which pass protons to the cathode, are very sensitive to the cation in the base that is used to raise the formic acid pH. The bulky sodium ion, for example, is dragged into the acid membrane and the membrane resistance rises rapidly (in a matter of seconds or minutes, depending on sodium concentration), rendering the fuel cell useless. Since

adjustments to the pH were shown to result in improvements to formic acid oxidation, future work involves adjusting the pH at the catalyst surface (rather than in the solution bulk) by mixing basic binders into the catalyst ink.

The second approach to address catalyst poisoning was to develop catalysts that have an adatom, such as antimony, tin, or lead, irreversibly adsorbed to the palladium surface. Such catalyst formulations have been shown to promote formic acid oxidation on palladium and platinum electrodes, but no work had been done prior to this work on palladium nanoparticles in either an electrochemical cell or a fuel cell. In this work, numerous catalyst formulations were studied, with the aforementioned three adatoms proving to be the most beneficial to formic acid oxidation. Promotion of formic acid oxidation in an electrochemical cell was substantial, but the promotion in a fuel cell was less. The promotion is attributed to a combination of a steric effect and an electronic effect.

The other research performed in this work involves the reduction of carbon dioxide in ionic liquid. The research group of the author's advisor has begun a substantial effort into conversion of carbon dioxide into hydrocarbon fuels that would lead to the development of carbon dioxide recycling devices. The author's contribution to this effort involves the use of an ionic liquid to stabilize a charged intermediate in the reduction of carbon dioxide. There is evidence that such stabilization is providing a substantial decrease (at least 0.5 V) in the amount of reduction potential necessary to electrochemically reduce carbon dioxide.

Chapter 4: Experimental Procedures

4.1 Fuel Cell Assembly and Testing

Fuel cell components. The direct formic acid fuel cell was demonstrated several years ago as an alternative to a battery in a commercial wireless phone as shown in Figure 4.1. In this configuration, its size and geometry was made comparable to that of the battery it replaced. However, in the research lab, the DFAFC used for testing is considerably larger for ease of handling. The fuel cell that is assembled for testing consists of the following components: membrane, catalyst layers, reference electrode, gas diffusion layers, gas/liquid flow fields, current collector plates, and heating tape. Each component will be discussed in order of assembly.

The membrane. The fuel cell membrane consists of the ionically conductive polymer, Nafion®, ranging in thickness from 0.002 to 0.010" for this study. We determined that Nafion® 117 (0.007" thickness) was the optimal membrane for the type of fuel cell analyzed in this work, providing the best balance between performance and robustness. Nafion® is a polymer which contains sulfonic acid groups that conduct protons from the anode to the cathode without leaking electrical current. The protons are drawn through the membrane either via a hydrogen bonding network of static water molecules or via bonding to mobile water molecules which escort the proton through the membrane. Since protons are drawn across the membrane, it is imperative that acid groups are protonated, but they are delivered to the end user in "sodium" form to enhance membrane stability during shipping. That is, the sulfonic acid groups are neutralized and must be protonated prior to use in the fuel cell.

To protonate a one square foot Nafion® sheet that is ordered from Ion Power, it is first cut into several smaller sheets, ranging in size from 4x4 to 10x10 cm^2. The smaller sheets are then heated in a bath consisting of 5 weight percent hydrogen peroxide (Alfa-Aesar, 35% w/w aqueous solution) and 18.2 MΩ Millipore® water, for 1 hour, at a temperature of 80° C. This bath removes organic contaminants from the surface of the Nafion®. After 1 hour, the sheets are carefully removed and washed with Millipore® water. After washing, they are placed in a bath of Millipore® water, and boiled for 1 hour to remove all hydrogen peroxide from the surface. After the water bath, a sulfuric acid (Sigma-Aldrich, ACS reagent) bath is prepared, consisting of 5 weight percent sulfuric acid, and Millipore® water. Again, the bath is heated to 80 °C and the Nafion® sheets placed in the bath, with extra caution taken due to the danger of sulfuric acid. In this step, the Nafion® membrane is protonated by displacing all the sodium ions with protons. Following the acid bath, the sheets are rinsed then boiled for 1 hour in Millipore® water to remove excess sulfuric acid on the membrane. Finally, the protonated Nafion® sheets are stored in Millipore® water for fuel cell assembly.

When one Nafion® sheet is used in a fuel cell assembly, it is painted with anode catalyst ink, cathode catalyst ink, and platinum reference ink. In preparation for painting the membrane is removed from the water storage solution, flattened, and dried on a heated vacuum table that was previously set to 60 °C in preparation for catalyst painting. A nylon or silicone gasket seals the membrane to the vacuum table to keep it flattened

since wrinkles that form during painting will ruin the membrane. Once the membrane is dried, after a few minutes, it is ready for catalyst ink painting.

Catalyst layers. The catalysts used for the direct formic acid fuel cell must be high surface area and highly active for their respective redox roles. For the anode catalyst, palladium black unsupported catalysts (Aldrich, 99.8%) were used due to their high performance for formic acid oxidation. Carbon-supported catalysts were tested but found to be far inferior to unsupported catalysts and were not further pursued for alloying studies. For the cathode catalyst, high surface area platinum catalysts, both unsupported (HiSpec 1000, Alfa Aesar) and carbon supported (~50wt % Pt, Tanaka) were studied. We found that the supported catalysts led to an earlier mass transport limiting region in the fuel cell polarization curves, which decreased the power output of such fuel cells. Therefore, only the results of the superior unsupported catalysts are shown in this work. Finally, a 1 cm^2 or less swath of the platinum catalyst was also painted off center (Figure 2) on the anode side of the membrane to create a hydrogen-platinum reference electrode that enabled probing of the individual reactions occurring at each anode.

While the Nafion® membrane is drying, the cathode catalyst ink is prepared. This is painted first because the unsupported platinum is the most difficult preparation step. It is crucial that the paint is applied evenly without cracks in the layer; the easiest way to observe cracks is if there is no catalyst yet painted on the other side of the membrane. The failure rate for painting this portion of the membrane is high (50%) but decreases with experience; a failed painting must be discarded entirely. The platinum

catalyst ink is prepared as follows. Approximately 50 mg of platinum is massed in a small glass vial and approximately 600 mg of water is added. This mixture is sonicated for 1-2 minutes surrounded by an ice bath. Then approximately 220 mg of Nafion® suspension (Ion Power, Equivalent Weight 1100) is added and the mixture is again sonicated for 1-2 minutes surrounded by an ice bath. The ice water bath prevents heating of the mixture, which could agglomerate particles and evaporate solvent. This final mixture is called the catalyst ink and is ready for painting; it is kept in the ice bath to prevent premature solvent evaporation. Note that the unsupported palladium ink is prepared in a similar fashion, but it is not prepared until after the platinum ink has been painted and dried.

The platinum catalyst ink is painted directly onto the membrane using a camel hair brush that is modified for a small paint area. [200] The ink is painted in long, slow swipes in a variety of directions. Unidirectional painting leads to poor catalyst layers that are prone to flaking, cracking, and holes. Even drying of the platinum catalyst is carefully watched for and when the ink appears to be on the verge of failure, painting is halted. Since the cathode reaction is not the limiting factor in the DFAFC, the amount of catalyst painted is not crucial as long as there is enough to keep up with the anode kinetics. After painting, the ink is dried for 30 minutes without removing the membrane from the heated vacuum table. (A heat lamp aids significantly in drying the catalyst layer during and after painting.)

Once the first catalyst application is dried, the membrane is flipped over and reflattened on the vacuum table. A few brush strokes are made off center with the platinum catalyst to create the reference electrode. Then the palladium ink is prepared using a similar preparation method to that of the cathode catalyst. The palladium ink applies more easily than the platinum, but care must still be taken to prevent cracking in the catalyst layer. Once it is dried the membrane can be removed from the vacuum table for assembly in the fuel cell; this membrane can now be called a membrane electrode assembly (MEA).

Electrochemically modified catalyst layer. One variation on this technique that was studied in this work is the division of the anode catalyst layer between the membrane and the carbon paper gas diffusion layer (0.008", Spectracarb), shown in Figure 4.2. The reason for the division of the catalyst layer is that catalyst painted directly on the membrane cannot be electrochemically modified. However, catalyst painted on the conductive carbon paper could be electrochemically modified as desired. Therefore, the electrochemically modified catalyst was necessarily only partly modified, which certainly led to some of the performance losses observed between the electrochemical cell and the fuel cell. Several experiments were run to determine the optimal ratio of catalyst ink between the two painting locations, and it was determined that an even division of catalyst ink provided the highest performance in the DFAFC. In order to paint the catalyst ink onto the carbon cloth, palladium ink was prepared (at lower proportions) as usual. A carbon paper piece was secured on a hot plate set at approximately 2 with a heat lamp used to help dry the ink. As usual, multidirectional brush strokes were used until all

the ink was painted. Care was taken to paint slowly so that the ink did not leak through the highly porous paper. The paper was left to dry overnight.

In order to modify the palladium that was painted onto the carbon paper, a standard three electrode electrochemical cell was employed. The paper was connected to the Solartron 1287 potentiostat via two pieces of gold foil (Alfa Aesar) connected to an alligator clip. The counter electrode was a platinum mesh (52 mesh, Alfa Aesar). The reference electrode was a silver silver chloride reference (BAS) calibrated by bubbling hydrogen (S.J. Smith) over the counter electrode. The electrochemical cell solution consisted of some adatom (Sb^{3+}, Sn^{2+}, Pb^{2+}, from Aldrich) dissolved in a supporting electrolyte (dilute sulfuric or perchloric acid, double distilled from GFS), and the potential was held at 0.45 V vs the reversible hydrogen electrode (RHE) for 5-20 minutes. Following electrochemical modification the carbon paper was again dried overnight prior to assembly in the fuel cell.

Fuel cell assembly. Once the MEA is completed, the fuel cell can be fully assembled with ease. The final preparation step is to hot press immediately prior to assembling the MEA into the rest of the fuel cell. The membrane containing all the catalyst layers, plus the carbon paper containing the remainder of the palladium catalyst layer, need to form a strong connection for proton conductivity to the membrane and electron conductivity out to the gas diffusion layer. The hot press is heated to approximately 80 °C. A few strokes of Nafion® suspension are painted between the catalyst layers on the carbon paper and the membrane, and the two are quickly assembled

together and placed in the hot press. They are pressed with light pressure (so as not to destroy the carbon paper) for 2-3 minutes. Following hot pressing, this MEA is now ready for fuel cell assembly.

The gold-plated current collector is first placed on the assembly table followed by the graphite flow field for the cathode side of the fuel cell. A few bolts are placed through these 2 pieces to stabilize the orientation of the MEA. A piece of carbon cloth (0.020", E-Tek) containing single-sided wet proofing is placed in the flow field such that the wet proofed side is in direct contact with the catalyst layer to wick water toward the flow field and out of the fuel cell. A silicone or Teflon® gasket with the same or slightly greater thickness is then placed onto the flow field to act as a spacer for the area that is not covered by the carbon cloth. Now the MEA is placed onto this assembly with the anode side facing up. On top of the MEA is then placed another gasket which is cut to perfectly surround the carbon paper gas diffusion layer that protrudes upward from the MEA. Finally, the anode flow field and another current collector are placed on top, and the bolts are tightened using a torque wrench. Heating tape, which is secured to each current collector, provides heat for the experiments when connected to a variable voltage power source.

Fuel cell testing. Diagnostic electrochemical tests were performed on the DFAFC using a Solartron 1287 potentiostat and a two electrode setup, with the working electrode on the cathode and the counter electrode on the anode; this configuration maintained a positive voltage output under normal operating conditions. Alligator clips

were attached to the current collectors in order to connect the fuel cell to the potentiostat. A reference electrode was employed separate from the potentiostat. Hydrogen gas was blown onto a platinum mesh that was pressed against the painted reference portion of the anode side of the fuel cell. This hydrogen reference electrode was then compared to the potentials of each electrode as measured by multimeters connected to each anode and grounded to the hydrogen reference electrode.

Voltage-current (VI) measurements. One of the methods used to characterize the performance of the DFAFC is the voltage-current (VI) experiment, an example of which was shown in Figure 2.1. It is similar to cyclic voltammetry experiments in electrochemistry since a linear potential sweep is employed and the resulting current is observed. In addition, the power, which is simply the current multiplied by the voltage, is calculated from this experiment. At low current, *activation polarization*, the energy required to overcome kinetic reaction barriers, severely reduces the cell voltage. In a hydrogen fuel cell, the significant kinetics losses occur at the cathode. However, in direct liquid fuel cells, kinetic losses occur at both electrodes, with the anode kinetics being more sluggish. In the Ohmic region of Figure 2.1, losses occur due to the *cell resistance*, to which contributions are made from the Nafion® membrane, the catalyst layers, the diffusion layers, and the current collectors. The third region shown in Figure 2.1 exhibits losses due to *mass transport* of the fuels to the catalyst. As high amounts of current are drawn through the cell, the reactions at the catalyst surfaces occur faster than the reactants can be replenished by diffusion. This region represents the practical limit of fuel cell operation without advanced methods of fuel delivery.

The potentiostat is set to measure the current at various potentials to construct the VI curve. The formic acid is set to flow at a rate of 1 mL min^{-1} over the anode so that the mass transport limiting region is not reached before high currents are produced. Air is blown over the cathode at ~300 sccm without backpressure.

Constant current measurements. A very important test that determines the stability of the fuel cell is a constant current test (although a constant voltage test can also be used to determine stability). In this experiment, the fuel cell is connected in the same way as for the VI test, except that the formic acid flow rate is lowered to 0.15 mL min^{-1} at the anode to conserve fuel and since the mass transport region of the VI will not be reached in such a test. Typically such a test is run for 8-12 hours at 100 mA cm^{-2}, and the voltage decay is measured with time. In the formic acid fuel cell, the main source of voltage decay is buildup of CO poison on the anode catalyst surface, and this is evident in a constant current test that employs a reference electrode, as shown in Figure 4.3. These tests also demonstrate catalyst stability over time. We find that the performance of the fuel cells employed in this work is fully regenerated following a step that removes the CO poison from the anode surface. In this step, the anode potential is pulsed to one volt (or is short circuited to the cathode that contains air flowing over it) for up to a minute, and the poison is fully removed.

4.2 Half Cell Electrochemistry

Catalyst preparations for the working electrode. Numerous electrochemical measurements were made employing a half cell to study the fuel cell anode reaction, formic acid oxidation. For the typical working electrode preparation, a catalyst ink was mixed and dried onto an electrode surface. The ink was a combination of 5.6 mg palladium, 30 mg Nafion® suspension, and 1 g water. Following sonication, the ink was placed on the electrode tip and dried either at ambient temperature or under a heating lamp. The electrode on which this ink was dried varied, depending on the experiment. For experiments in which a rotating disk was employed, the electrode options were gold and glassy carbon. The catalyst typically stuck better to the gold electrode, especially in the cases where Nafion® was not used as a binder. However, in some cases, such as electrochemical surface modification with lead, it was desirable to use the glassy carbon so as to avoid any undesired side reaction between the gold, which is inert to formic acid oxidation, and the adatom being studied. For experiments without the RDE, the catalyst was also dried on either a gold electrode or glassy carbon electrode. Finally, some experiments were done in which the catalyst was painted onto a carbon paper using the method described in the fuel cell preparation section. Very small strips (a few mm^2) were used as working electrodes to mimic the fuel cell environment as closely as possible in a three electrode cell.

Other electrodes and the electrochemical cell. The counter electrode used in electrochemical measurements was a platinum mesh (52 mesh, Alfa Aesar) connected to a platinum wire of 1 mm diameter (Alfa Aesar). The mesh was cleaned in a hydrogen

flame prior to use in the cell. The reference electrode was a standard silver-silver chloride reference (BAS) calibrated by bubbling hydrogen (S.J. Smith) over the counter electrode. The reference was stored in concentrated potassium chloride to maintain a constant chloride concentration, and therefore a constant reference potential (±2 mV) over several months.

The electrochemical cell is constructed entirely of glass and is cleaned in an acid and/or nochromix bath. It is a 100 mL flask with a 24/40 joint at the top and two 14/20 joints on the sides. The large joint permits insertion of the RDE, and the other joints permit insertion of a counter electrode, and solution additions as necessary. The flask is further modified by flattening the bottom to reduce its volume, adding Luer joints to permit gas flow, and adding a reference capillary that can be closed off while maintaining electrical connection with the solution. Ultra high purity argon (S.J. Smith) was used to remove oxygen from solution by bubbling for 30 minutes prior to experiment, and blowing over the top of the solution during experiments. A gas exit stream passed through a bubbler consisting of water (or mineral oil for water sensitive experiments) to prevent back diffusion of oxygen.

This cell was designed entirely by the author and constructed at the university campus glass blowing facility. Alternate electrochemical cells were also employed, but the bulk of the work used this very useful cell design.

Cyclic Voltammetry. Several electrochemical techniques were employed to permit characterization of catalysts used for formic acid oxidation. The most commonly used technique was cyclic voltammetry (CV), a technique that characterized the catalysts prior to testing in formic acid. CV was performed in only the supporting electrolyte, although tests in formic acid were also performed but not discussed here because the steady state measurements were deemed more informative. The supporting electrolyte typically consisted of dilute sulfuric or perchloric acid in concentrations ranging from 0.1 to 1 M. CV was used to determine the cleanliness of an electrode surface and the electrochemical surface area (ECSA). The palladium electrode scanned in 0.1 M sulfuric acid was shown in Figure 2.4. In the hydrogen region, protons interact with the catalyst surface, adsorbing to the surface in the cathodic scan and desorbing in the anodic scan. In the oxygen region, hydroxide ions oxidize the surface in the anodic scan and are reduced from the surface in the cathodic scan. Between these regions is the double layer region, in which only double layer charging occurs. The increased surface area from nanoparticles (as compared with smooth polycrystalline electrodes or single crystals) results in a higher current magnitude in this region.

A CV can also be used to determine the ECSA of a high surface area fuel cell catalyst. Figure 2.5 showed the voltammogram of a palladium catalyst which has been saturated with carbon monoxide. In the first cycle, no hydrogen activity is observed because the surface is poisoned by the CO. As the potential reaches ~0.9 V, the CO is oxidized from the surface, and the surface oxidation and reduction activities resume. In the second cycle, with a clean palladium surface, the hydrogen surface interactions also

resume. Integration of either the hydrogen peaks or the CO stripping peak can be used to calculate the charge passed for the one or two electron process, respectively. It is widely accepted that both platinum and palladium can be characterized in this manner, where the surface area from the hydrogen peaks is determined from the relationship of 210 $\mu C\ cm^{-2}$ and from the CO peaks by the relationship of 420 $\mu C\ cm^{-2}$. [36-41]

Chronoamperometry. Experiments were also performed in which the potential was held constant for a period of time. In these experiments, called chronoamperometry (CA), the stability of the catalyst can be studied; CA is the analogue to the constant current or constant voltage tests of the fuel cell. The typical experiment of this nature was carried out at 0.3 V vs RHE for formic acid oxidation. The experiment duration was as short as a few seconds to construct Tafel plots using 0.1 M HCOOH + 0.1 M H_2SO_4. Many experiments lasted several minutes to 12 hours using 1 or 12 M HCOOH + 0.1 M H_2SO_4. The formic acid was HPLC grade, 50% formic acid from Aldrich. A rotating disk electrode was often used for these experiments for two reasons: to probe kinetics without contributions from mass transport and to remove carbon dioxide bubbles formed at the catalyst surface during formic acid oxidation. Prior to deciding on a rotation speed of 2000 rpm, the dependence of formic acid oxidation on rotating speed was investigated. It was found that there was very little variation in current at different rotation speeds since the reaction is sluggish enough to be kinetically limited. Therefore, the rotation speed was chosen primarily to permit adequate removal of carbon dioxide bubbles from the electrode surface.

Electrochemical surface modification. The palladium catalyst was modified electrochemically in a three electrode cell, either for further study in the electrochemical cell or for study in the fuel cell. When used entirely in the electrochemical cell, the palladium catalyst was placed on the glassy carbon electrode used with the RDE. After cleaning the palladium surface with CV (and, depending on the experiment, running experiments in formic acid for baseline activity values), the palladium was placed into an adatom solution containing dilute sulfuric or perchloric acid electrolyte. A potential was set at 0.45 V vs RHE for a few minutes and the catalyst was rinsed and removed from solution. The catalyst could then be further characterized by CV and CA.

4.3 Carbon Dioxide Electrochemistry

Electrochemical Methods. The glassware and counter electrode for the electrochemical cell used in carbon dioxide electrochemistry was of exactly the same configuration as that used for the half cell electrochemistry, except that additional measures were taken to ensure that the cell was completely dry for introduction of the ionic liquid. The solution for the silver-silver ion reference electrode consisted of acetonitrile, 0.01 M silver nitrate, and 0.1 M tetrabutylammounium phosphate, and the reference was calibrated to the ferrocene redox couple. [201, 202] The reference potential was found to be +0.535 V vs SHE and repeatable over several experiments in EMIM BF_4. The working electrode was platinum black (HiSpec 1000, Alfa Aesar) on a rotating disk electrode (Pine) set to 2000 rpm.

Ionic Liquid Preparation. The ionic liquid was used as the electrolyte. Although the size of the ions and the high viscosity result in lower conductivity than aqueous solutions with support electrolytes, the conductivity is still greater than organic solvents with support electrolytes; the conductivity of the ionic liquid is sufficiently high to perform the voltammetric experiments in this work without the addition of a support electrolyte. [203] The ionic liquid was prepared by heating overnight just above 100 °C under convection and vacuum in order to remove any residual water or dissolved gases. During electrochemical experiments, the ionic liquid was purged with argon (UHP, S.J. Smith) to take baseline measurements assuring a large potential window and the absence of water. For carbon dioxide reduction, the ionic liquid was purged with carbon dioxide (99.99%, S.J. Smith).

4.4 X-Ray Photoelectron Spectroscopy

Electrochemical Methods. XPS was used to supplement the electrochemical and fuel cell data that was collected on the palladium-based catalysts and confirm the presence of an electronic effect by the adatom. To prepare the catalyst for XPS measurements, care was taken to protect as much as possible from contaminants including atmospheric oxygen. The only way to completely eliminate oxygen from the sample is to use an in situ electrochemical XPS instrument. However, since the focus of this work is not the electronic effect, care was taken to reduce oxygen exposure in order to provide supplemental XPS data in support of our hypothesis that the adatoms produce some electronic effect on the palladium.

The electrochemical cell configuration was the same for these experiments as for the others. The working electrode was palladium black catalyst ink (consisting of only palladium and water) deposited onto a gold plug and allowed to dry. One gram of water was added to 5.6 mg of palladium, and it was placed in the sonicating bath for a few minutes. The catalyst ink (50 uL) was then deposited quickly onto the gold plug, and the plug was completely covered with an even layer of palladium once it dried; only an even layer with full disk coverage was used for experiments. The counter electrode and reference electrodes were the same: palladium mesh and silver-silver chloride, respectively.

The solutions were degassed for at least 30 minutes with UHP argon. At the same time, pure water solutions were also degassed in large flasks that were used for sample transfer. Once degassed, a sulfuric acid solution was used to clean the catalyst surface by several CVs. Then the catalyst was quickly transferred to the adatom solution. In this solution, several CVs were run again, and then a potential was applied for several minutes to reduce the adatom to the surface. Depending on the experiment, the catalyst was then either ready for analysis or CVs were performed prior to analysis. Once the catalyst was ready for analysis, it was quickly transferred from the electrochemical cell to the sample transfer flask while protected with a solution droplet. After five more minutes of degassing, valves were sealed on the transfer flask and it was carried promptly to the Materials Research Laboratory for analysis.

XPS Parameters. The samples were quickly transferred to a sample holder while protected with a water droplet. The sample holder was placed into the XPS instrument and the sample chamber was pumped down immediately. Measurements were performed by Dr. Richard Haasch using a Physical Electronics PHI 5400 system with an Mg Kα X-ray source. For each sample, a spectrum of all kinetic energies was taken, followed by higher resolution spectra in the carbon region (for calibration), the palladium 3d region, and one region of interest for the adatom. Using CasaXPS software, the spectra were calibrated to a carbon binding energy of 285.0 eV.

4.5 Broad-Band Sum Frequency Generation

Electrochemistry apparatus. A custom electrochemical cell was designed very similar to an existing glass and Kel-F cell that had been previously used for electrochemical BB-SFG. The cell constructed for this work used a calcium fluoride window and a 50 um spacer to define the thin layer electrochemistry geometry. The work done here used a platinum polycrystalline electrode of 6 mm diameter as the working electrode. The crystal was polished and/or flame annealed as necessary. The counter electrode was a clean platinum wire. The reference electrode was a silver-silver ion electrode in a solution which consisted of acetonitrile, 0.01 M silver nitrate, and 0.1 M tetrabutylammounium phosphate, and the reference was calibrated to the ferrocene redox couple. [201, 202] The reference potential was found to be +0.535 V vs SHE and repeatable over several experiments in EMIM BF_4. The reference electrode was connected to the cell through a long capillary (~1 m).

Ionic liquid preparation. The ionic liquid was used without additional supporting electrolyte in all experiments. Although the size of the ions and the high viscosity result in lower conductivity than aqueous solutions with support electrolytes, the conductivity is still greater than organic solvents with support electrolytes; the conductivity of the ionic liquid is sufficiently high to perform the voltammetric experiments in this work without the addition of a support electrolyte. [203] The ionic liquid was prepared by heating overnight just above 100 °C under convection and vacuum in order to remove any residual water or dissolved gases. During electrochemical experiments, the ionic liquid was purged with argon (UHP, S.J. Smith) to take baseline measurements assuring a large potential window and the absence of water. For carbon dioxide reduction, the ionic liquid was purged with carbon dioxide (99.99%, S.J. Smith).

Electrochemical methods. The most important initial electrochemistry experiments were performed in the custom electrochemical cell outside the BB-SFG chamber but still under positive argon pressure. These experiments involved numerous fast scan (200 mV s^{-1}) cycles to clean the electrode surface and to ensure quality of the ionic liquid. Typically 40-100 cycles were needed, and the final cycles were always compared with previous electrochemistry to ensure the electrode and ionic liquid were of optimal quality for experiments. This method was performed each morning prior to laser alignment. If the electrode was deemed to be of poor quality it was polished until its quality was sufficient. If the ionic liquid was deemed to be of poor quality, it was removed and new (previously prepared) ionic liquid was added to the cell. Experiments

will not be reliable unless these measures are taken, especially because of the interaction of water with the ionic liquid.

Once the system was electrochemically stable and of high quality, the electrochemical cell was moved to the BB-SFG chamber (Figure 4.5) for laser alignment. At this point, carbon dioxide is bubbled into the electrochemical cell in order to saturate the cell. Once the cell was saturated (~30 minutes), fifteen fast scan (200 mV s^{-1}) potential cycles (~0.5 to -1 V vs SHE) were performed to adsorb enough CO on the surface to finish laser alignment.

Kinetic scans were run in which the electrochemical measurements were performed simultaneously with collection of BB-SFG spectra at the CCD detector. These scans were run within the TLE configuration and therefore were run at slow scan rates, typically 5 mV s^{-1}. Such scans were run in carbon dioxide as well as argon-only liquids in order to determine which peaks should be attributed to the ionic liquid. Spectra were also taken while a specific potential was held without synchronization. Finally, some spectra were taken in which the beams were polarized in order to obtain some preliminary data on the orientation of the ionic liquid at the platinum surface.

Spectroscopic parameters. The BB-SFG apparatus shown in Figure 4.5 was used to probe molecules at the platinum electrode surface in the ionic liquid EMIM BF_4. An IR beam and a visible beam were focused to a 400 μm spot size on the crystal surface with a pulse rate of 10^3 s^{-1}. The timing of these two pulses was staggered by a few

picoseconds in order to deplete the non-resonant contribution to the signal if necessary. The visible beam power was 4.0 μJ while the IR was centered at 6300 or 6500 nm to probe the ionic liquid peaks. The power was reduced to 2.5 μJ when probing the CO and other peaks (at an IR wavelength of 4250 or 4800 nm) in order to prevent laser-assisted desorption of the CO.

4.6 Figures

Figure 4.1. A formic acid fuel cell demonstrated as a power source for a wireless phone.

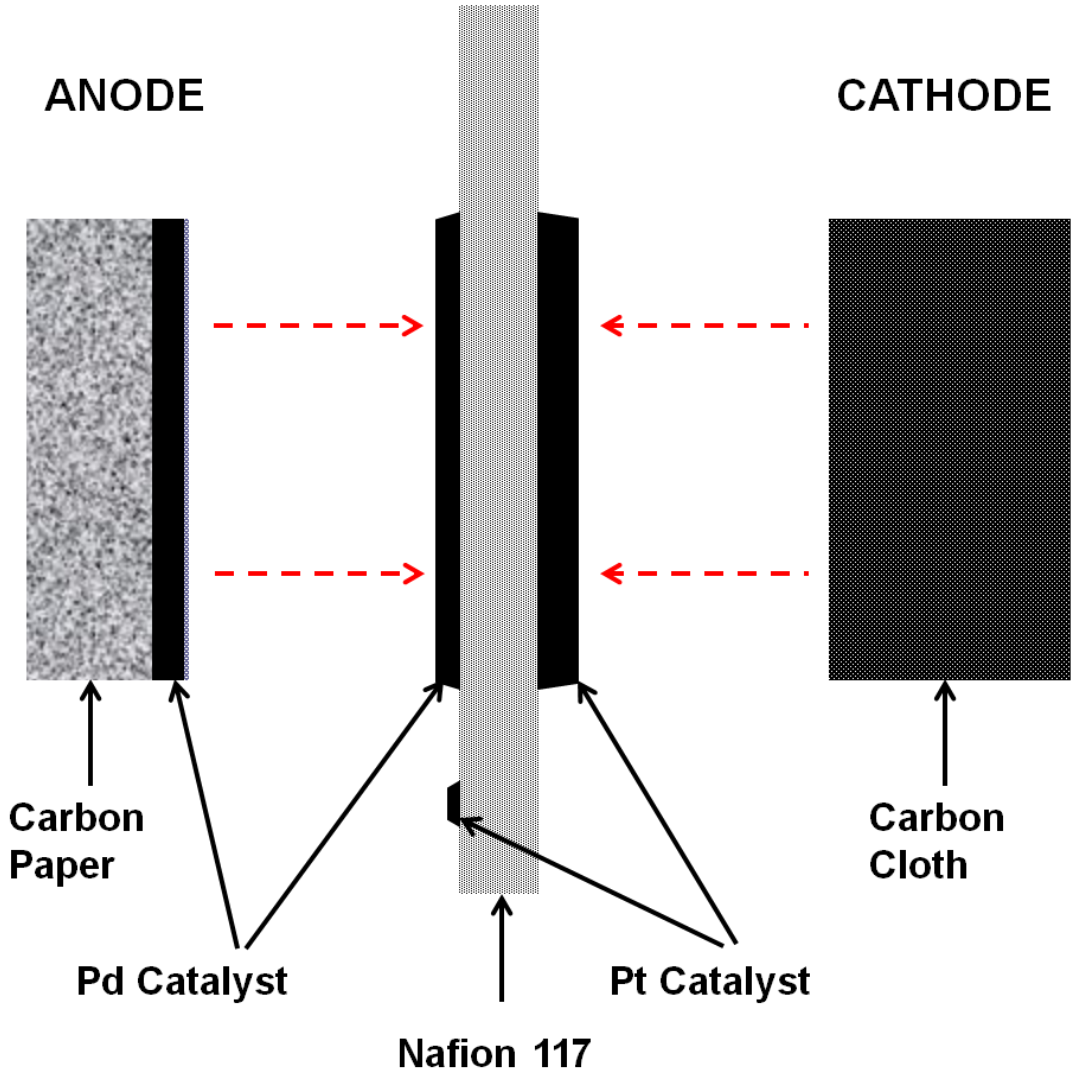

Figure 4.2. A diagram of the membrane electrode assembly showing the location of each catalyst painting on the Nafion® membrane. The small section of platinum catalyst is used as a reference electrode. This figure shows Nafion 117, which was deemed the optimal membrane thickness, but others were tested in this work. The carbon paper/cloth were used as liquid/gas diffusion layers.

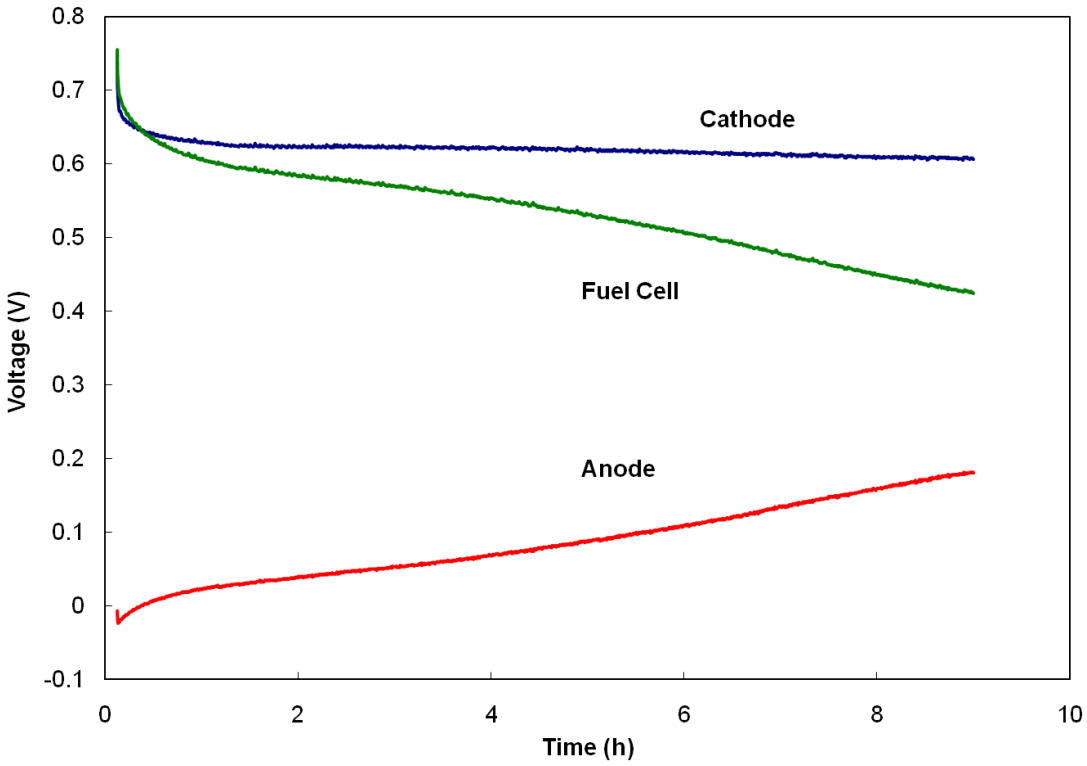

Figure 4.3. Constant current test demonstrating performance of a typical DFAFC operating at ambient temperature with 0.15 mL min^{-1} 10 M formic acid on the anode and 300 sccm air on the cathode. A reference electrode is employed to determine the anode and cathode potentials and the voltage of the fuel cell. The cathode is stable, while the fuel cell performance loss can be attributed primarily to the anode overpotential due to CO buildup on the catalyst surface. [33]

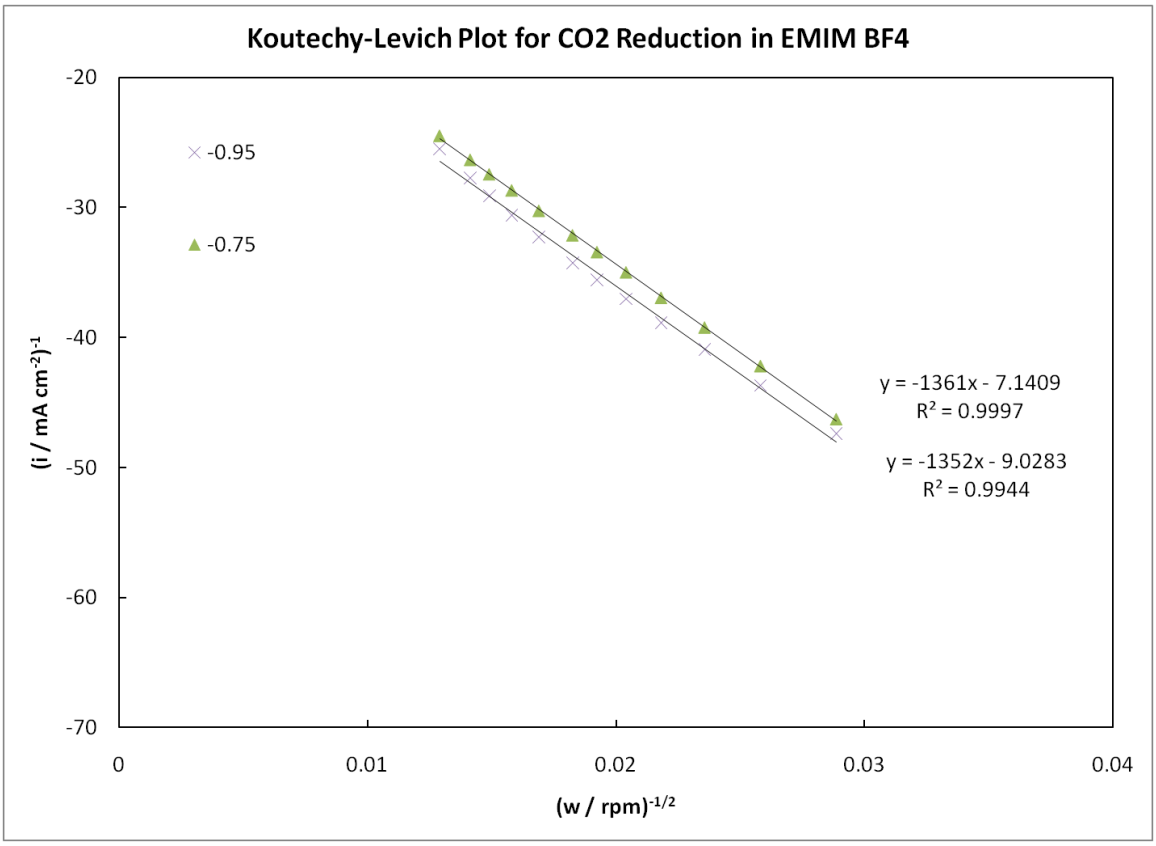

Figure 4.4. Koutechy-Levich plot for CO_2 reduction in EMIM BF_4 saturated with CO_2. The plot is linear from rotation rates of ~1000 to 6000 rpm.

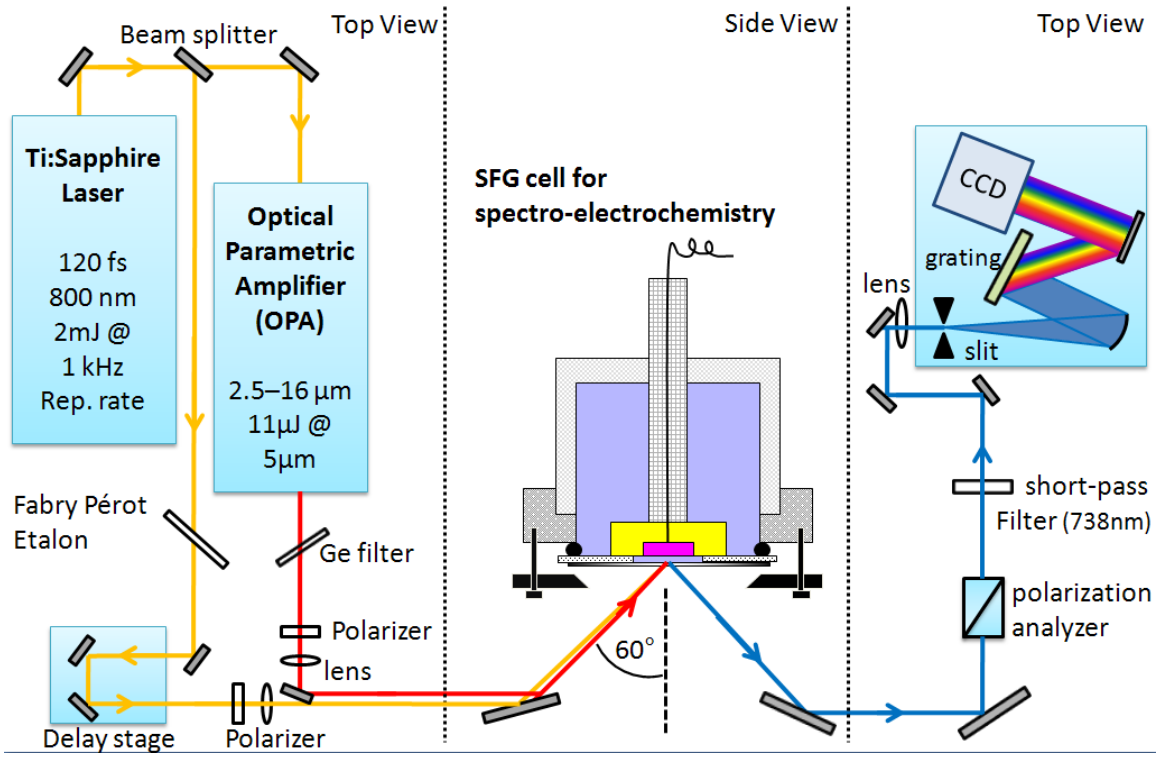

Figure 4.5. The spectroelectrochemical setup that is used for the BB-SFG work reported in this work; the laser is setup in the research lab of Dr. Dana Dlott at the University of Illinois. The chamber in which the electrochemical cell is placed is under positive argon pressure. The yellow beam, which passes through the delay stage, is the IR beam. The red beam, which passes through the OPA is the visible beam. As they overlap on the surface, the sum frequency beam, in blue, exits the electrochemical cell and is detected at the CCD. Figure courtesy Bjoern Braunschweig and is used with permission.

Chapter 5: The Influence of Solution pH on Rates of an Electrocatalytic Reaction: Formic Acid Electrooxidation on Platinum and Palladium

This chapter is adapted from a paper published in Electrochimica Acta in 2009 by Haan, J.L., and Masel, R.I., and used with permission. [204]

5.1 Introduction

The direct formic acid fuel cell (DFAFC) demonstrates promise to meet the demand of high power density off the electrical grid for portable electronics such as wireless phones and laptop computers. [24, 25, 30, 31, 62-65, 83, 95, 96, 98, 205-229] The direct formic acid fuel cell (DFAFC) is capable of power comparable to a battery, and it performs better at ambient temperature than the direct methanol fuel cell (DMFC), in which significant amounts of fuel cross through the membrane, and the fuel can cause blindness in humans. [28-31] Stronger ambient performance and lower crossover rates allow the DFAFC to produce higher energy density, even though its theoretical energy density is lower than that of the DMFC.

The overall reaction of formic acid oxidation occurs as the following reaction on palladium (at a theoretical standard potential of -0.220 V) [230]:

$$HCOOH \rightarrow CO_2 + 2\,H^+ + 2\,e^- \qquad (5.1)$$

Initial work on the DFAFC anode catalyst involved the use of platinum and its alloys. [54, 55] However, formic acid oxidation on platinum proceeds primarily through an indirect pathway that includes a strongly-bonded CO intermediate [45, 49, 50, 52, 53]:

$$HCOOH + Pt^0 \rightarrow Pt\text{-}CO + H_2O \quad (5.2)$$

$$H_2O + Pt^0 \rightarrow Pt\text{-}OH + H^+ + e^- \quad (5.3)$$

$$Pt\text{-}CO + Pt\text{-}OH \rightarrow CO_2 + 2\,Pt^0 + H^+ + e^- \quad (5.4)$$

Significant amounts of CO quickly build up on the catalyst surface, blocking reaction sites. Therefore, platinum is not a useful anode catalyst for the DFAFC. A more direct pathway is followed when palladium is used to catalyze the oxidation of formic acid through a reactive intermediate, *X*, preventing buildup of CO on the catalyst surface [45, 49, 60, 61]:

$$HCOOH \rightarrow X \rightarrow CO_2 + 2\,H^+ + 2\,e^- \quad (5.5)$$

Indeed, palladium has been shown to provide better current density when used as the anode catalyst for the DFAFC. Experimentally, we do not observe any CO buildup when we oxidize 1 M formic acid in an electrochemical cell. However, the commercial fuel cells use 22-24M formic acid. Experimentally, we have found that CO slowly accumulates on the anodes of the commercial fuel cells running on 22 M formic acid. In a previous patent application we found that purification of the formic acid, to remove methyl formate and formic anhydride (HCOOHCO) impurities in the commercial formic acid led to a substantial reduction in the rate of CO formation. [65] However, we were never able to completely suppress the CO buildup, and so the commercial fuel cells need to be periodically regenerated. [25, 31, 63, 64]

The object of this paper was to see if an increase in the pH of the solution could lead to either a reduction in the rate of CO formation or an increase in the rate of CO

removal. According to Marcus' theory, changes in the free energy driving force for reaction should change the rate of an electrochemical reaction, even under conditions where the surface composition is constant. [231-234] One can change the free energy for an electrochemical reaction by changing the pH in solution, but so far no one has examined the effect of pH, under conditions where the effect of other variables is constant. For example, previous investigators have compared formic acid electrooxidation under acidic, neutral and basic conditions [235-239], but these measurements were done under conditions where the pH changes lead to substantial changes in hydroxyl or proton concentration on the surface. The objective of the work here was to see if solution pH would change the rate under conditions where the proton and hydroxyl are small, so that the effects of changes in the free energy of the reaction can be isolated.

In particular, our measurements have been done at pH from 1-5 and potentials where adsorption of hydroxyls is negligible. At a pH of 1-5, hydroxyls do not substantially adsorb on platinum or palladium at potentials below about 0.5 V with respect to a standard hydrogen electrode (SHE). [44, 240] The hydrogen concentration is negligible above about 0.3 V vs. SHE. [44, 240] Thus, if we do our measurements at a potential between 0.3 and 0.5 V vs. SHE and a pH of 1-5, one can make measurements without substantially changing the hydrogen and hydroxyl concentration on the electrocatalyst. With careful experiments, one can do the experiment so the counter ion concentration does not change. Further Reaction 5.1 is almost irreversible. [241] Thus, if there are changes in the rate with acidic pH at potentials between 0.3 and 0.5 V vs.

SHE, they must be associated with a change in the driving force for the reaction in solution and not a buildup of hydroxyl species on the surface.

The powerful effect of CO in the oxidation of formic acid and methanol has resulted in numerous studies of CO bound to catalyst surfaces. The oxidation of CO to CO_2 was observed to occur more easily in alkaline solution (pH 11) than in acidic solution (pH 1) in which strong surface binding is present. [242] The presence of OH bound to platinum defect sites was found to aid in CO oxidation in alkaline media, but only at high CO coverage. [243] Detailed work on the oxidation of CO on palladium and platinum in solutions of weakly acidic pH has not been reported previously.

In this study, we present the effects of pH in weakly acidic solution on the oxidation of formic acid and CO on palladium and platinum black catalysts.

5.2 Experimental

Reagents. High surface area palladium black (Aldrich) and high surface area, Johnson Mathey platinum black (Alfa Aesar) unsupported nanoparticles were used for all electrochemical measurements. All solutions were made in 18MΩ Milli-Q water. Electrolyte solutions containing perchlorate, sulfate, or phosphate at 0.1 M concentration were made by diluting 70% HClO4 or 95% H2SO4 (both GFS, double distilled) or 85% H3PO4 (Aldrich). Formic acid solutions were initially made by diluting 50% HCOOH (Fluka, HPLC grade) to 1 M in 0.1 M supporting electrolyte (either perchlorate, sulfate, or phosphate). The pH was then adjusted by titration with sodium hydroxide. Finally, the sodium ion concentration was adjusted using sodium perchlorate to remain constant

in all solutions. Additional experiments were performed with excess amounts of sodium perchlorate to create nearly constant ionic strength. In addition, some initial experiments were performed without adjustment of sodium ion concentration via sodium perchlorate. In either case, the current-potential trends were similar. In preparation for each electrochemical experiment, each solution was thoroughly degassed using ultra high purity argon (S.J. Smith). Carbon monoxide (S.J. Smith) was used for CO adsorption experiments. Hydrogen (S.J. Smith) was used for reference electrode calibration.

Electrochemical Methods. A standard three electrode electrochemical cell with a Solartron potentiostat (SI 1287) was used for electrochemical measurements. Catalyst ink (containing palladium or platinum black mixed with water via sonication) was applied to the tip of a glassy carbon electrode and dried for use as the working electrode. The working electrode was rotated at 6000 rpm (Princeton Applied Research, Model 616) for current-potential experiments. Experiments were carried out at lower rotations, but 6000 rpm was chosen to minimize the noise and maximize removal of carbon dioxide product in constant potential experiments due to the high currents found at elevated pH. Both hydrogen and CO oxidation peaks were used to determine the electrochemical surface area of the catalyst. [39-41] Platinized platinum gauze (Alfa Aesar, 52 mesh woven from 0.1 mm diameter wire, 99.9%) was used for the counter electrode. An Ag/AgCl/sat'd KCl reference electrode (BAS) was separated from the working electrode via a Luggin capillary. The reference was calibrated by bubbling hydrogen gas over the platinum gauze electrode. The junction potentials between solution electrolyte and KCl solution were calculated for various pH using the Henderson equation, and were found to

be no more than 2 mV. All potentials reference the standard hydrogen electrode, unless otherwise noted.

Current-potential measurements were obtained using formic acid with both perchlorate and sulfate electrolyte. Phosphate electrolyte was also studied and demonstrated similar behavior. The catalyst surface was stabilized by several sweeps of cyclic voltammetry in base electrolyte. Constant potential measurements were taken in uniform steps at various potentials above the open circuit potential (OCP). Data is reported after 2 min of oxidation. Studies also were performed by holding the potential for as long as 60 min, and similar current-potential trends were observed.

For CO stripping voltammetry, the catalyst surface was first stabilized by cyclic voltammetry in 0.1 M electrolyte. Then CO was bubbled into the 0.1 M electrolyte solution (at pH 1) to adsorb it to the catalyst surface at 57 mV vs. RHE for 60 minutes. Finally, the adsorbed CO was oxidized by cyclic voltammetry in degassed electrolyte solutions with pH ranging from 1 to 10.

5.3 Results

Current-potential measurements. Figure 5.1 shows how the reaction rate on palladium varies with pH for pH's between 1 and 5. One finds that the electrooxidation current varies with both the pH and the applied potential. Generally the rate (i.e. the current) increases exponentially with the applied voltage as expected from the Butler-Vollmer equation. Figure 5.1 also shows that the rate increases with increasing pH, i.e. if one holds the potential constant at, for example 0.29 V, the current increases from 0.12

to 0.53 mA cm^{-2} as the pH increases from 1 to 5. Interpolation of the same experiment at 0.22 V on platinum (Figure 5.2) shows that the current increases from 0.005 to 0.17 mA cm^{-2} as the pH increases from 1 to 5. Each data set can also be interpolated at constant current, for example, 0.1 mA cm^{-2}. On palladium, the potential at which this current was reached changed by 56 mV per pH, while on platinum the potential shifted 62 mV per pH.

Figure 5.3 shows that there is no correlation between the increased reaction rate and the increased formate ion concentration as pH increases, which agrees with Adzic, et al. [235] The formate ion concentration increases rapidly between pH 3 and 4, while the increase in reaction rate remains steady.

These experiments were done by varying the pH, by varying the ratio of perchloric acid and sodium perchlorate keeping the sodium concentration constant. We show data in Figure 5.1 that is taken after 2 minutes at constant potential. CO slowly builds up during formic acid electrooxidation on palladium and we wanted to prevent the CO from confounding the effects. However, we have also plotted data taken by holding the potential constant for 20 minutes or 1 hour and see similar trends.

These experiments were repeated in sulfate solutions with the same parameters, and the data is shown in Figures 5.4 and 5.5. We observe some difference in the actual values when compared with perchlorate electrolyte, but the trends are very similar. The

well-known adsorption of sulfates is affecting the current values but not the observed trends.

The current density was also measured from pH 6 through 10, but no significant deviation from the current density measured at 5 was observed. Therefore, it was determined that the current density of interest for this study lied between pH 1 and 5.

Long-term current measurements. Figure 5.6 demonstrates the long-term stability of the pH effects. At pH 1, near the pH of the anode in an operating fuel cell, we observe that the performance at 40 h is only 3.0% that of the performance at 1 h. For this reason, frequent regeneration steps are necessary during fuel cell operation. However, at pH 3, we observe that performance at 40 h is 25% that of performance at 1 h. Although this would not eliminate the need for regeneration in the fuel cell, it could greatly reduce the frequency. For example, it takes over 15 h for the oxidation current at pH 3 to fall below the current observed after 1 h at pH 1. Finally, it can be noted that the oxidation current in pH 3 is ~3x greater than in pH 1 after 1 h, but it is ~20x greater after 40 h because the current decay with time is not as rapid.

The oxidation of CO. The significant enhancement in steady state current, particularly on the Pt catalyst that is more influenced by CO, leads to the question of influence of pH on the oxidation of CO. The cyclic voltammogram in Figure 5.7 represents the difference in surface chemistry of Pd in sulfate electrolyte at pH 1 and 2. The regions for hydrogen adsorption and desorption, surface oxidation and reduction, and

CO oxidation are all shown. They each shift approximately 59 mV per pH, demonstrating the expected Nernstian behavior. The most interesting of these shifts is that of the CO oxidation peak, which the focus of this portion of the work is.

The CO oxidation peak potential was observed on palladium and platinum in each electrolyte as shown in Figure 5.8. Phosphate electrolyte was also used during this portion of the experiment in order to create a buffer system that enabled the study of neutral pH values where the data in sulfate and perchlorate electrolytes became unreliable because the pH was difficult to control. The peak position of the CO oxidation on palladium was observed to shift by ~57 mV per pH within and between the buffer regions of pH 1 to 3 for each electrolyte, and 6 to 8 in phosphate. Reliable measurements beyond pH 3 were not possible in sulfate or perchlorate. The peak position of CO oxidation on platinum followed a trend somewhat similar to that of Pd, but the peak position decreased by only ~36 mV per pH as the pH was increased from 1 to 3. As with the palladium, reliable measurements were not made at higher pH with sulfate or perchlorate electrolytes.

Open circuit potential in formic acid. The open circuit potential (OCP) is a measure of the equilibrium state of the reaction where no net current is passing. For formic acid oxidation this should theoretically occur at -0.22 V, the standard reduction potential, E^o. As the pH is raised and the hydrogen ion concentration decreases, the open circuit potential follows the Nernst equation:

$$E = E^o - \frac{0.059}{n} \log \frac{[red]}{[ox]} \qquad (5.6)$$

where *n* is the number of electrons transferred and *red* and *ox* are the concentration of species that are reduced or oxidized, respectively, during the reaction. When the formic acid pH is changed, the only species in Equation 5.1 to change concentration is the hydrogen ion, which is an oxidized species, and therefore appears in the denominator of the logarithmic term in Equation 5.6. Therefore, an increase of one pH unit will lower *E* by 0.059 V for the two electron oxidation of formic acid. The theoretical and measured OCPs for several pH are shown in Table 5.1.

5.4 Discussion

The effect of solution pH on the electrochemical driving force for formic acid electrooxidation. We have measured the oxidation of formic acid on both platinum and palladium in solutions in which the pH ranges from 1 to 5. On palladium, formic acid oxidation proceeds via a direct mechanism, where Reaction 5.1 is rate determining. [25, 30, 55, 61, 63, 241] On platinum, though, the reaction goes through a CO intermediate (Equation 5.2). [25, 30, 55, 61, 63, 241] CO oxidation quickly becomes rate determining as it poisons the surface in a matter of seconds. We also note that perchlorate does not adsorb strongly on platinum under any of the conditions of our experiment, and we explored the effect of sodium and have found that it does not substantially change the rate.

Notice that changes in pH change the rate of Reaction 5.1 even between 0.3 and 0.5 V where neither hydroxyls nor protons strongly adsorb on platinum or palladium. For example, at a potential of 0.3 V, the current produced by Reaction 5.1 on palladium changes by a factor of 3 when the pH is increased from 1 to 5, as shown in Figure 5.1.

The current is a direct measure of the rate. Therefore we can conclude that the rate changes with changing pH even under conditions where neither hydrogen nor hydroxyls adsorb strongly on the surface. Clearly, the properties of the solution are changing the rate under conditions where the composition on the catalyst surface is not changing substantially.

Next we wished to check a hypothesis about how that occurs. Our hypothesis is that a hydronium ion or related species is produced during the rate determining step in Reaction 5.1. The hydronium could be on the surface[244] or in the solution near the surface. The changes in pH change the free energy driving force for hydronium formation, and that in turn changes the rate. Note that free energy of Reaction 5.1 in solution changes with changing pH by 5.7kJ/mol/pH per electron. (Note 0.059V/pH×F = 5.7 kJ/mol/pH, where F is faraday's constant) and so if we are producing a hydronium, the rate should change.

One can quantify this idea using Marcus theory of electrochemical reactions. [231-234] According to the Marcus model, the rate of reaction changes as the free energy of the reaction changes. Thus, according to Marcus's model, the rate of reaction 5.1 should increase as the pH increases.

In order to test that we replotted the data in Figures 5.1 and 5.2 as a function of the electrochemical driving force for the reaction in solution, η, where η is given by

$$\eta = V + \alpha(\Delta G_1)/F \qquad (5.7)$$

In Equation 5.6, V is the applied voltage with respect to a standard hydrogen electrode, ΔG_1 is the free energy of Reaction 5.1 relative to that of a standard hydrogen electrode as a function of pH and α is the transfer coefficient. We expected the transfer coefficient to be 1 for Reaction 5.1, since the heat of reaction is more than 4 times the intrinsic barrier. [245, 246]

Figure 5.9 shows the results. Data for platinum is also shown. Notice all of the curves for each metal seem to collapse to a single line, independent of pH. For example, the voltage to achieve a current of 0.29 mA cm^{-2} on palladium varies by 0.41 V with pH in Figure 5.1 and 0.023 V in Figure 5.9. Thus, it appears that the variations with pH seen in Figure 5.1 are mainly associated with a change in the free energy driving force for Reaction 5.1 in solution.

We have also replotted the experiments from Figures 5.4 and 5.5 in a sulfuric acid electrolyte to insure that anion affects are not confounding the effects. Figure 5.10 shows the results. There is some anion poisoning with sulfuric acid, and that produces some extra variations at high potential. Still the general trends are the same. There are wide variations in rate with changing pH, but all of the curves collapse to a single line when plotted as a function of the electrochemical driving force for reaction. Thus, the presence of counterions in the solution is not affecting the result.

These results demonstrate that changes in pH can have a large effect on electrochemical reactions even when the reactions are largely irreversible, and there is no

substantial adsorption of hydrogen or hydroxyls on the surface of the electrocatalyst. The long term effects (Figure 5.6) of this rate enhancement demonstrate that the pH effect is not transient; rather it is stronger over time.

The oxidation of CO. The oxidation potential of CO was found to decrease on palladium by ~57 mV per pH (Figure 5.8), which was approximately the same amount as the decrease in OCP. This behavior has not been reported before, but can be explained by application of the Nernst equation to Equation 5.4 for removal of CO from noble metal surface. The impact of this confirmation is that the strongly-bound CO can be removed from a poisoned catalyst surface at significantly lower potentials when a solution of higher pH is used. Decrease of this oxidation potential could reduce the need for the regeneration step during fuel cell operation.

The open circuit potential in formic acid. The theoretical and measured OCPs for several pH shown in Table 5.1 to decrease by about 59 mV pH^{-1} are in agreement with literature data for platinized platinum electrode in 1 M HCOOH. [230] The significance of this observation is underscored by the difference in current density with respect to pH as observed in Figures 5.1, 5.2, 5.4, and 5.5 compared with the current density in Figures 5.9 and 5.10. The latter two figures demonstrate clearly that there is no change to the overpotential of the reaction when the pH is changed. While the pH does not affect the amount of overpotential required to obtain a certain current density, it significantly affects the value of the onset potential for formic acid oxidation, the OCP. Therefore, the large enhancement to oxidation current can also be viewed as a significant

decrease in potential that is required to achieve the same current. This has obvious implications for a fuel cell, in which a lower oxidation potential would theoretically produce a larger overall cell voltage.

5.5 Conclusion

This study demonstrates the strong effect of pH on formic acid oxidation on palladium and platinum catalyst. Increasing the pH of weakly acidic solutions decreases the reaction potential with respect to SHE, and it enhances the current density at a given potential. The current density on platinum is enhanced thirty fold at 0.22 V, while a lesser, four-fold enhancement is observed on palladium at 0.29 V. The catalyst which is more typically poisoned, platinum, exhibits the greatest enhancement by change in pH, due in part to the negative shift of the CO oxidation potential with increased pH.

We have demonstrated that pH changes can have a large effect on electrochemical reactions even when the reactions are largely irreversible and there is no substantial adsorption of hydrogen and hydroxyls on the electrocatalyst surface. These results can be explained by the Marcus model of electrode kinetics.

5.6 Acknowledgements

This work was supported by the Army Research Office Under Contract W911NF-05-C-0110 and Defense Advanced Research Projects Agency (DARPA) under grant DST 2007-0299513- 000-1. Qian Chen assisted in the initial stages of the research.

5.7 Tables and Figures

Table 5.1. Open circuit potential for formic acid oxidation on platinum and palladium black in 1 M HCOOH + 0.1 H_2SO_4 and 1 M HCOOH + 0.1 $HClO_4$ solutions at various pH.

pH	$[H^+]$	E_{theo} (V)	H_2SO_4 electrolyte		$HClO_4$ electrolyte	
			$E_{meas,Pt}$ (V)	$E_{meas,Pd}$ (V)	$E_{meas,Pt}$ (V)	$E_{meas,Pd}$ (V)
1	0.1	-0.279	0.041	0.016	0.015	0.003
2	0.01	-0.338	-0.036	-0.053	-0.046	-0.063
3	0.001	-0.397	-0.117	-0.150	-0.107	-0.129
4	0.0001	-0.456	-0.160	-0.195	-0.171	-0.197
5	0.00001	-0.516	-0.217	-0.248	-0.232	-0.271

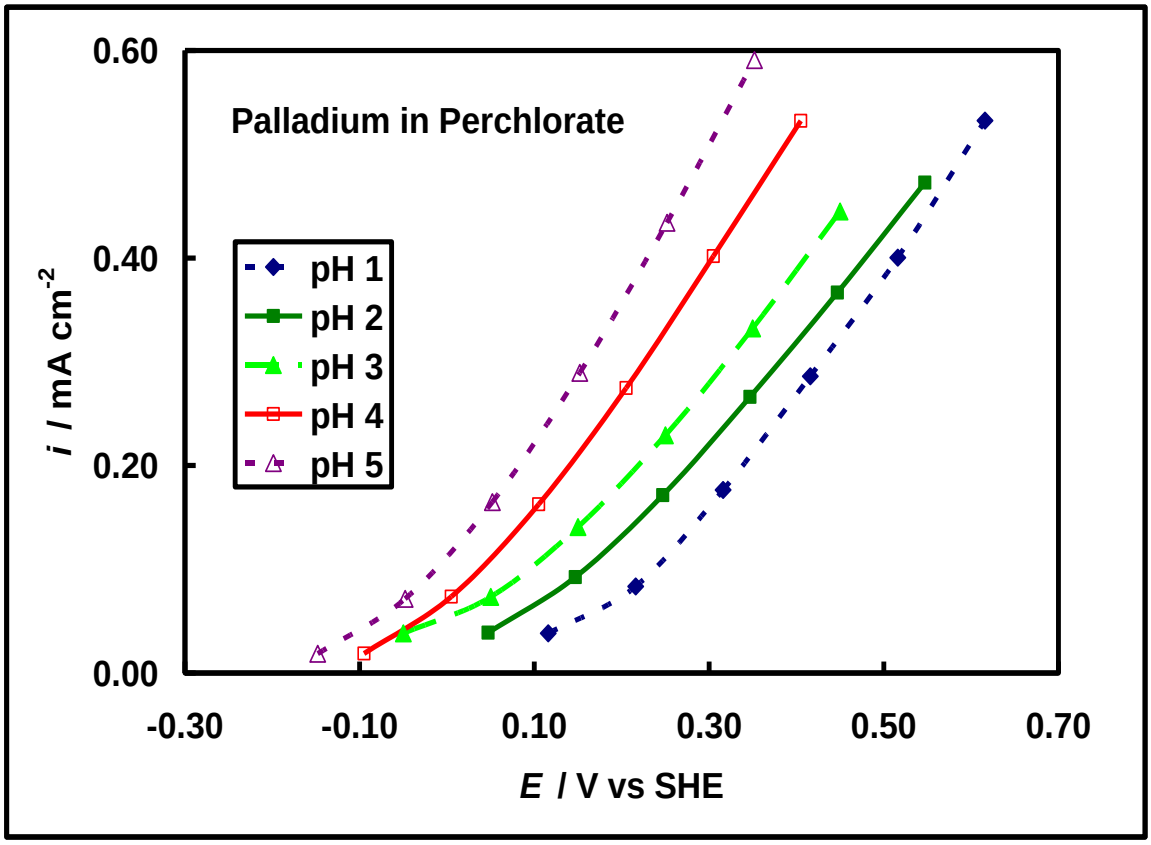

Figure 5.1. The formic acid oxidation current per unit surface area on Johnson Mathey palladium black in 1 M HCOOH plotted as a function of the potential vs a standard hydrogen electrode Each data point is taken by holding the potential constant and measuring the current after after 2 min of oxidation with a rotating disk electrode at 6000 rpm. The solution contained a mixture of perchloric acid and sodium perchlorate to control the pH and keep the sodium concentration constant.

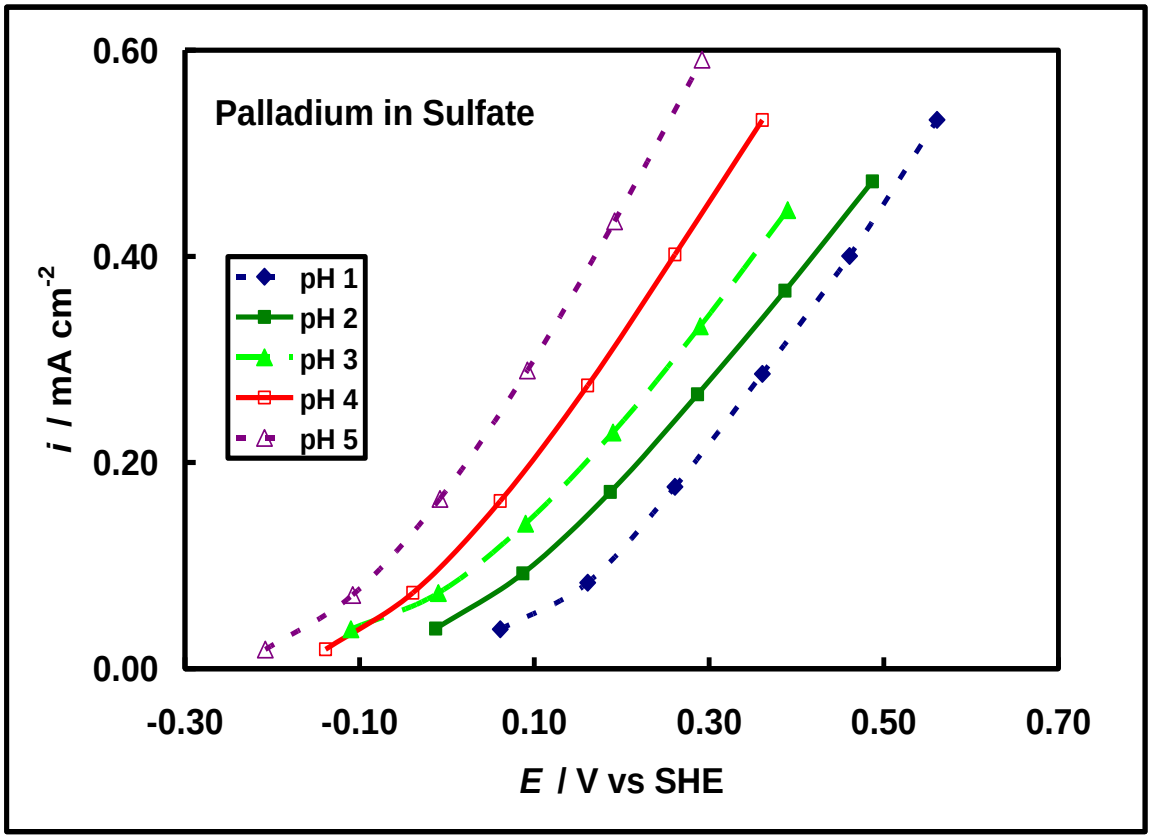

Figure 5.2. The same experiment as Figure 1, but in a solution that contained a mixture of sulfuric acid and sodium sulfate electrolyte.

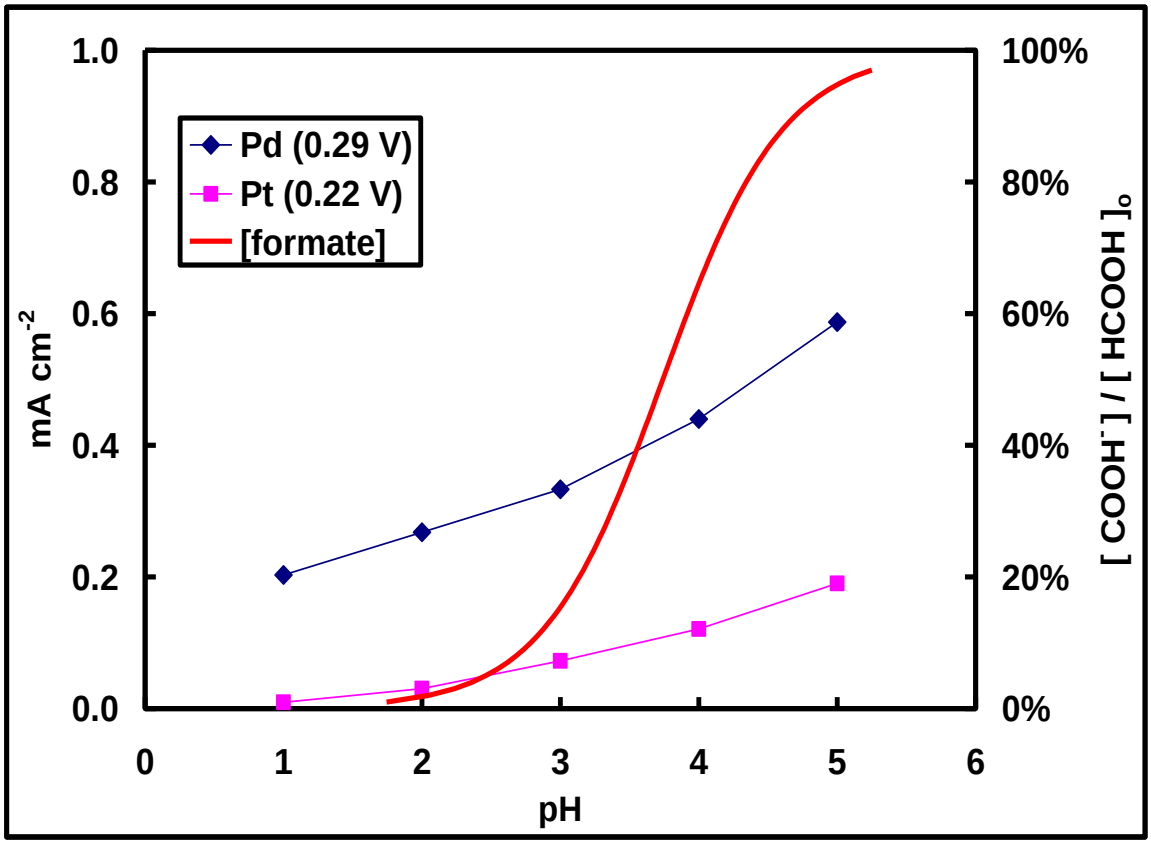

Figure 5.3. The formate concentration shows s-like behavior with a very rapid change between pH of 3 and 4. In contrast, the reaction rate data shows a smooth, nearly linear change. If the increase in reaction rate was due to formate ion formation there should be a large increase in the current as pH is raised from 3 to 4, but that is not observed. Therefore, the changes in formate ion concentration are not responsible for the changes in reaction rate.

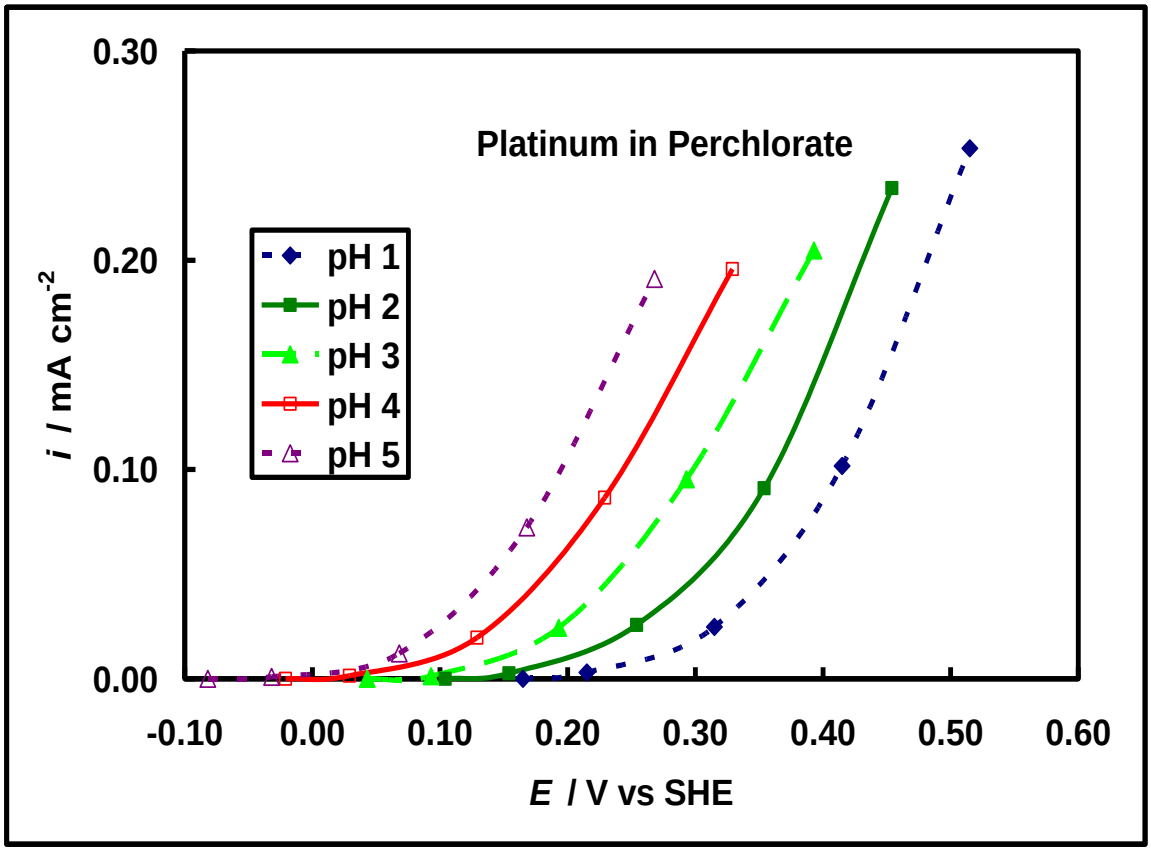

Figure 5.4. The same experiment as Figure 1, but on platinum black catalyst in a solution containing a mixture of perchloric acid and sodium perchlorate electrolyte.

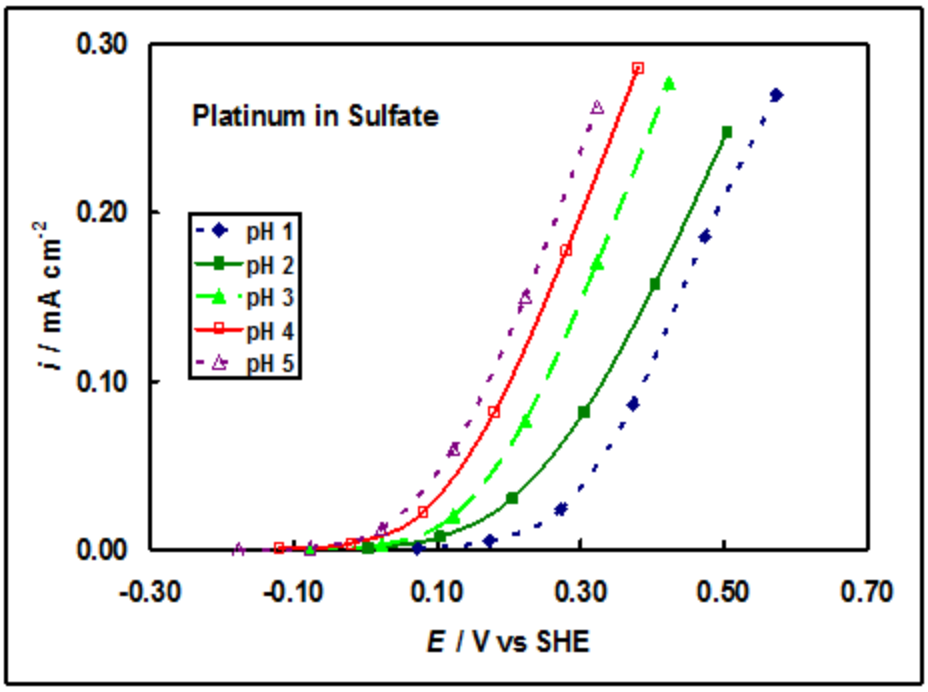

Figure 5.5. The same experiment as Figure 4, but in a solution containing a mixture of sulfuric acid and sodium sulfate electrolyte.

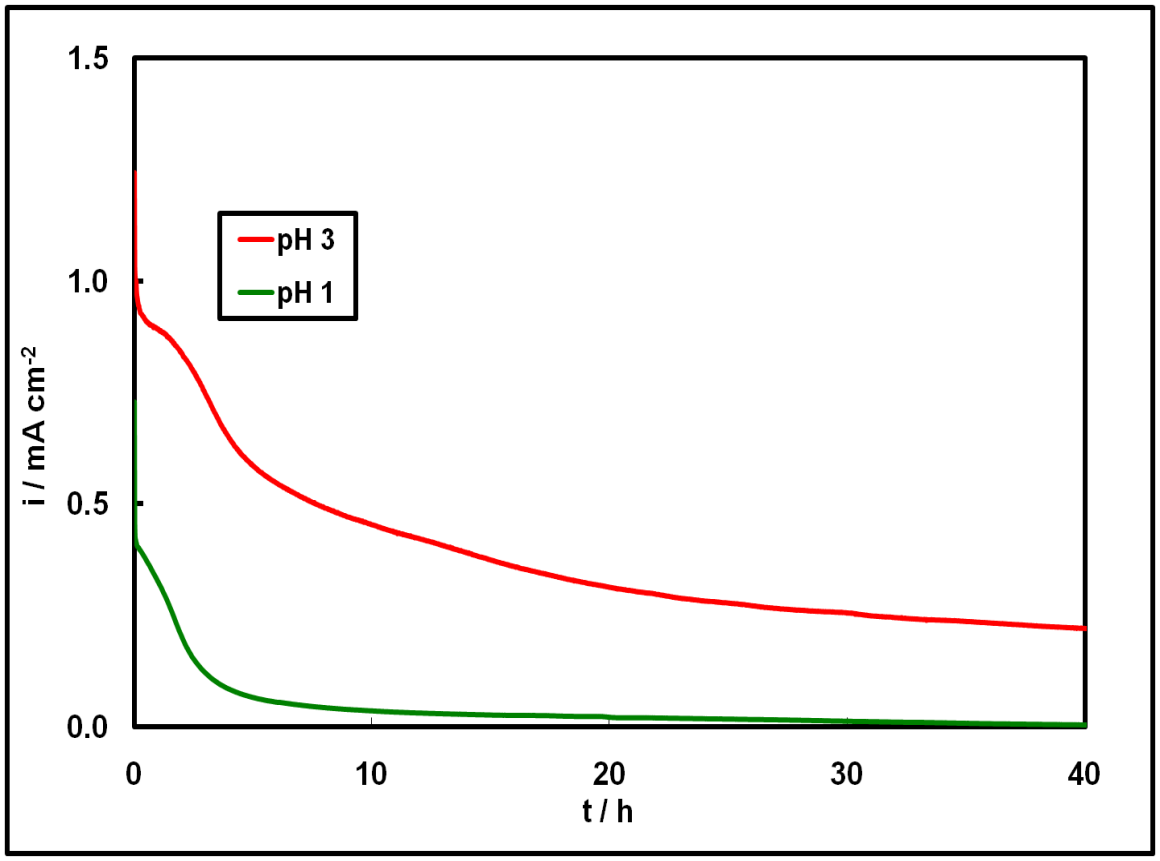

Figure 5.6. Formic acid oxidation current measured for 40 h at 0.3 V vs SHE on palladium black catalyst in a solution of 1.0 M HCOOH and 0.1 M mixture of perchloric acid and sodium perchlorate at pH of 1 and 3. The current in pH 3 does not decay nearly as strongly as the current in pH 1.

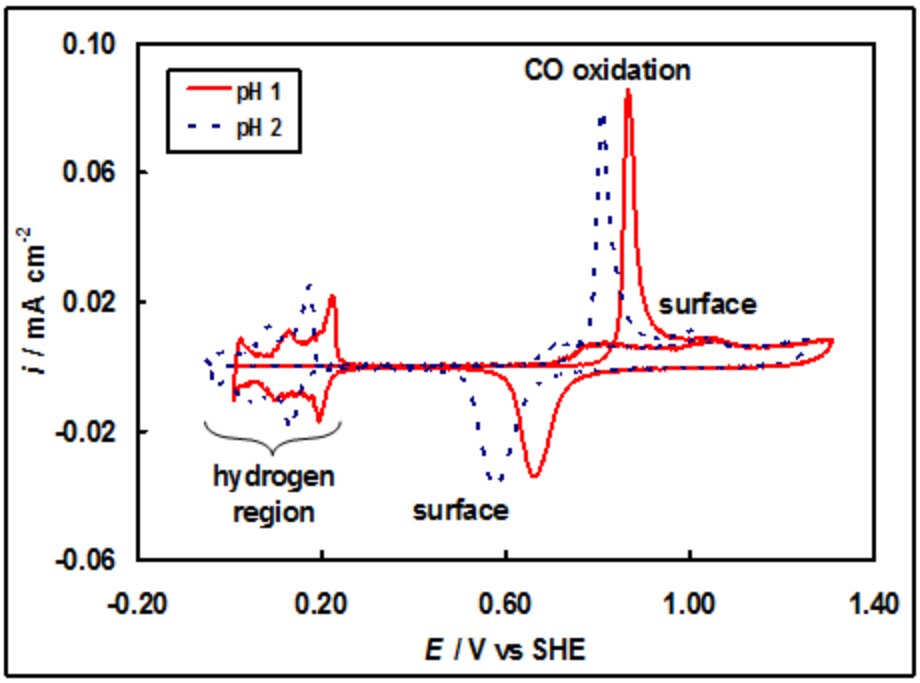

Figure 5.7. Cyclic voltammogram of palladium black in perchloric acid solution with sodium perchlorate added such that pH 1 and 2 was established. The peaks for hydrogen underpotential deposition, oxide formation and removal, and CO oxidation shift negatively by approximately 59 mV per pH, in accordance with the Nernst equation.

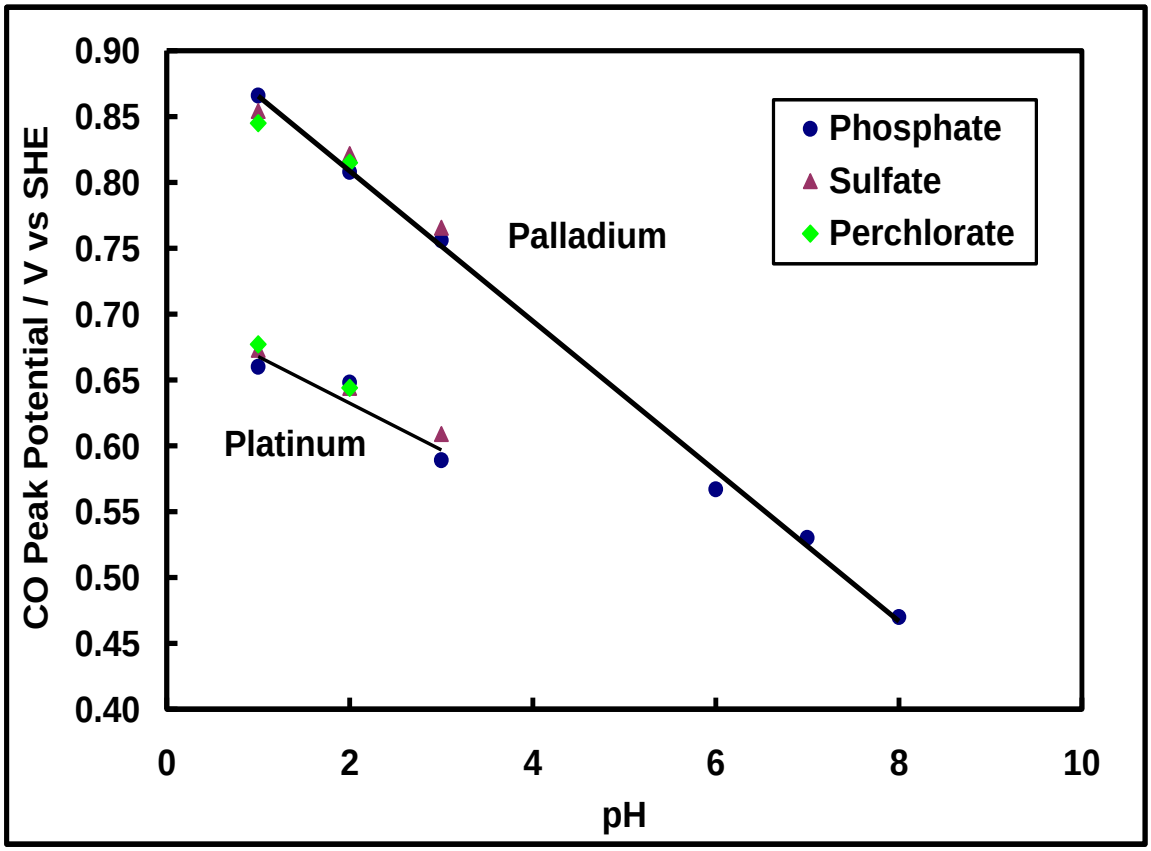

Figure 5.8. The position of the CO oxidation peak on palladium and platinum is shown as a function of pH in the buffer regions of each electrolyte. On palladium, the peaks shift at ~57 mV per pH, close to the Nernstian shift. However, on platinum the peak shift is closer to ~30 mV per pH. Again, the electrolyte was a combination of the acid and the salt, in order to target the desired pH.

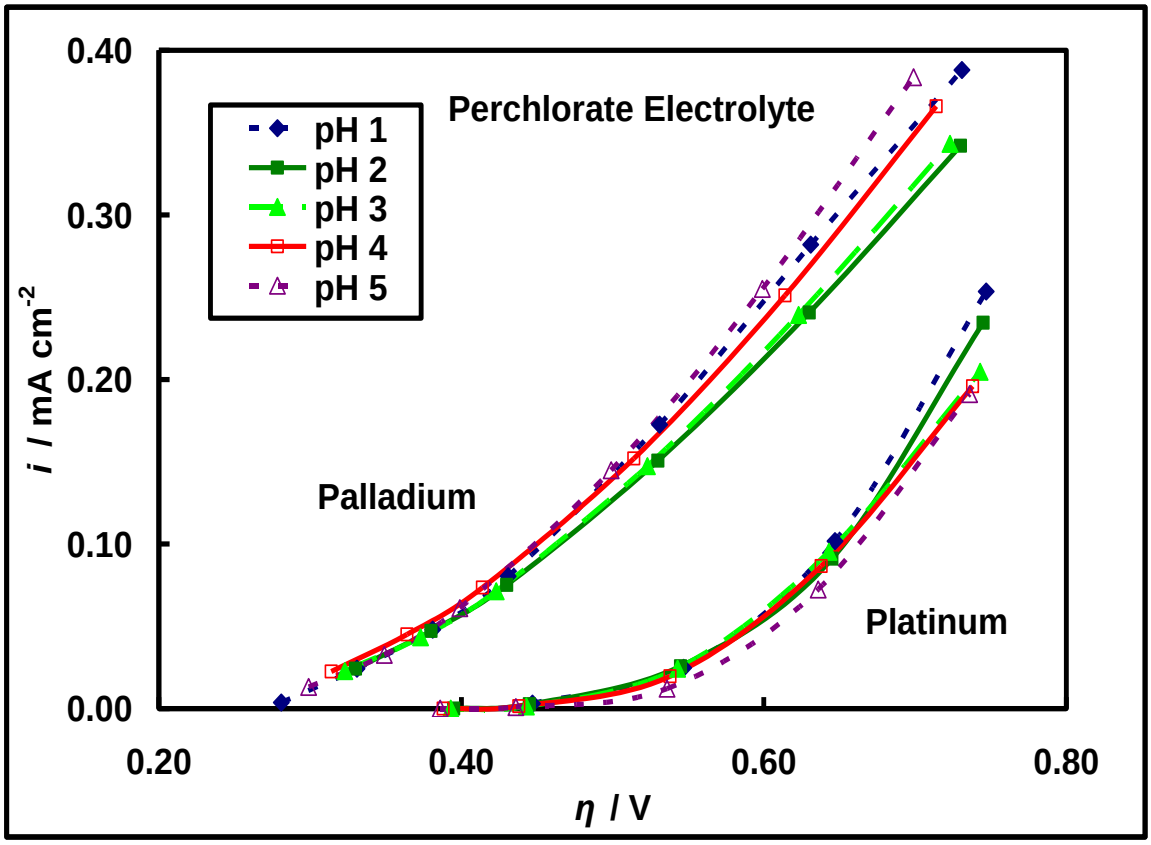

Figure 5.9. A replot of the data from Figure 1 as a function of the electrochemical driving force, η, with α=1. Similar data with a platinum catalyst is also shown, which is replotted from Figure 4. Notice that all of the curves for each metal collapse to a single line independent of pH.

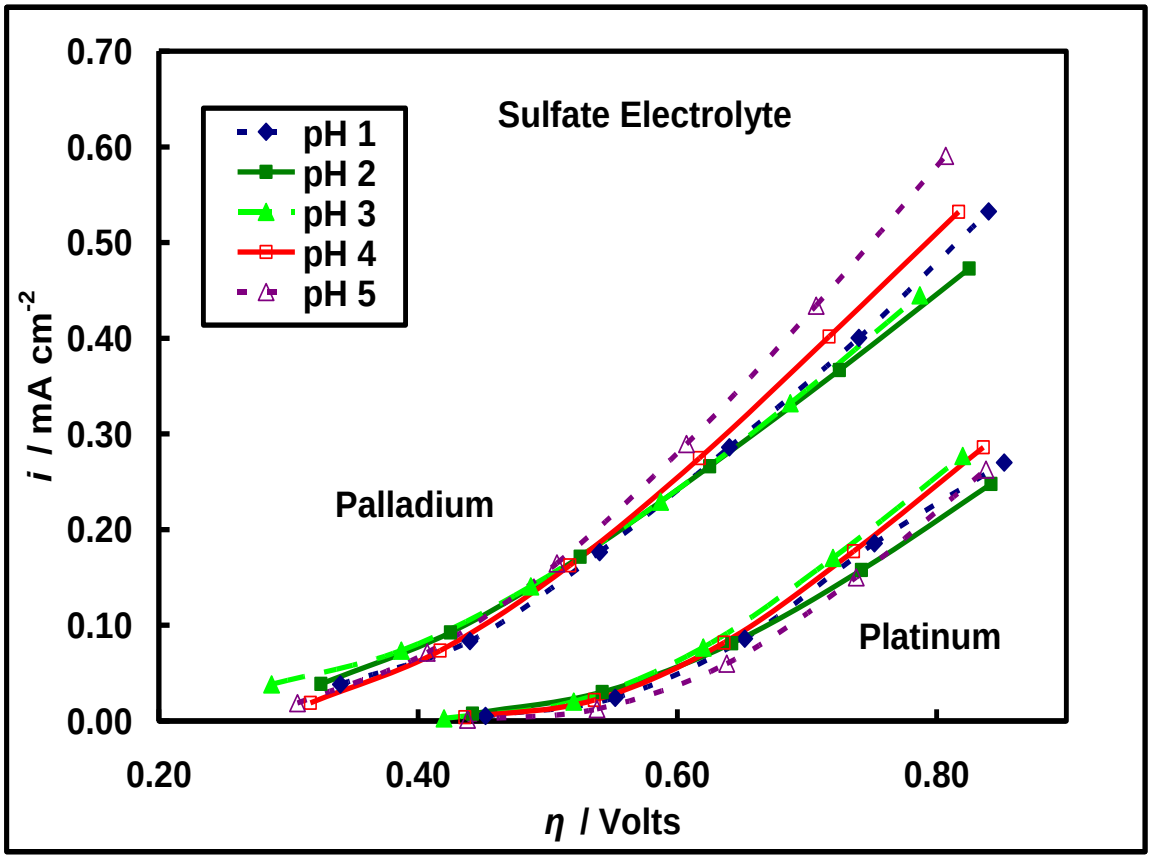

Figure 5.10. A replot of the data from Figure 2 as a function of the electrochemical driving force, η, with α=1. Similar data with a platinum catalyst is also shown, which is replotted from Figure 5. Notice that all of the curves for each metal collapse to a single line independent of pH.

Chapter 6: Performance of the Direct Formic Acid Fuel Cell with Electrochemically Modified Palladium-Antimony Anode Catalyst

This chapter is adapted from a paper published in Electrochimica Acta in 2010 by Haan, J.L., Stafford, K.M., Morgan, R.D., and Masel, R.I., and is used with permission. [33]

6.1 Introduction

The direct formic acid fuel cell (DFAFC) has been studied recently as a means to provide high power density for portable devices without requiring connection to the electrical grid for device recharging. [24, 25, 30, 31, 62-65, 72, 83, 95, 96, 98, 204-229] The DFAFC power is comparable to that of a battery, and its performance at ambient temperature is stronger than a direct methanol fuel cell (DMFC), with less crossover. [28-31] Stronger performance and lower crossover rates result in higher energy density in the DFAFC, although its theoretical energy density is lower.

The first anode catalyst that was used in the DFAFC was platinum black, but the oxidation of formic acid on platinum occurs via an indirect pathway that includes a strongly-bound CO intermediate [45, 49, 50, 52, 53]:

$$HCOOH + Pt^0 \rightarrow Pt\text{-}CO + H_2O \quad (6.1)$$

$$H_2O + Pt^0 \rightarrow Pt\text{-}OH + H^+ + e^- \quad (6.2)$$

$$Pt\text{-}CO + Pt\text{-}OH \rightarrow CO_2 + 2\,Pt^0 + H^+ + e^- \quad (6.3)$$

The CO builds up quickly on the platinum catalyst, poisoning the surface, and rapidly degenerating the fuel cell performance. [54, 55]

A more efficient catalyst is palladium black, on which the oxidation of formic acid occurs via a more direct pathway which involves a reactive intermediate, *X*, minimizing the buildup of CO on the catalyst surface [45, 49, 60-62]:

$$HCOOH \rightarrow X \rightarrow CO_2 + 2\ H^+ + 2\ e^- \qquad (6.4)$$

As expected, very little CO buildup is observed in an electrochemical cell while oxidizing 1 M formic acid. However, in a commercial fuel cell using 22-24 M formic acid, CO slowly accumulates on the anode catalyst during operation. Purification of formic acid to remove methyl formate and formic anhydride impurities leads to substantial reduction in the rate of CO buildup. [65] However, CO buildup has not been eliminated, and the anode catalyst must be regenerated periodically in an operating fuel cell. [25, 31, 63, 64]

6.2 Experimental

Reagents. High surface area palladium black unsupported nanoparticles (99.8%, Aldrich) were used as the fuel cell anode catalyst and high surface area platinum black unsupported nanoparticles (HiSpec 1000, Alfa Aesar) were used as the fuel cell cathode catalyst. Sulfuric acid (Veritas® double distilled from Vycor, GFS) was diluted to 1 M H_2SO_4 as the supporting electrolyte for electrochemical modification. Antimony (III) oxide (99.999%, Alfa Aesar) was used to make ~1 mM Sb^{3+} in 1 M H_2SO_4. Ten molar formic acid was used for fuel cell testing as diluted from fifty percent formic acid (Fluka, HPLC grade). All solutions were made using 18MΩ Milli-Q water as the solvent. Compressed air (S.J. Smith) was used for fuel cell testing.

Electrochemical Modification. A standard three electrode electrochemical cell was used with a Solartron potentiostat (SI 1287) to modify the anode catalyst. The working electrode was a 4 cm^2 carbon paper with palladium black painted on one side, and this electrode was used in the fuel cell assembly. A platinum mesh was used for the counter electrode. The Ag/AgCl/sat'd KCl reference electrode (BAS) was calibrated by bubbling hydrogen gas (S.J. Smith) over a platinum mesh electrode in 1 M H_2SO_4.

X-ray Photoelectron Spectroscopy. X-ray photoelectron spectroscopy (XPS) was performed using a PPHI 5400 XPS system with an Mg Kα X-ray source. A sample of carbon paper (area 4 cm^2, as in the fuel cell assembly) was painted with palladium black and modified with antimony using the same parameters as those used in fuel cell preparation.

Electrochemical Testing. A sample of carbon paper (area 0.5 cm^2) with the same approximate catalyst ink loading as the fuel cell was tested in the three electrode cell. First, the current was measured after five minutes of formic acid oxidation in 3 M formic acid and 0.1 M sulfuric acid. Next, the electrode was modified in 1 mM Sb^{3+} and 1 M H_2SO_4 at 0.2 V for 2 and 5 minutes. Finally, the current was measured again after five minutes of formic acid oxidation.

Fuel Cell Testing. The membrane electrode assembly (MEA) used in fuel cell testing is shown in Figure 6.1. The cathode consisted of approximately 10 mg cm^{-2} platinum black painted directly onto a Nafion 117 membrane (Ion Power). Carbon cloth

with single-sided wet-proofing (0.020", E-Tek) was used as the cathode gas diffusion layer (GDL). A very small amount of platinum (four paint layers; geometric coverage: 0.3 cm^2) was also painted in an off-centered area on the anode side of the membrane for use as a reference electrode. Palladium black was painted onto the fuel cell anode for a total loading of approximately 10 mg cm^{-2}. Approximately half the anode catalyst was painted directly onto the Nafion, while the remainder was painted onto a carbon paper GDL (0.008", Spectracarb). The palladium that was painted on the carbon paper was then electrochemically modified at 0.45 V vs the reversible hydrogen electrode (RHE) during suspension in ~1 mM Sb^{3+} and 1 M H_2SO_4 in an electrochemical cell. This modified carbon paper then completed the MEA and was inserted into a fuel cell. This same MEA painting method was used without electrochemical modification to test the palladium black anode catalyst for comparison to antimony-modified palladium black anode catalyst.

Fuel cell current-potential tests were performed at 30° C using the Solartron potentiostat running 1.0 mL min^{-1} 10 M formic acid and 300 sccm air. Constant current tests were performed with 0.15 mL min^{-1} flow of formic acid. The formic acid fuel cell contained a reference electrode established by bubbling humidified hydrogen over platinum foil in contact with the platinum layer that had been painted off-center on the anode side of the Nafion membrane.

Anode polarization was measured at 30°C by preparing carbon paper with palladium black catalyst as in the fuel cell assembly, except that no additional anode

catalyst was painted onto the Nafion and the MEA was not hot pressed. Hydrogen at 300 sccm was passed over platinum catalyst on the other side of the Nafion as a reference, and 1.0 mL min^{-1} formic acid was pumped on the anode.

6.3 Results

XPS Characterization. Carbon paper (4 cm^2) was painted with palladium black catalyst on one side. The paper was then modified in an electrochemical cell for 20 minutes at 0.4 V vs RHE in a solution of ~1 mM Sb^{3+} and 1 M H_2SO_4. The presence of antimony was confirmed by XPS, and the atomic composition was 62% Pd and 38% Sb.

Electrochemical Characterization. The effect of adding antimony to palladium black for formic acid oxidation in a three electrode cell is shown in Figure 6.2. The antimony deposition period for Sample A was 2 minutes and for Sample B it was 5 minutes. In sample A, the current for formic acid oxidation increased from 48 mA cm^{-2} before deposition to 90 mA cm^{-2} after deposition, a 90% enhancement. In sample B, the current increased from 52 to 114 mA cm^{-2}, a 120% enhancement.

Fuel Cell Characterization. Anode polarization curves are shown in Figure 6.3 in 3 M formic acid (the concentration used in the electrochemical cell) and in 10 M formic acid (the concentration used in the fuel cell). Considering a constant current of 300 mA cm^{-2}, the palladium catalyst in 10 M formic acid is at a potential of 0.155 V, while the palladium-antimony catalyst is at a potential of 0.109 V, a 40% reduction in

potential. In 3 M formic acid there is a potential reduction of 50% for the palladium-antimony catalyst.

Fuel cell polarization curves comparing two different MEAs are shown in Figure 6.4 as a function of geometric surface area. The experiments were run at ambient temperature using 1 mL min^{-1} 10 M formic acid and 300 sccm air. At 0.6 V, the current of the fuel cell using antimony-modified palladium black catalyst at the anode was approximately 340 mA cm^{-2}. At this same potential, the current of the fuel cell using a palladium black anode catalyst was approximately 299 mA cm^{-2}. By comparison, a MEA produced via the more standard direct paint procedure produces about 300 mA cm^{-2}. This demonstrates that the antimony additions produced a slight initial 14% improvement to the fuel cell performance at 0.6 V. At approximately 550 mA cm^{-2}, the peak power is reached. The power in the fuel cell with antimony-modified anode is 247 mW cm^{-2}, which is ten percent higher than the power in the fuel cell with palladium black anode, 225 mW cm^{-2}.

A constant current test at 100 mA cm^{-2} demonstrating the performance of the palladium-antimony anode catalyst in a fuel cell operating for several hours is shown in Figure 6.5. Initially the performance is stronger, as expected from Figure 6.4. For the first several hours, the rate of decay is comparable for the two catalysts. However, after about five hours the performance of the palladium black catalyst weakens at a faster rate due to increased deactivation from CO poisoning. After nine hours, the palladium-

antimony catalyst has a cell voltage of 0.495 V, which is 18% higher than the cell voltage of the palladium black catalyst, 0.419 V.

The performance of a typical DFAFC is shown in Figure 6.6 when a reference electrode is added to the fuel cell in order to differentiate performance losses at the anode and cathode. The cathode performance remains relatively constant for the duration of the experiment. However, the anode potential increases steadily and is shown to increase more rapidly after five hours. The fuel cell voltage curve mirrors the anode potential curve, decreasing at nearly the same rate. This confirms that the key performance loss in the DFAFC is at the anode.

6.4 Discussion

We have found a significant enhancement to formic acid electrooxidation when antimony is added to palladium catalyst in a three electrode cell with 3 M formic acid. Figure 6.2 shows that the effect of antimony adsorption is dependent on adsorption time, and we found a 120% improvement to oxidation current after 5 minutes of antimony adsorption. We also see some improvement in the anode polarization curves in Figure 6.3. However, the improvement does not carry over as strongly to real fuel cell conditions; we do not observe much evidence of suppression of CO formation.

The observation that the initial IV curves do not change substantially with the addition of antimony is not a surprise. Previous workers have found that initially the current out of a formic acid fuel cell is largely cathode limited [63, 65, 206, 247, 248].

One would not expect the changes in the anode catalyst to have a significant effect under cathode limited conditions.

The observation that antimony additions do not suppress CO poisoning was a surprise, however. Previous workers have found that antimony additions suppress CO formation on platinum. [73-75, 80] There are three key effects. First, the coverage of less than one monolayer of catalyst with an adatom that is inert to formic acid isolates individual catalyst sites and reduces the amount of CO poison that can build up on the surface, particularly CO that is multiply bonded to the surface. [42, 73, 74, 84-89] This is known as the *steric effect* and is strongly supported by empirical evidence in which an adatom such as lead is shown to completely block CO buildup on platinum during formic acid oxidation. [80] Second, the adatom can create a *bi-functional catalyst*, in which the inert adatom may still be inert to formic acid, but performs some other role [90-92]. For example, ruthenium readily adsorbs water, which is necessary for removal of CO from a platinum surface during formic acid oxidation, as shown in Equations 6.2 and 6.3, although ruthenium itself will not oxidize formic acid. [54] Third, the adatom may shift the binding energy of the catalyst, changing the adsorption characteristics of formic acid and CO on the catalyst surface, which is known as the *electronic effect*. [45, 93, 94]

Platinum and palladium are quite similar chemically. Theoretically, anything that suppresses CO formation on platinum should also suppress CO formation on palladium. Yet, we find that the anode is poisoned by CO even in the presence of antimony.

We have been puzzling over why so little suppression of CO formation/ poisoning is observed. We can exclude the possibility that the antimony does not adsorb on the palladium or that it is removed during the reaction. Note that we observe significant enhancement in the anode polarization experiments in Figure 6.3 in the presence of the antimony. Clearly there is antimony on the surface of the catalyst since we still see a significant enhancement in anode polarization. We did lifetime studies and found that the anode polarization does not change significantly after 24 hours. Thus we know that the antimony is present on the catalyst and not being removed during the reaction. Further, antimony has been shown to irreversibly adsorb on platinum surfaces when the catalyst is held at underpotential for a period of time, typically minutes. [78, 79] Such adatoms do not strip off the surface during anodic potential scans as do reversibly adsorbed atoms. We observe similar irreversible adsorption of antimony on our palladium catalyst. Our conclusion therefore, is that we have significant antimony on our catalyst, but the antimony does not sufficiently suppress CO formation in an operating formic acid fuel cell.

One possibility that could explain such a result is that the CO, or some CO precursor such as formic anhydride, is formed on the Nafion, and that this eventually migrates to the catalyst, poisoning it. We previously showed that there is very little CO formation on a pure palladium catalyst after 1 hour in 5 M formic acid, even though CO formation is detected in less than 1 hour in a fuel cell. [60] As noted earlier, Gates et al. previously found that polystyrene sulfonic acid catalyzes the dehydration of formic acid to yield carbon monoxide and water. [66] Nafion is more acidic than polystyrene sulfonic

acid. Thus if polystyrene sulfonic acid can catalyze the formation of CO, it is very likely that Nafion would too. Antimony additions would have little effect on the Nafion, since the antimony is only present on the palladium surface. Our suggestion, therefore, is that CO being formed on the Nafion is contributing to the catalyst poisoning, and the antimony additions cannot suppress this CO formation.

6.5 Conclusion

We have shown that electrochemical surface modification of palladium by antimony adatoms enhances the oxidation of formic acid by more than two-fold in an electrochemical cell. However, when the catalyst is scaled up to an operating DFAFC, the enhancement is much less. In the fuel cell we find that the initial performance is improved 14% by the palladium-antimony catalyst, and the performance is improved by 18% after several hours.

6.6 Acknowledgements

This work was supported by the Army Research Office under contract W911NF-05-C-0110 and the Defense Advanced Research Projects Agency (DARPA) under grant DST 2007-0299513- 000-1. The opinions are the authors and do not reflect the findings of the Army Research Office, DARPA or the US government. XPS analysis was carried out by Dr. Richard T. Haasch in the Frederick Seitz Materials Research Laboratory Central Facilities, University of Illinois, which is partially supported by the U.S. Department of Energy under grants DE-FG02-07ER46453 and DE-FG02-07ER46471.

6.7 Figures

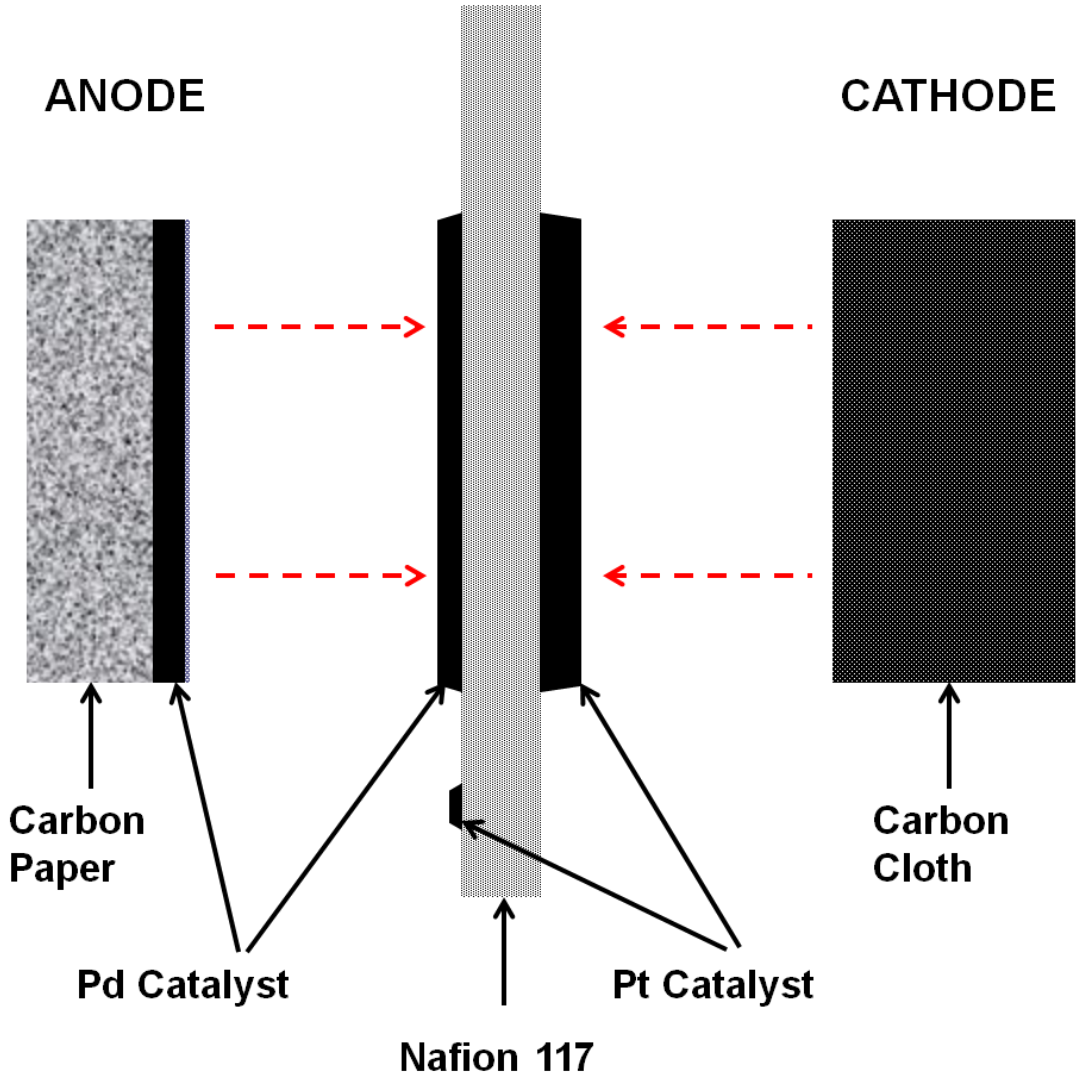

Figure 6.1. Novel MEA design. This is a cross-section diagram of fuel cell MEA design that demonstrates the features of an MEA designed so that some of the anode catalyst can be electrochemically modified.

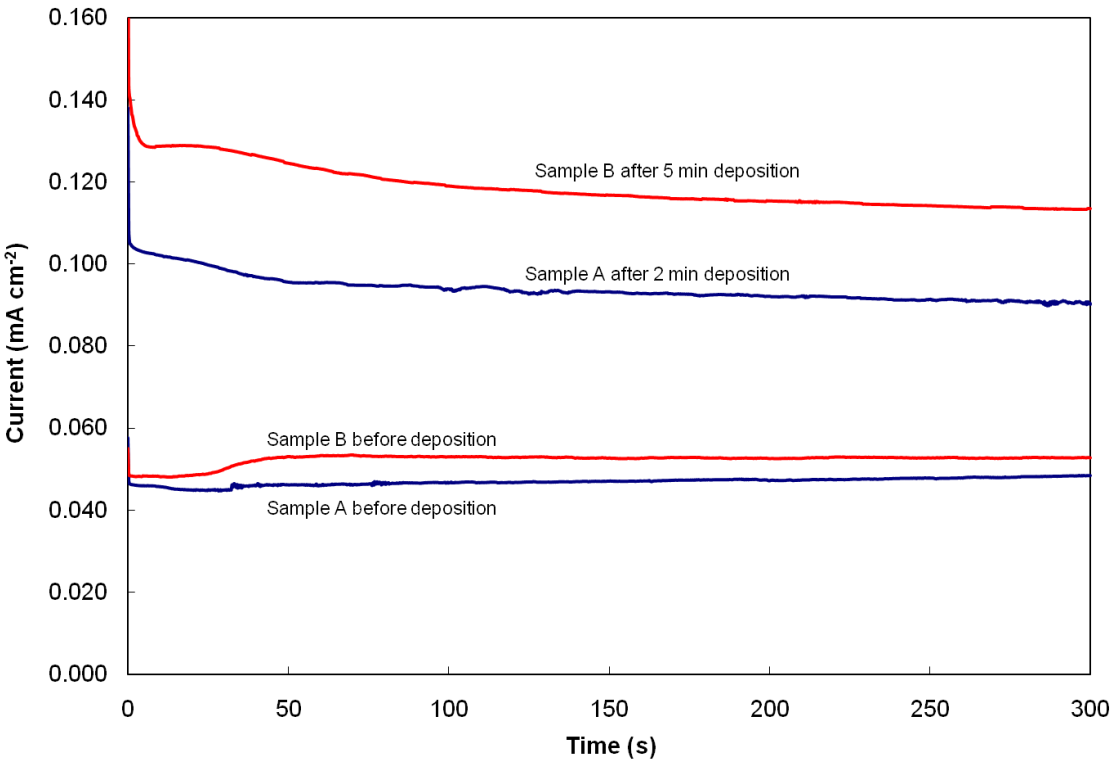

Figure 6.2. The oxidation of formic acid in a three electrode cell before and after antimony deposition. The deposition was carried out for 2 or 5 minutes, as indicated, in 1 mM Sb^{3+} and 1 M H_2SO_4 at 0.45 V vs RHE. The formic acid was oxidized at 0.3 V vs RHE. An approximately two-fold increase in formic acid oxidation is observed for each sample.

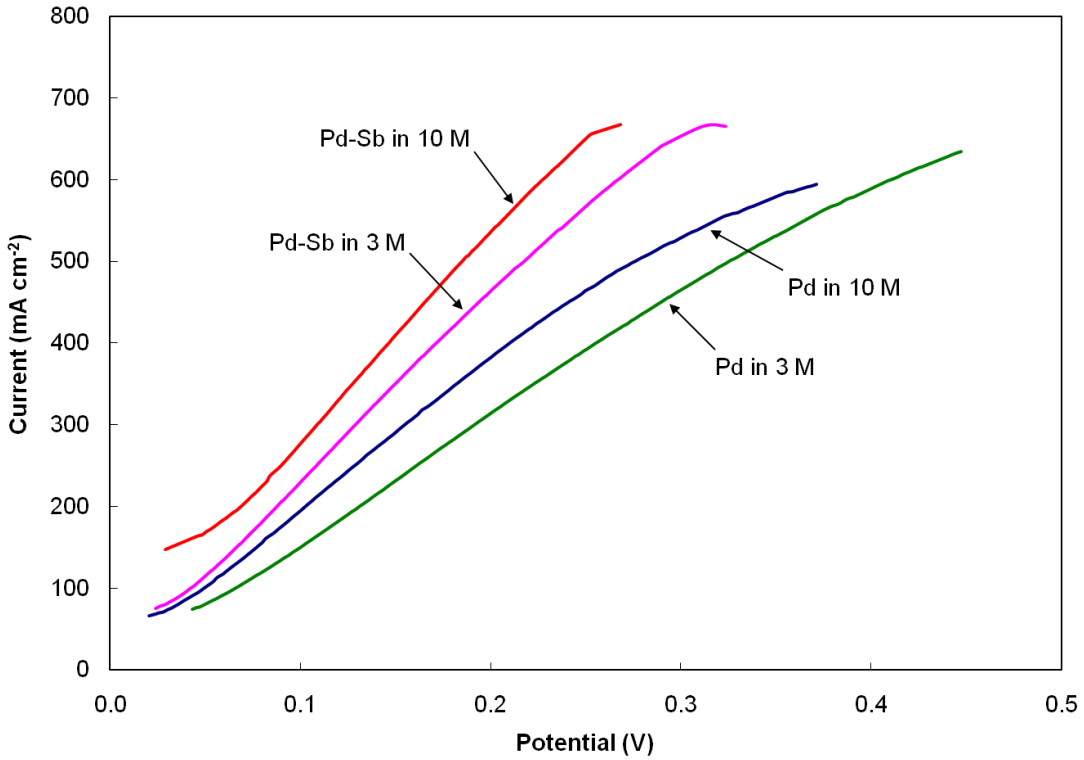

Figure 6.3. Anode polarization curves comparing palladium black and palladium-antimony catalyst. The catalyst was painted onto carbon paper and inserted into a fuel cell assembly with 1 mL min^{-1} of 50% formic acid on the anode and hydrogen on the cathode. For the 10 M formic acid at a current of 300 mA cm^{-2} , the Pd-Sb catalyst is at a potential of .109 V, while the Pd catalyst is at .155 V, a 42% difference. For the 3 M formic acid, the difference in potential at 300 mA cm^{-2} is 50%. There is a lower anode potential in 10 M formic acid for each catalyst compared with 3 M formic acid.

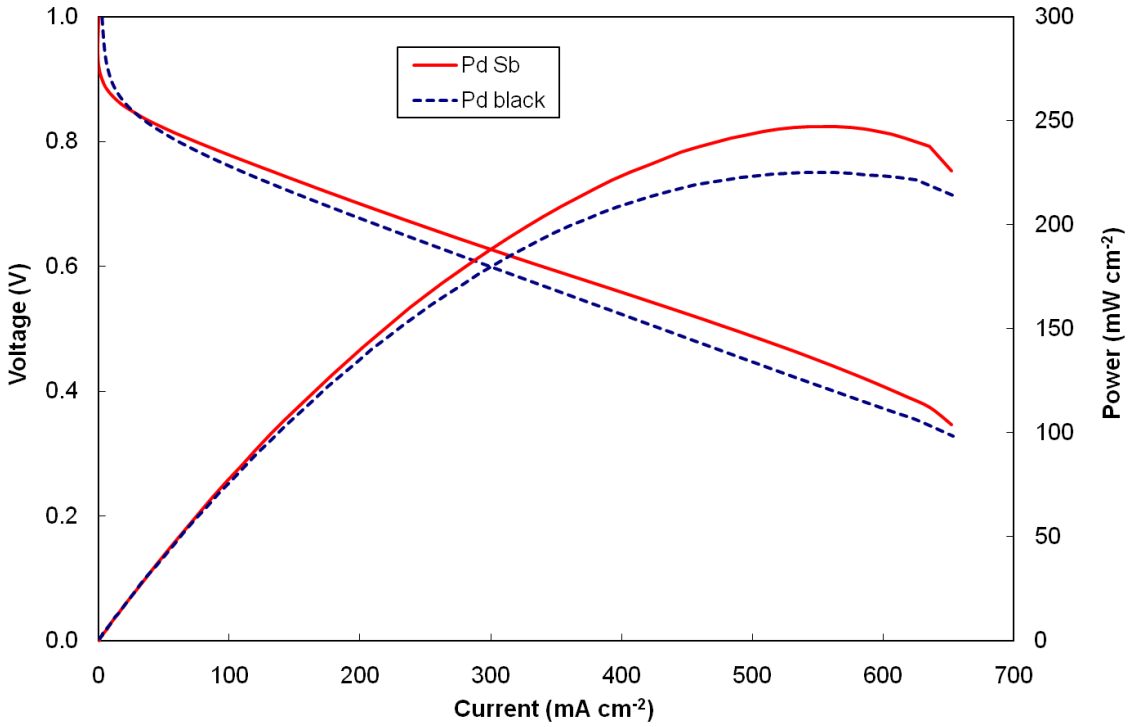

Figure 6.4. Polarization curves of two different MEAs in an operating DFAFC at 30°C with 1 mL min^{-1} 10 M formic acid on the anode and 300 sccm air on the cathode. The Pd black fuel cell has unmodified palladium black as the anode catalyst, while the Pd-Sb fuel cell has antimony-modified palladium black as the anode catalyst.

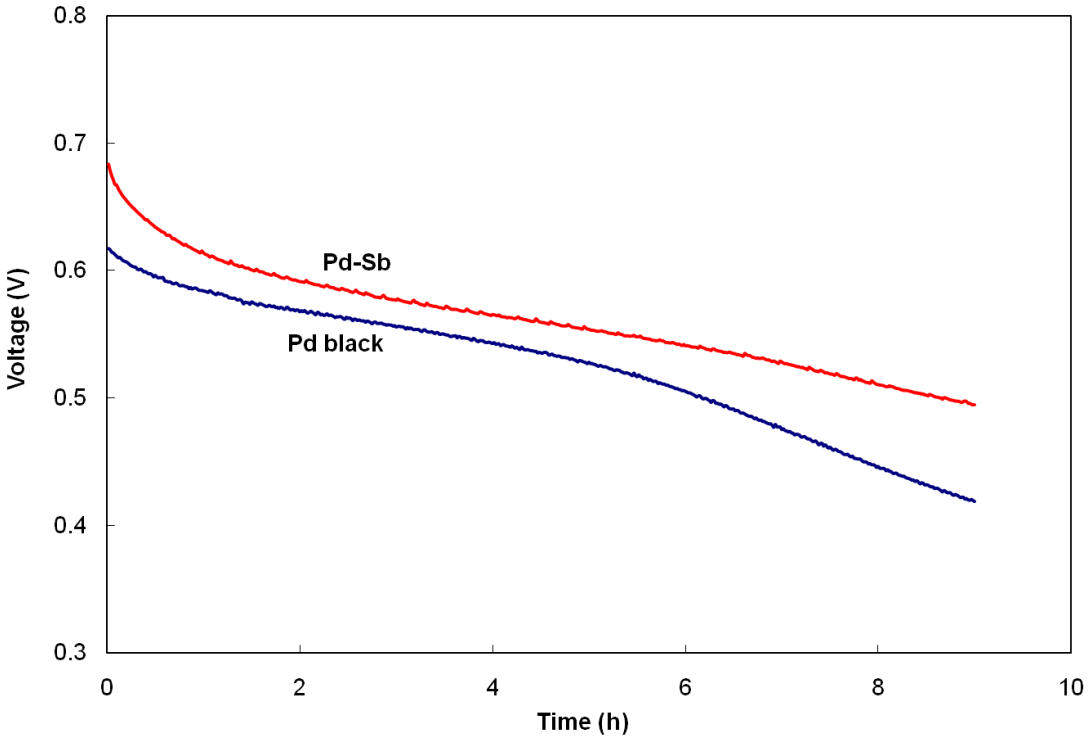

Figure 6.5. Constant current test for 9 hours at 100 mA cm^{-2} for two different MEAs in an operating DFAFC at ambient temperature with 0.15 mL min^{-1} 10 M formic acid on the anode and 300 sccm air on the cathode. The Pd black fuel cell has unmodified palladium black as the anode catalyst, while the Pd-Sb fuel cell has antimony-modified palladium black as the anode catalyst.

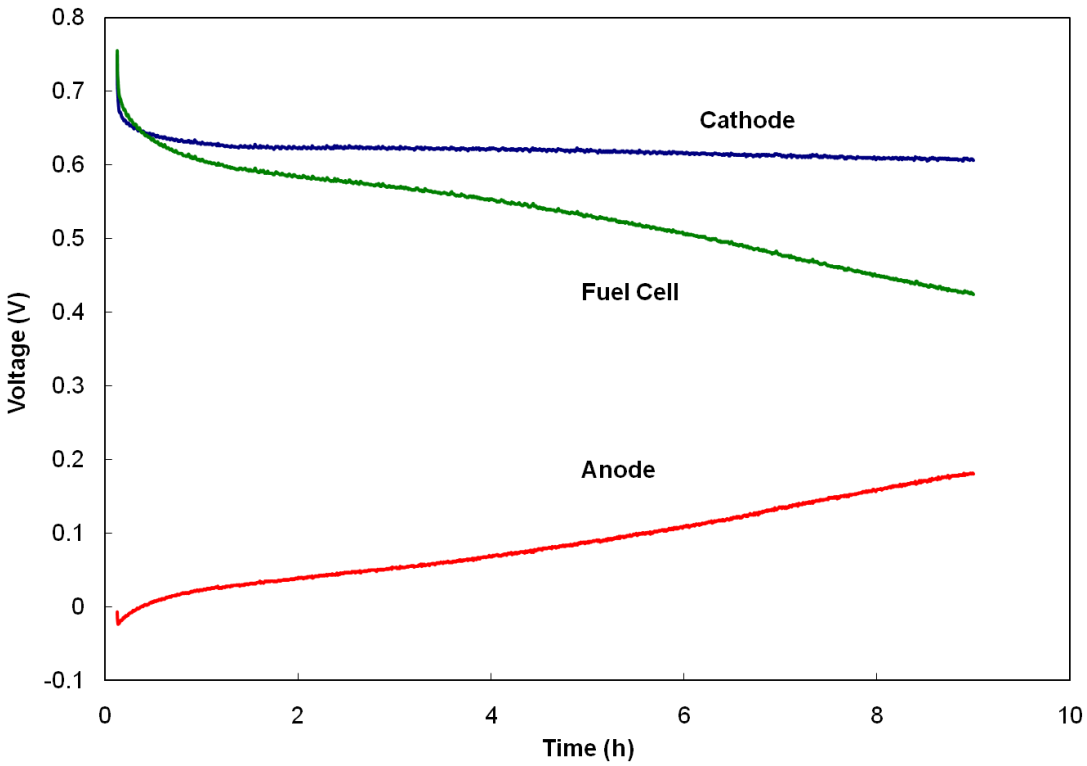

Figure 6.6. Constant current test demonstrating performance of a typical DFAFC operating at ambient temperature with 0.15 mL min^{-1} 10 M formic acid on the anode and 300 sccm air on the cathode. A reference electrode is employed to determine the anode and cathode potentials and the voltage of the fuel cell. The cathode is stable, while the fuel cell performance loss can be attributed primarily to the anode overpotential due to CO buildup on the catalyst surface.

Chapter 7: The Effects of the Addition of Antimony, Tin, and Lead to Palladium Catalyst Formulations for the Direct Formic Acid Fuel Cell

This chapter is adapted from a manuscript that was submitted for publication in April 2010 to the Journal of Physical Chemistry C.

7.1 Introduction

Fuel cells operated with small organic molecules as the anode fuel source have gained significant interest as a viable alternative to hydrogen fuel cells for portable power applications; such fuel cells can be used as primary energy sources or for recharging of these devices. [24, 25, 30, 31, 33, 62-65, 72, 83, 95, 96, 98, 204-229] The direct formic acid fuel cell (DFAFC) has been studied recently because its power is comparable to that of a battery, and its performance at ambient temperature is stronger than a direct methanol fuel cell (DMFC) with lower fuel crossover and higher energy density. [28-31]

Initial catalysis work on the DFAFC was dominated by studies of platinum black as the anode catalyst, but it was known that one oxidation pathway of formic acid on platinum includes a strongly-bound CO intermediate [45, 49, 50, 52, 53]:

$$HCOOH + Pt^0 \rightarrow Pt\text{-}CO + H_2O \quad (7.1)$$

$$H_2O + Pt^0 \rightarrow Pt\text{-}OH + H^+ + e^- \quad (7.2)$$

$$Pt\text{-}CO + Pt\text{-}OH \rightarrow CO_2 + 2\,Pt^0 + H^+ + e^- \quad (7.3)$$

At fuel cell potentials, the CO builds up in a matter of minutes on the anode, which rapidly diminishes DFAFC performance and makes platinum an infeasible anode catalyst. [54, 55]

A more efficient catalyst is palladium black, on which the oxidation of formic acid occurs via a more direct pathway which involves a reactive intermediate, *X*, minimizing the buildup of CO on the catalyst surface [45, 49, 60-62]:

$$HCOOH \rightarrow X \rightarrow CO_2 + 2\ H^+ + 2\ e^- \qquad (7.4)$$

The rate of formic acid oxidation is very low on low surface area palladium as compared with high surface area nanoparticles. As a result, there is no evidence of CO poisoning on low surface area palladium during formic acid oxidation. However, as palladium surface area is increased, the formic acid oxidation rate also increases. Zhou, et al, showed that there is also a correlation between particle size and core level binding energy, in which the binding energy increases with decreasing particle size. [105] In 5 M formic acid, very little CO poison is found after one hour of formic acid oxidation. [25] However, in fuel cells with higher formic acid concentration, significant amounts of CO build up after several hours and must be removed in order to restore full operating power. Studies have shown that purification of the formic acid to remove impurities reduces the rate of poisoning but does not eliminate it. [25, 31, 63-65, 72]

Catalyst modifications to platinum (e.g., antimony, bismuth, cadmium, and lead) have been shown to increase the rate of formic acid oxidation and, in some cases, eliminate CO poisoning. [73-75, 80] This is likely due to any or all of the following:

steric effect [42, 73, 74, 84-89], by which poison formation is inhibited by site blocking; the bifunctional effect [54, 90-92], by which the adatom aids in adsorption of water to the surface and thus removal of poison; the electronic effect [45, 93, 94], by which the adatom alters the electronic nature of the platinum. Recently, studies have shown that fuel cells made with these anode catalysts are still inferior to fuel cells with palladium anode catalyst. [82, 83] Therefore, in this study, we determine what effects palladium catalyst modifications have on formic acid oxidation in both an electrochemical cell and a fuel cell using high surface area palladium catalysts.

We have found that antimony, tin, and lead modifications to palladium catalyst increase the rate of formic acid oxidation in an electrochemical cell and to a lesser extent in a fuel cell. We also found that these adatoms reduce short-term CO poisoning in an electrochemical cell, but they do not eliminate the poisoning in the long-term. Finally, we show that these adatoms shift the core level binding energy of the palladium and decrease the Tafel slope for formic acid oxidation.

7.2 Experimental

Electrochemistry. A standard three-electrode electrochemical cell was used with a Solartron potentiostat (SI 1287), a platinum mesh counter electrode, and an Ag/AgCl/sat'd KCl reference electrode (BAS). The reference was calibrated by bubbling hydrogen gas (S.J. Smith) over the counter electrode in 1 M H_2SO_4 (Veritas® double distilled from Vycor, GFS). The working electrode was palladium black (99.8%, Aldrich; suspended with Nafion and water then dried) on a glassy carbon rotating disk electrode (Pine) for Tafel analysis and palladium-painted carbon paper (Toray, 0.008")

for the CO formation analysis and the fuel cell assemblies. For XPS analysis, the working electrode was palladium black ink (with water but no Nafion) dried on a gold plug.

Fuel Cell Testing. The membrane electrode assembly (MEA) used in fuel cell testing was developed so that the palladium black anode catalyst could be modified in an electrochemical cell prior to use in the fuel cell. [33] Anode palladium black catalyst was painted partially on the carbon paper gas diffusion layer (GDL), and partially on the Nafion membrane. Cathode platinum black catalyst (Alfa Aesar) was painted directly onto a Nafion 117 membrane (Ion Power), and the GDL was a single-sided wet-proofed carbon cloth (0.020", E-Tek). The portion of the anode catalyst painted on the carbon paper was then modified electrochemically at 0.45 V vs RHE in a solution containing both an electrolyte and the adatom. Fuel cell polarization experiments were performed with the Solartron potentiostat at 30° C, 1.0 mL min^{-1} 10 M formic acid, and 300 sccm air. Constant current tests were performed at 100 mA cm^{-2} with 0.15 mL min^{-1} flow of formic acid.

X-ray Photoelectron Spectroscopy. X-ray photoelectron spectroscopy (XPS) was performed using a PHI 5400 XPS system with an Mg Kα X-ray source. The palladium catalyst was prepared for XPS by potential cycling to clean the surface, followed by holding the potential at 0.45 V vs RHE in a solution containing the metal adatom and an electrolyte. A blank was prepared by holding this potential, which lies in the double layer charging region of palladium, in an electrolyte containing no adatom.

7.3 Results

Chronoamperometry. Several adatoms were tested for their promotion of formic acid oxidation in the electrochemical cell using 12 M HCOOH and 0.1 M H_2SO_4 and a potential of 0.3 V vs RHE. Palladium catalyst modified with tin, lead, or antimony was found to increase the rate of oxidation as shown in Figure 7.1. The palladium-tin catalyst was made by electrochemically modifying palladium black in a solution of 0.5 M $HClO_4$ and 1 mM SnO while holding the potential at 0.45 V vs RHE for two minutes. The palladium-lead catalyst was made by modifying palladium in 0.5 M $HClO_4$ and 1 mM $Pb(NO_3)_2$, while also holding the potential at 0.45 V vs RHE for two minutes. The palladium-antimony was made by modification in 1 M H_2SO_4 and 1 mM Sb_2O_3 at a potential of 0.45 V vs RHE for two minutes. Previous work had shown that, over several minutes, antimony additions nearly doubled the rate of formic acid oxidation on palladium [33], and Figure 7.1 shows that antimony remains a strong promoter after three hours of oxidation in 12 M HCOOH and 0.1 M H_2SO_4. After three hours, the current density on palladium black is 8.1 uA cm^{-2}, while on palladium-antimony it is 21 uA cm^{-2}. We also found that lead is a strong promoter of formic acid oxidation, and the formic acid oxidation current is 32 uA cm^{-2} at three hours, which is significantly more than the palladium black. Palladium-tin catalyst was found to be a strong promoter in the first hour, but after three hours, the current density was 10 uA cm^{-2}, which is still 25% stronger than the palladium black, but not as substantial as lead and antimony.

Fuel Cell Tests. The palladium-tin and palladium-lead catalyst formulations from Figure 7.1 were tested in the fuel cell to determine how much of the promotion seen

in the electrochemical cell would carry over into the fuel cell. The fuel cell was operated at 100 mA cm^{-2} for nine hours, and the results are shown in Figure 7.2. Also included in Figure 7.1 is data from [33] to compare the new catalysts to the palladium black and palladium-antimony results previously reported. The PdPb catalyst performs better than any other catalyst for the first three hours, which correlates *qualitatively* with the results from the electrochemical cell. However, the fuel cell with PdPb only operates at 580 mV at 3 h, while the fuel cell with Pd operates at 556 mV at 3 h. *Quantitatively*, this difference in voltage is far less than predicted from Figure 7.1, where the oxidation rate is four times greater for PdPb than for Pd. In addition, the voltage of the fuel cell with PdPb decreases substantially after 3 hours and eventually does not perform much different than the fuel cell with Pd.

The fuel cell with PdSn catalyst initially performs well, but then performs comparably to the fuel cell with Pd catalyst until about 4 hours, at which time its performance decays slightly slower. This behavior also matches that in the electrochemical cell qualitatively, but the difference in fuel cell performance is not very significant; the fuel cell with PdSn has a voltage of 478 mV, which is 14% greater than the fuel cell with Pd (421 mV) after 9 hours. The fuel cell reported previously with PdSb catalyst performs better than the others after 9 hours, but the performance difference of close to 20% is much less than what is observed in the electrochemical cell.

Polarization curves are shown in Figure 7.3, in which it is observed that the fuel cells with bimetallic catalysts all perform slightly better than the fuel cell with palladium

catalyst, which achieves a current density of 299 mA cm^{-2} at 0.6 V. The fuel cell with PdPb achieves 345 mA cm^{-2} at 0.6 V, which is about 15% higher, while the other fuel cells are only slightly lower, achieving the following current densities at 0.6 V: PdSb, 340 mA cm^{-2}; PdSn, 335 mA cm^{-2}.

CO Stripping Experiments. While we do not expect much CO to build up on the palladium surface during formic acid oxidation as compared with platinum, we did find that at the concentration of formic acid we used (12 M) and in the presence of ~20wt% Nafion in the catalyst ink (which is the quantity used in the DFAFC) CO does indeed buildup on the surface. Figure 7.4 shows a representative cyclic voltammogram at 10 mV s^{-1} following 3 hours of formic acid oxidation at 0.3 V vs RHE. We observe stripping of CO from the surface between 0.8 and 1 V vs RHE. Once the CO is removed from the catalyst, there is a poison-free palladium surface, indicated by the voltammetric peaks related to hydrogen adsorption and desorption between 0.1 and 0.3 V and the surface oxidation (beyond 0.7 V) and reduction (0.9 V to 0.7 V). The area under the oxidation curve in cycle 2 can be subtracted from the area under the CO stripping peak in cycle 1, and then integrated to obtain the charge passed while the CO was stripped from the surface.

Figure 7.5 shows the difference between the first and second cycles for the CO stripping CVs that follow formic acid oxidation for 1 hour with each of the four catalysts. Integration of these curves shows that after 1 hour of oxidation, the CO covered 58% of the available electrochemical surface area on the palladium catalyst and it covered 50%

on the PdSb and PdSn catalysts and 39% on the PdPb catalyst. Figure 7.6 shows CO stripping data on the catalysts after 3 hours of formic acid oxidation, at which time the CO buildup is 59% on the palladium catalyst, but it is much more on the bimetallic catalysts than after only 1 hour: PdPb, 54%; PdSb, 57%; PdSn, 60%. It is quite clear that there is a reduction in CO buildup on the modified catalysts, but that this effect does not last for several hours.

It is also interesting to note that there is a subtle shift in the CO stripping peak potentials on each catalyst. After 1 hour of formic acid oxidation the CO stripping peak on palladium is at 913 mV, while the peak shifts to 906 mV on PdPb, to 895 mV on PdSb, and 941 mV on PdSn. After 3 hours of formic acid oxidation the CO stripping peaks all shift to higher potentials: Pd at 939 mV, PdPb at 933 mV, PdSb at 908 mV, and PdSn at 945 mV.

Tafel Analysis. Tafel plots were created for the four catalysts and shown in Figure 7.7. The catalysts were suspended on a glassy carbon electrode that was rotated at 2000 rpm to eliminate mass transfer effects so that the kinetics could be probed directly. Various potentials were held for 3 seconds in 0.1 M HCOOH and 0.1 M H_2SO_4 to build the Tafel plot. The Tafel slope for palladium catalyst was found to be 141 mV dec^{-1}, with a correlation of 0.98. For the PdPb catalyst the slope was 124 mV dec^{-1} (0.98), for PdSb the slope was 116 mV dec^{-1} (0.99), and for PdSn the slope was 103 mV dec^{-1} (0.99). Clearly, the presence of an adatom decreases the Tafel slope, although not to a large extent.

X-Ray Photoelectron Spectroscopy. The core level binding energy of the palladium was analyzed using XPS to determine the effect of the adatoms on the electronic structure of the palladium. Catalyst inks were prepared with the catalyst nanoparticles and water (with Nafion excluded from the ink), and the ink was dried on a gold plug. The dried catalyst was then transferred to an electrochemical cell for potential cycling and then a potential hold at 0.45 V vs RHE. For the palladium catalyst, this potential hold was done in a solution of 1 M H_2SO_4, but for the bimetallic catalysts, the solutions contained the dissolved adatom. Following the potential hold, the catalyst was quickly transferred (while protected with a solution droplet) to a degassed water flask. The catalyst was then quickly transferred (while protected with a water droplet) to the XPS chamber, which was immediately pumped down. Figure 7.8 shows the binding energy for Pd $3d_{5/2}$ and $3d_{3/2}$. The black vertical line indicates the peak position, 335.60 eV for the Pd $3d_{5/2}$ in the unmodified catalyst. The same peak in the PdPb catalyst is 335.76 eV, an upshift of 0.16 eV. A stronger shift of 0.41 eV to 336.01 eV is observed in the PdSn catalyst is 336.01 eV, and a stronger shift of 0.50 eV to 336.10 eV is observed in the PdSb catalyst.

XPS was also used to determine the ratio of palladium to adatom for each sample. For the PdSn sample, there was 75at% Pd and 25at% Sn, while for the PdPb sample, there was 86% Pd and 14% Pb. We previously reported the PdSb sample to contain 62% Pd and 38% Sb. [33] The deposition times were chosen not to target a specific coverage but to target maximum activity for formic acid oxidation. [249]

7.4 Discussion

Electrochemical Cell: Strong Promotion of Formic Acid Oxidation by Adatoms. We found that there was a substantial promotion of formic acid oxidation in an electrochemical cell by adatoms of lead, antimony, and tin on the palladium surface. Adzic, et al, reported a substantial increase in transient formic acid oxidation current on low surface area palladium by lead adatoms [87], and others have reported that lead deposited at underpotentials can be irreversibly adsorbed. [250, 251] It has also been reported that lead and tin suppresses CO buildup on platinum surfaces [80, 252], and we hoped that we would find a long-term suppression of CO buildup on palladium. We previously reported that the formic acid oxidation rate doubles on a high surface area palladium antimony formulation after 5 min and that antimony is stable on the palladium surface, while others have shown that antimony is stable on platinum, also. [33, 78, 79] Recent work pending publication by Pickup, et al., shows that antimony suppresses CO formation on palladium over short time periods. Tin has been shown to promote formic acid oxidation on platinum and is also known to irreversibly adsorb on a palladium surface, so we wanted to determine its effect on formic acid oxidation on palladium, also. [253, 254] Since none of this previous work studied the effects of adatoms after a few hours of formic acid oxidation on high surface area palladium in the presence of Nafion during formic acid oxidation, we sought to determine the effects of lead, antimony, and tin after one and three hours of oxidation. We found a substantial increase in the rate of formic acid oxidation after 1 hour on each of the catalysts when compared with pure palladium, as shown in Figure 7.1. After 3 hours, we observed a four-fold increase in current with the lead catalyst, a 2.5-fold increase with antimony, and a 25% increase with

tin. These results demonstrate that each adatom has a significant promotion effect for formic acid oxidation on palladium in an electrochemical cell.

Fuel Cell: Weak Promotion of Fuel Cell Performance by Adatoms. Despite our results shown in Figure 7.1, we were disappointed that more of the promotion of formic acid oxidation did not carry over as strongly into the fuel cell when we employed palladium catalysts with lead, antimony, and tin adatoms. The fuel cell data in Figure 7.2 shows a qualitative relationship to the electrochemical cell data in Figure 7.1 in that the lead and antimony promote the fuel cell up to 3 hours as in the electrochemical cell, while the tin promotes the fuel cell initially but fails to promote at 3 hours. After 9 hours of fuel cell operation, the order of promotion is PdSb, followed by PdSn, and PdPb. We also show polarization curves in Figure 3, in which we note that the adatoms each promote initial fuel cell performance, although not to the extent we had hoped. The best performing catalyst is PdPb, which produces 345 mA cm^{-2} at 0.6 V, which is 15% more than the 299 mA cm^{-2} of the palladium catalyst. This performance difference is much less than the two-fold initial difference between PdPb and Pd catalysts that we see in the electrochemical cell; the performance difference at 3 hours is also significantly less in the fuel cell than the electrochemical cell.

In our previous study we isolated the cell potentials via a hydrogen reference electrode to confirm that the most significant losses were occurring at the anode, as the potential increased during several hours of oxidation due to the buildup of CO poison on the surface of the anode catalyst. [33] The initial performance can be quickly regenerated

by electrochemically cleaning the CO from the surface, which can be accomplished by short-circuiting the anode and cathode while air flows over the cathode. Therefore, we know that our general performance losses in the fuel cell over several hours are occurring at the anode where CO poisoning is occurring at a rate that severely restricts fuel cell performance.

Our data in Figure 7.2 suggests that, while we have made some improvement to the fuel cell performance, we have not seen the improvement of formic acid oxidation in the electrochemical cell carry over as strongly to the fuel cell. There are several sources of efficiency losses in the fuel cell, such as mass transfer limitations, fuel crossover (although lower in the DFAFC than other liquid fuel cells), membrane resistance, etc. [34] We expect that a change to the anode catalyst would affect the DFAFC performance since it is a great source of performance loss over time, but we do not expect to see the four-fold increase in performance in the fuel cell that we see in the electrochemical cell. In our previous study, we showed nearly 100% improvement in the electrochemical cell (with PdSb vs. Pd), nearly 50% improvement in anode polarization curves (only the anode operates as in the fuel cell), and 20% improvement in the fully operational fuel cell. [33] In other words, as the device becomes more complicated by adding components, the performance gains in one component (e.g., the anode catalyst) are masked by the other components so that there is a smaller performance gain in the fully operational fuel cell. Although we could accept that the new catalysts afford less performance gain in the fuel cell than the electrochemical cell, we were disappointed to find that CO buildup is *not* eliminated on these catalysts, as discussed in the next section.

The Buildup of CO Poison during Formic Acid Oxidation. During formic acid oxidation, we have found that CO does not buildup as rapidly on palladium catalyst as it does on platinum. [25] However, under conditions that are similar to an operating fuel cell, such as higher formic acid concentrations, longer durations of experiments, and the presence of Nafion® both as a binder and a membrane, we find that CO does buildup to poison the catalyst surface during a time frame of hours (rather than seconds, as on platinum. We also know that polystyrene sulfonic acid catalyzes the dehydration of formic acid to yield carbon monoxide and water. [66] Since Nafion® is more acidic than polystyrene sulfonic acid, it is likely that Nafion® can catalyze the formation of CO. Adatoms would not affect this process since they are only present on the palladium surface. What we have found in the electrochemical cell under these conditions, using carbon paper painted with a palladium-Nafion ink with the same formulation as that of the fuel cell is that we have significant CO build up that occurs after formic acid oxidation. A sample CO stripping voltammogram is shown in Figure 7.4. The area under the CO peak (i.e., the charge for CO oxidation), which starts ~0.8 V on the first scan can be integrated and compared with the charge due to palladium surface oxidation on the second scan to determine the amount of CO coverage on the palladium surface. This figure confirms the presence of CO on the palladium surface after 3 hours of formic acid oxidation, and it also confirms the removal of CO after one cycle to high enough potentials.

In Figures 7.5 and 7.6, the CO oxidation peak on each catalyst after 1 hour and 3 hours, respectively, is shown after the current due to oxidation of the palladium in the second cycle is subtracted. After 1 hour of oxidation, as shown in Figure 7.5, there is more buildup of CO on the palladium catalyst (58%) than on the catalysts with adatoms (PdSb: 50%, PdSn: 50%, PdPb: 39%). There is also a shift in peak potentials, where CO oxidation shifts the most from 913 mV on Pd to 895 mV on PdSb, indicating a weaker adsorption of CO on the PdSb catalyst. This data shows that the presence of the adatoms does have an effect on the short-term buildup of CO poisoning which we anticipated, but we were disappointed to find that after 3 hours, the presence of the adatom did not have much impact. Figure 7.6 shows that a similar amount of CO builds up on all the catalysts in a range from 54% on the PdPb to 60% on the PdSn, while the Pd was 59%. This data suggests that there is a steric effect from the presence of the adatoms over short time periods, but that after a few hours, the propensity to build up CO poison overwhelms this steric effect. It is possible that significant amounts of CO are being produced at the Nafion®, which would be unaffected by the presence of the adatoms and produce a gradual buildup of CO as it migrates to the palladium surface.

It is also interesting to note that the CO peak positions after 3 hours are qualitatively similar to the peak positions after 1 hour, but they are all shifted to higher potentials, indicating that the CO is more strongly adsorbed after 3 hours than after 1 hour of oxidation. This difference in CO adsorption is due to contributions from the adatoms to the activation of water in Equation 7.2 (bifunctional effect) or to the electronic structure of the palladium (ligand effect). [55, 255] For example, the peak

position on Pd shifts from 913 to 933 mV with the additional 2 hours of oxidation. It is important to also note that the effect of the adatoms on both the oxidation current (Figure 1) and the amount of CO buildup (Figures 7.5 and 7.6) can be restored when the CO is stripped from the surface, just as the fuel cell performance is fully restored when CO is stripped from the anode. Therefore, the fact that the CO buildup on all the modified catalysts is comparable to that of the unmodified catalysts after 3 hours is not due to a disappearance of the adatoms.

Tafel Plots of Formic Acid Oxidation. So far we have determined that the weak steric effect resulting in reduced CO buildup is limited to short time periods that are not of interest to fuel cell operation. We also have shown that the promotion of formic acid oxidation by the adatoms goes beyond the short time period in which the steric effect is present, so it cannot be attributed merely to a slowed buildup of CO poison. The adatoms must be either creating a bifunctional catalyst or causing an electronic effect, both of which we might observe by studying the reaction kinetics. Since formic acid oxidation occurs primarily via the direct route (Equation 7.4) on palladium, it is unlikely that a bifunctional catalyst would have much effect as it would on platinum, where it would essentially promote Equation 7.2, the attraction of an oxide to the surface to aid in CO removal. To probe the kinetics, we found a potential region (~0.05 to 0.15 V vs RHE) in which Tafel behavior was observed on our catalysts with a strong correlation for linear behavior (0.98 to 0.99). We found that the Tafel slope was 141 mV dec^{-1} on Pd, which is very close to the slope of 136 mV dec^{-1} reported for palladized platinum electrodes [241], and that it was lower for each adatom, with the lowest observed at 103 mV dec^{-1} on

PdSn. Since all Tafel slopes measured here are reasonably close to the 120 mV dec^{-1} expected for a single electron transfer reaction, the following reaction mechanism has been suggested for palladium, which does not strongly support the indirect oxidation route [105, 241, 256]:

$$HCOOH \rightarrow (COOH)_{ads} + H^+ + e^- \quad (7.5)$$

$$COOH \rightarrow CO_2 + H^+ + e^- \quad (7.6)$$

where Equation 7.5 represents the rate determining step of C-H bond breaking, and Equation 7.6 is a fast step that completes the oxidation to CO_2. It is important to consider, however, that the Tafel behavior takes place within the potential window in which hydrogen interacts with the palladium surface. [241] Therefore it is not reasonable for us to speculate further on the values of the Tafel slopes calculated in this work, except to suggest that our palladium Tafel slope compares well with previous work and that the adatoms clearly impact the kinetics of the reaction since they do change the Tafel slope.

X-Ray Photoelectron Spectroscopy: A Shift in Palladium Binding Energy.

We have suggested that there must be an electronic effect to explain the behavior we see in Figure 7.1 (3 hours of oxidation) and Figure 7.7 (Tafel slopes), where we see both promotion of formic acid oxidation and high surface coverage of CO poison. We also know that an electronic effect plays a role in platinum-based catalyst formulations for formic acid oxidation, including catalysts with irreversibly adsorbed lead and bismuth surface modifications. [219, 257] Because of the similarities between palladium and platinum, we expect to see an electronic effect when adatoms are irreversibly adsorbed to the palladium surface as well.

To probe this, we considered the binding energy of the Pd $3d_{5/2}$, looking for shifts that would demonstrate that the adatoms had affected the electronic structure of the palladium. We found that the binding energy of the Pd $3d_{5/2}$ peak in the palladium catalyst was 335.60 eV, which is in agreement with recent studies of particles 7 nm or less in diameter [106, 107]; our particles are 7.5 nm [258], which is the optimal size for formic acid oxidation on palladium. [106] On the blank palladium sample we do not find evidence of oxygen in the O 1s or 2s regions. Addition of antimony or tin to the palladium results in higher binding energies for the Pd $3d_{5/2}$: we see a shift of 0.50 eV to 336.10 eV in the PdSb and a shift of 0.40 eV to 336.01 eV in the PdSn. However, the slight shift of 0.16 eV to 335.76 eV in the PdPb is attributed to a range of instrument error (±0.10 eV) or a slight charging effect. The difference in electronegativity between the palladium and the antimony or tin indicates that the adatoms donate electrons to the palladium metal, but in the case of the lead adatom, the donation is reversed. In addition, the Pourbaix diagrams suggest that, in the potential regions in which we are adsorbing the adatoms, the tin and antimony will be in an oxide form on the surface; the lead should be elemental. [259] Indeed, we find that the binding energies for Sn $3d_{5/2}$ and Sb $3d_{5/2}$ are well within the range of binding energies indicating the presence of their respective oxides.

Previously, it has been reported that an increase in binding energy (due to a decrease in particle size in this case) is strongly correlated with an increase in the rate of formic acid oxidation. [105] Yang, et al., have recently shown a shift from 335.5 to

336.0 eV with the alloying of phosphorus to carbon supported palladium, while the peak potential in the voltammetry for formic acid oxidation increases significantly with the addition of phosphorous. [107] In addition, others have shown by XPS that there is an electronic effect on platinum by both tin and lead. [219, 252] However, since platinum and carbon supported palladium catalysts are inferior for the DFAFC, we are interested in whether we can produce similar effects on our unsupported palladium catalysts. [25] Our PdSb and PdSn catalysts in particular show some promotion for formic acid oxidation over 9 hours in the fuel cell, and we cannot entirely attribute this to reduced CO buildup (see Figure 7.6). We are seeing a shift to higher binding energy, which suggests an electronic effect that promotes formic acid oxidation on PdSb and PdSn. We do not see a significant shift in binding energy with the PdPb catalyst. Although the PdPb catalyst demonstrates the strongest resistance to CO buildup after 1 hour and even after 3 hours, the catalyst performs as poorly as the Pd catalyst beyond 3 hours, which suggests that once it is no longer resistant to CO build up, there is not much electronic effect in PdPb that would promote formic acid oxidation.

7.5 Conclusion

We have studied palladium catalysts for the oxidation of formic acid. Although we do not expect much CO buildup on palladium during formic acid oxidation, we do observe enough CO buildup over several hours that causes severe performance losses in the DFAFC. We added antimony, lead, and tin to these palladium catalysts in hope that we would block CO formation, but we found that CO formation is lower only at time periods less than 3 hours. We did see a strong promotion of formic acid in the electrochemical cell up to 3 hours, and to a much lesser extent in the fuel cell beyond 3

hours. Since we have significant CO coverage after short time periods, we attribute some of the oxidation rate promotion to the electronic effect, whereby we observe a positive shift in palladium core level binding energy with the addition of antimony or tin. We have not solved the problem of CO poisoning in the DFAFC. But we have made some suggestions for evidence that there is a weak steric effect in PdSb and PdPb and some electronic effect on PdSb and PdSn; these effects each lead to the promotion of formic acid that we observe in the electrochemical cell to a large extent and in the fuel cell to a lesser extent.

7.6 Acknowledgements

This work was supported by the Army Research Office under contract W911N F-05-C-0110 and the Defense Advanced Research Projects Agency (DARPA) under grant DST 2007-0299513- 000-1. The opinions are the authors and do not reflect the findings of the Army Research Office, DARPA or the US government. XPS analysis was carried out with Dr. Richard T. Haasch in the Frederick Seitz Materials Research Laboratory Central Facilities, University of Illinois, which is partially supported by the U.S. Department of Energy under grants DE-FG02-07ER46453 and DE-FG02-07ER46471.

7.7 Figures

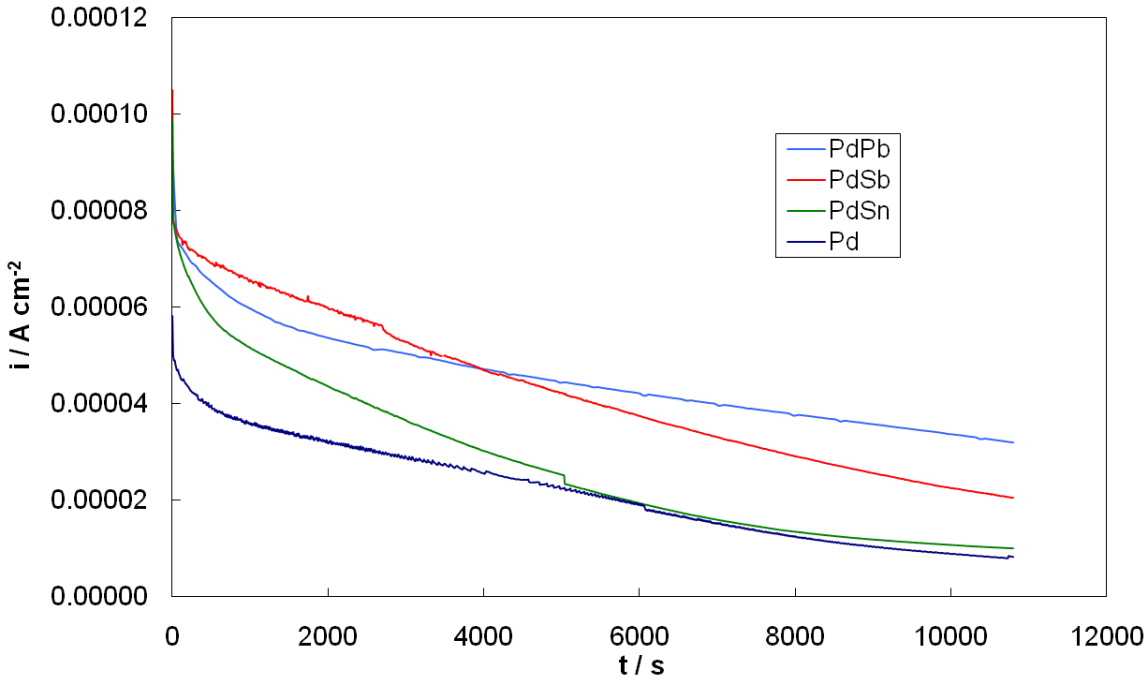

Figure 7.1. Constant voltage tests (0.3 V vs RHE) with four different high surface area palladium-based catalysts for formic acid (12 M) oxidation in an electrochemical cell at room temperature (~22°C) for 3 hours. After three hours the oxidation rate with the PdPb catalyst is four times that of the Pd catalyst, while with PdSb it is about 2.5 times greater, and with PdSn it is 25% greater.

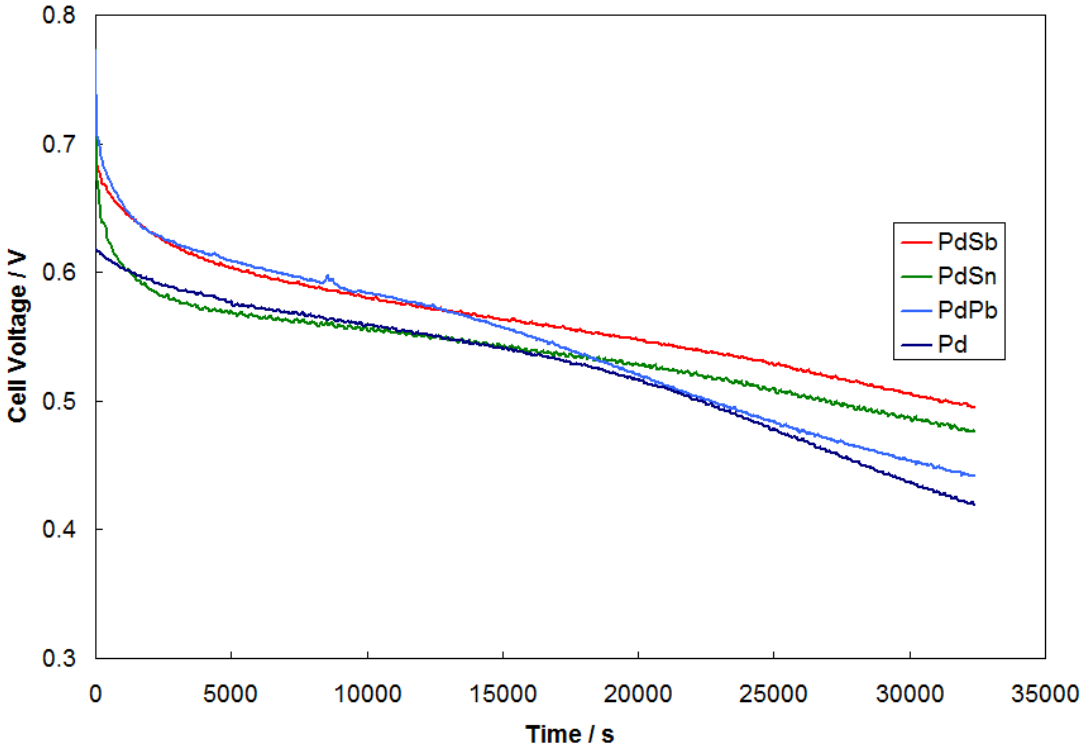

Figure 7.2. Constant current (100mA cm^{-2}) tests for four different palladium-based high surface area anode catalysts in the direct formic acid fuel cell operating at room temperature (~22 °C) for 9 hours. Formic acid is flowed at 0.15 mL min^{-1} on the anode and air is pumped over the cathode at 300 sccm. The Pd and PdSb data is from [33], and is included here for comparison to the other catalysts. The promotion of formic acid oxidation is much less in the fuel cell than it is in the electrochemical cell.

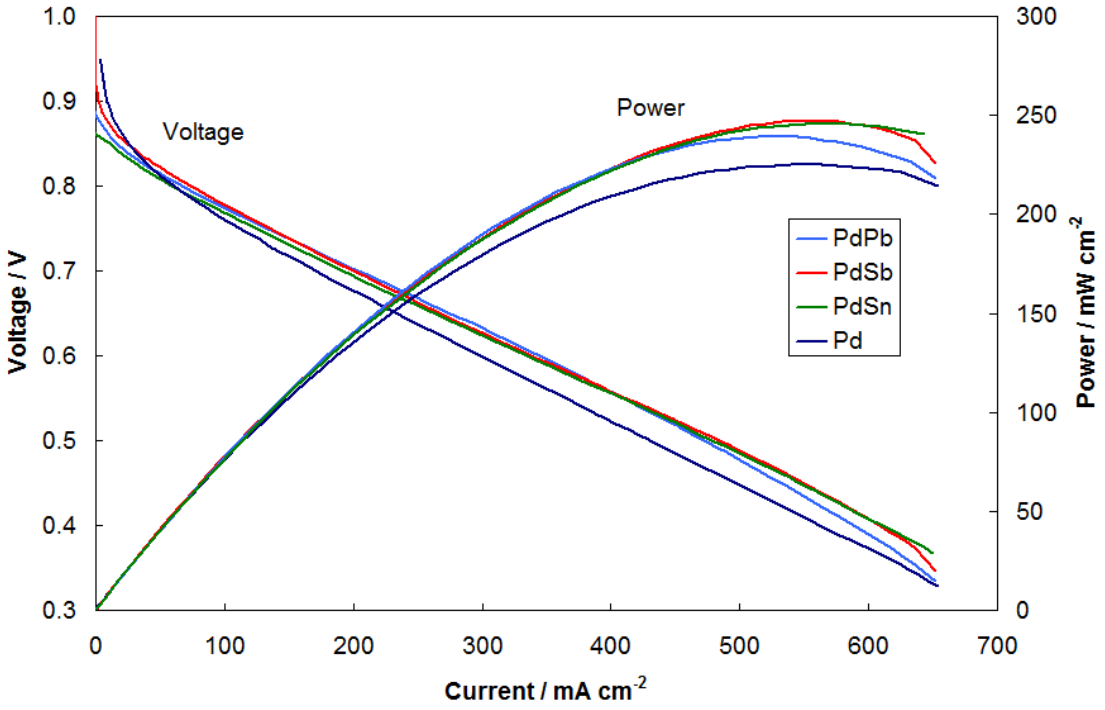

Figure 7.3. Polarization curves for four different palladium-based high surface area anode catalysts in the direct formic acid fuel cell operating at 30 °C. Formic acid is flowed at 1.0 mL min^{-1} on the anode and air is pumped over the cathode at 300 sccm. The Pd and PdSb data is from [33], and is included here for comparison to the other catalysts.

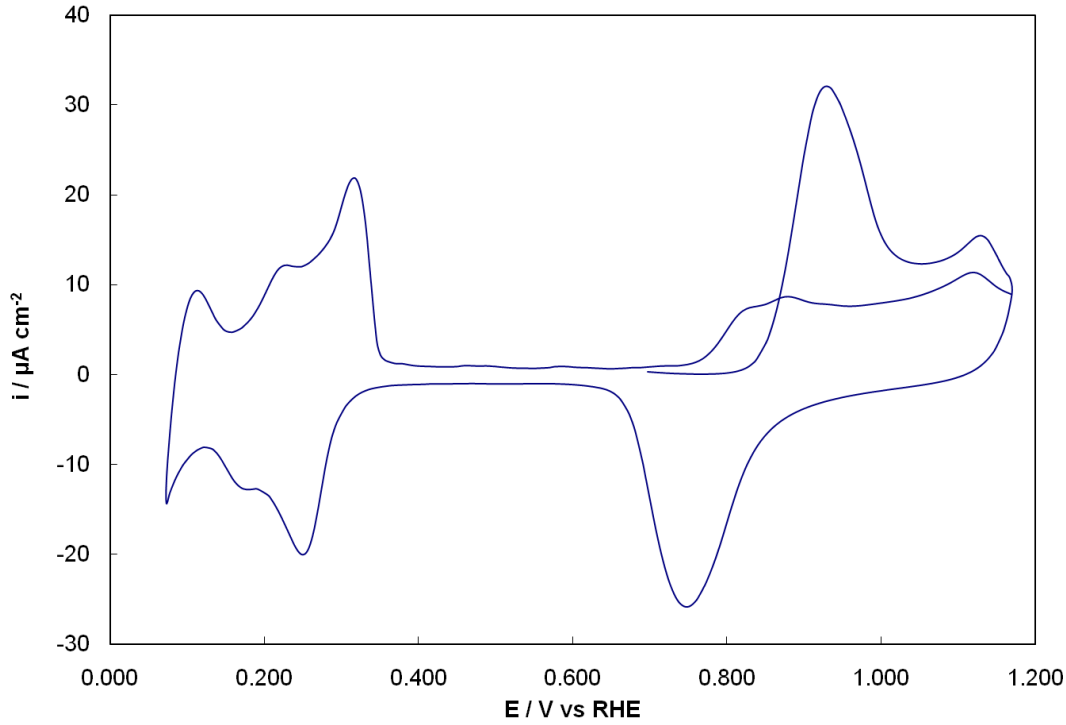

Figure 7.4. A sample CO stripping voltammogram (10mV/s) on palladium black following 3 hours of formic acid (12 M) oxidation at 0.3 V vs RHE. The CO peak is evident on the first scan between 0.9 and 1.0 V vs RHE. Once the CO is oxidized from the surface, peaks are observed both in the hydrogen adsorption/desorption regions (0.1 to 0.3 V vs RHE) and the surface oxidation (beyond 0.7 V vs RHE) and reduction (0.9 to 0.7 V vs RHE) regions.

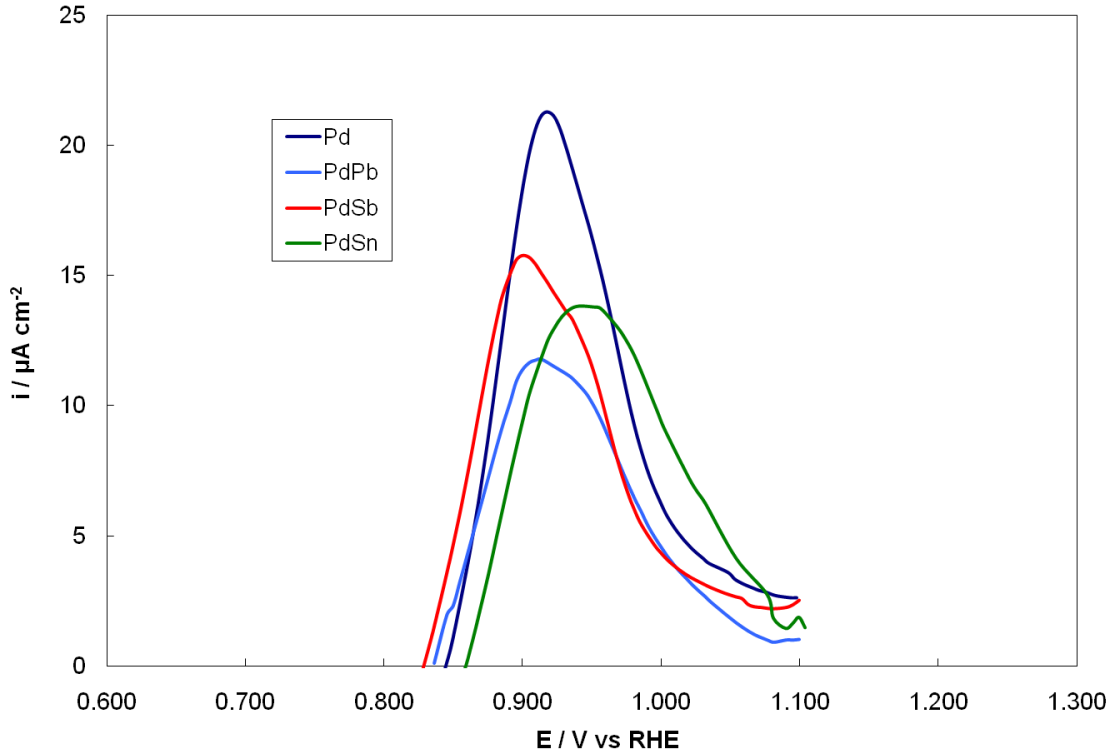

Figure 7.5. CO stripping voltammograms (10mV/s) following 1 hour of oxidation in 12 M formic acid at 0.3 V vs RHE. The data shown is the difference between the current density while the CO is removed from the surface in the first sweep and the current density while oxidizing the surface in the second sweep.

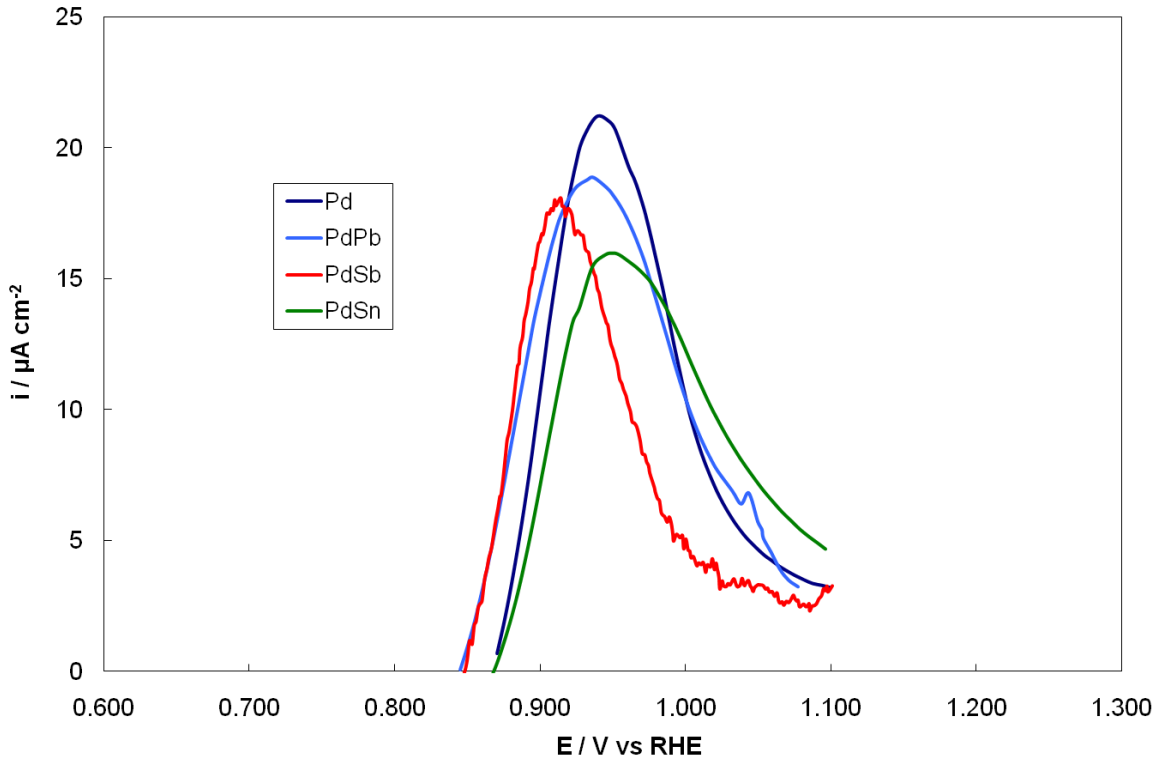

Figure 7.6. CO stripping voltammograms (10mV/s) following 3 hours of oxidation in 12 M formic acid at 0.3 V vs RHE. The data shown is the difference between the current density while the CO is removed from the surface in the first sweep and the current density while oxidizing the surface in the second sweep.

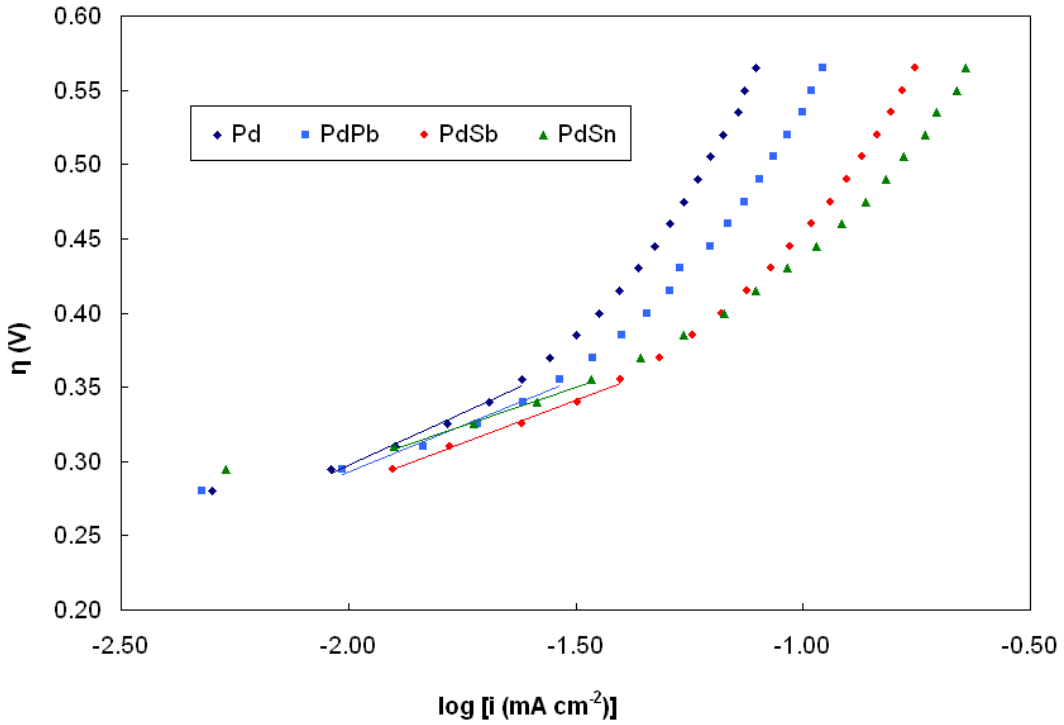

Figure 7.7. Tafel plots for formic acid oxidation on the four catalysts in 0.1 M HCOOH + 0.1 M H_2SO_4. Data points were obtained after holding the potential for 3 s. The palladium catalyst exhibits the highest Tafel slope (164 mV/decade), while the PdSn catalyst exhibits the lowest slope (105 mV/decade).

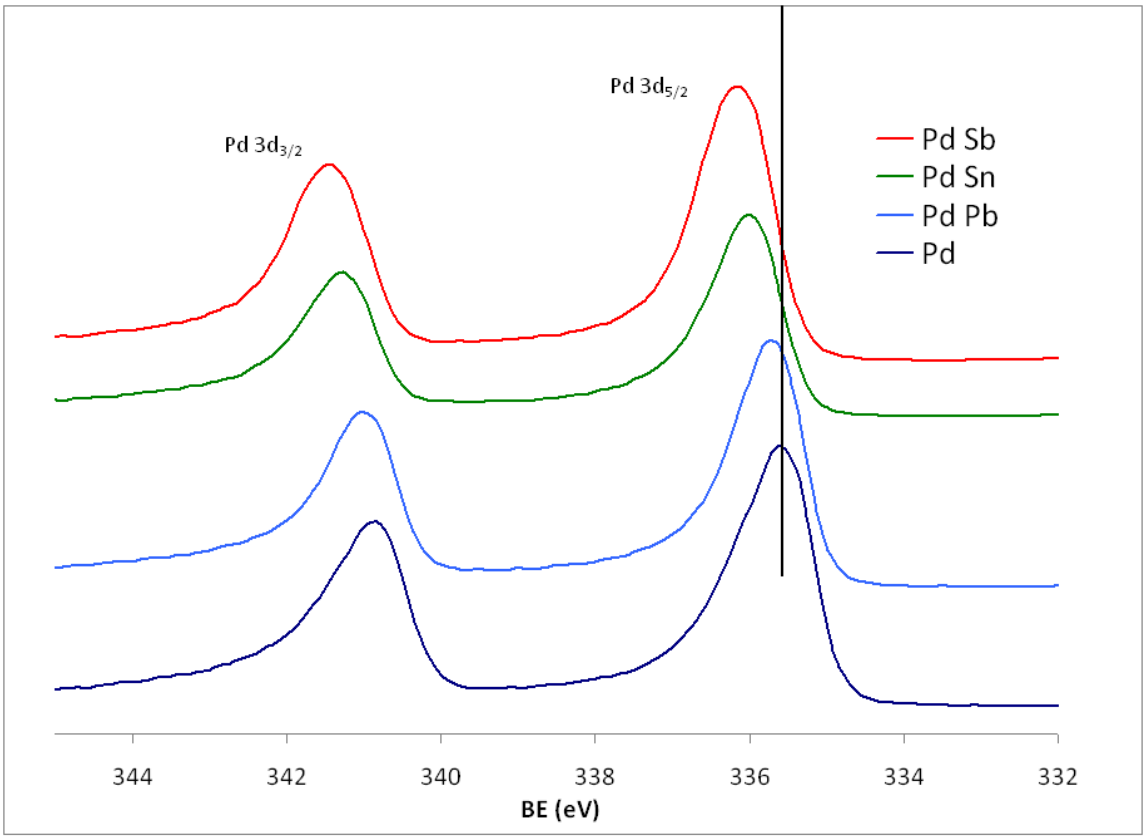

Figure 7.8. The core level binding energy of palladium $3d_{5/2}$ and $3d_{3/2}$ when the adatoms are added to the palladium via electrochemical surface modification. The vertical line at 335.60 eV indicates the peak position for Pd $3d_{5/2}$ when no adatom is present. Deviation from this peak position is due to the presence of the adatom.

Chapter 8: Electrochemistry of Carbon Dioxide Reduction in the Ionic Liquid 3-Ethyl-1-Methyl-Imidazolium Tetrafluoroborate

This chapter represents contributions of the author to three manuscripts in preparation that will be submitted for publication shortly.

8.1 Introduction

The earth contains an abundance of fossil fuels which provided energy for the industrial revolution and remain the primary source of energy in most developed and developing nations. However, the combustion of such fuels produces a highly stable carbon dioxide product. Carbon dioxide is known to be a greenhouse gas, contributing to recent climatic warming trends as its concentration climbs to high levels not observed in the past 50 million years. [2, 3] Therefore, there have been significant efforts in recent years to control emission of carbon dioxide, by capturing it in the waste stream of combustion reactions or by resorting to alternative low-emission fuels. The first strategy would permit the underground storage of carbon dioxide to prevent release into the atmosphere that would further increase atmospheric carbon dioxide concentration. However, there is a significant energy cost to this process, which would either negate the benefit or substantially drive up energy costs. [5] The strategy of using alternative fuels as primary energy sources is not economically feasible especially in developing countries, because of the availability and low cost of fossil fuels. In addition to concerns about carbon dioxide emission, there is a growing awareness that the supply of fossil

fuels is not limitless. Therefore, we are interested in a new strategy that captures carbon dioxide in a waste stream and converts it into a hydrocarbon fuel. [6] This would reduce the amount of carbon dioxide that is released from energy usage and would also reduce our dependence on fossil fuels that are extracted directly from the ground. It has been suggested recently that this process of carbon dioxide capture and conversion can be done using sunlight, a renewable energy source that does not produce harmful waste products. [2]

Electrochemical reduction of carbon dioxide has been extensively studied during the last decade in aqueous solutions and organic solvents on a variety of electrodes. [108-157] In aqueous solutions, the following products can be formed: formic acid, carbon monoxide, formaldehyde, methanol, and methane; the product depends on the electrode, its potential, and the electrolyte. [158] The advantage of using aqueous solutions is that the water provides a proton source; for example the overall equation for the formation of carbon monoxide is:

$$CO_2 + 2\ H^+ + 2\ e^- \rightarrow CO + H_2O \quad E^o = -0.104\ V\ vs\ SHE \quad (8.1)$$

However, one disadvantage of using aqueous solutions is that the hydrogen evolution reaction (HER) begins at 0.000 V vs the standard hydrogen electrode (SHE). The competition between the two reductions decreases the Faradaic efficiency of carbon dioxide reduction. [109, 119, 120, 159, 160] Another complication with aqueous solutions is that carbon dioxide is not very soluble, especially at lower pH. At a pH of 9, where carbon dioxide is more soluble, the reduction potential for Equation 8.1 is -0.635 V vs SHE.

In aprotic organic solvents, the primary products formed are carbon monoxide and oxalic acid [158, 161]:

$$2\ CO_2 + 2\ e^- \rightarrow CO + CO_3^{2-} \qquad E^o = -0.642\ V\ vs\ SHE \qquad (8.2)$$

Although the reaction is not as thermodynamically favorable as in aqueous solutions, the absence of HER allows for a more efficient reduction to CO. However, carbon dioxide still is not very soluble in aprotic organic solvents.

In order to efficiently reduce carbon dioxide to carbon monoxide in the absence of hydrogen evolution, we used room temperature ionic liquids (RTILs) as solvents. RTILs are thermally stable, can be tailored to specific applications, and the cations can stabilize anion intermediates. They also provide a large potential window for electrocatalysis when compared with aqueous solutions, which are bounded for practical surface electrochemistry by hydrogen and oxygen evolution reactions. In addition, carbon dioxide is quite soluble in RTILs compared with aqueous solutions. [170, 173-177] In aprotic solvents, a charged intermediate is formed during the rate-determining step (rds) in the reduction of carbon dioxide to carbon monoxide and carbonate [109 , 158, 162-167]:

$$CO_2 + e^- \rightarrow {}^{\cdot}CO_2^- \qquad \text{(rate-determining step)} \qquad (8.3)$$

$$2\ {}^{\cdot}CO_2^- \rightarrow C_2O_4^{2-} \qquad (8.4)$$

$$C_2O_4^{2-} \rightarrow CO + CO_3^{2-} \qquad (8.5)$$

It has been shown that the ${}^{\cdot}O_2^-$ intermediate formed during oxygen reduction in 1-butyl-3-methyl-imidazolium bis(trifluoromethylsulfonyl)imide (BMIM NTf_2) forms a complex

between the intermediate and the $BMIM^+$ cation. [168, 169] This intermediate causes a positive shift in the reduction potential by 0.65 V. We expected that we also could use ionic liquids to lower the reduction potential required to form the $\cdot CO_2^-$ radical intermediate, which could significantly reduce the amount of energy needed to produce carbon monoxide from carbon dioxide reduction. In addition, CO_2 forms a weak complex with some imidazolium cations, which suggests that the charged $\cdot CO_2^-$ would also form such a complex. [170-172]

We used broad-band sum frequency generation (BB-SFG) to study the mechanism of carbon dioxide reduction on platinum in ionic liquid so that we could compare the ionic liquid solvent with previous studies in aprotic organic solvents. BB-SFG has been demonstrated recently as a useful tool for probing an electrode surface during electrochemical reactions in thin-layer electrochemistry (TLE). [194-196] Specifically, the adsorption of CO molecules on platinum polycrystalline and single crystal surfaces has been studied, with an ability to differentiate between singly- and multiply-bonded CO molecules. [194] CO stripping experiments demonstrated that the electrochemistry in the TLE correlates directly with the presence, then disappearance, of CO signal in the SFG spectra during an anodic potential scan. Platinum strongly promotes the formation of CO from carbon dioxide reduction in aprotic solvents. Since CO adsorbs strongly to platinum and has a strong vibrational signal, SFG is an excellent tool to study carbon dioxide reduction on platinum in ionic liquids; this work has not been done previously.

8.2 Experimental

Rotating Disk Electrochemistry. A standard three-electrode electrochemical cell was used with a Solartron potentiostat (SI 1287), a platinum mesh counter electrode, and a silver/silver wire reference electrode (BAS). The reference solution was acetonitrile, 0.01 M silver nitrate, and 0.1 M tetrabutylammounium phosphate, and the reference was calibrated to the ferrocene redox couple. [201] The reference potential was found to be +0.535 V vs SHE and repeatable over several experiments in EMIM BF_4. The working electrode was platinum black (Alfa Aesar) on a rotating disk electrode (Pine) set to 2000 rpm, according to the Koutecky-Levich plot in Figure 8.1. The ionic liquid was used as the electrolyte. Although the size of the ions and the high viscosity result in lower conductivity than aqueous solutions with support electrolytes, the conductivity is still greater than organic solvents with support electrolytes; the conductivity of the ionic liquid is sufficiently high to perform the voltammetric experiments in this work without the addition of a support electrolyte. [203] The ionic liquid was prepared by heating overnight just above 100 °C under convection and vacuum in order to remove any residual water or dissolved gases. During electrochemical experiments, the ionic liquid was purged with argon (UHP, S.J. Smith) to take baseline measurements assuring a large potential window and the absence of water. For carbon dioxide reduction, the ionic liquid was purged with carbon dioxide (99.99%, S.J. Smith).

Thin Layer Electrochemistry. Electrochemistry was carried out in a three electrode, thin-layer configuration for simultaneous surface spectroscopy with BB-SFG as reported previously. [194-196] We used a 50 μm Teflon spacer to create a gap in

which the correlation between the electrochemistry and the spectroscopy was correct. Constructing the electrochemical cell was a Kel-F and glass cylinder and an optical window made of CaF_2. A glass plunger held the polycrystalline platinum disk of diameter 6 mm, which was the working electrode. Experiments reported here in the TLE configuration were carried out at 5 mV s^{-1}. The counter electrode was a platinum wire, and the reference electrode was the silver/silver wire reference. A PAR 263A potentiostat was used for electrochemical measurements.

Broad-Band Sum Frequency Generation. The laser apparatus used in this experiment has been shown previously. [194-196] An IR beam and a visible beam were focused to a 400 μm spot size on the crystal surface with a pulse rate of 10^3 s^{-1}. The visible beam power was 4.0 μJ while the IR was centered at 6300 or 6500 nm to probe the ionic liquid peaks. The power was reduced to 2.5 μJ when probing the CO peaks (at an IR wavelength of 4250 or 4800 nm) in order to prevent laser-assisted desorption of the CO. Individual spectra were taken at each IR wavelength while the potential was held but not scanned. Potential scans at 5 mV s^{-1} were taken while the CCD detector was synchronized with the potentiostat to allow for direct correlation between the electrochemistry and the spectra; this synchronization was verified prior to data analysis. Such scans were also taken at specific IR wavelengths in order to probe different spectral regions and intensify the peaks of interest.

8.3 Results

Rotating Disk Electrochemistry. Koutecky-Levich plots are shown in Figure 8.1 at two different potentials for CO_2 reduction on platinum black in CO_2-saturated

EMIM BF_4. At these potentials there is a linear dependence of $(current)^{-1}$ and $(rotation\ rate)^{-1/2}$ in the rotation rate range of 1200 to 6000 rpm. The slope of these curves is approximately -1350, and the current at the intercept for no rotation is extrapolated to be 7.14 mA cm^{-2} at -0.75 V and 9.03 mA cm^{-2} at -0.95 V. To construct these plots, the potential was held at steady state for 30 seconds at each scan rate, and the current at 30 seconds was plotted. Linear sweep voltammograms are shown in Figure 8.2 demonstrating the reduction wave for CO_2 reduction on platinum black in CO_2-saturated EMIM BF_4. The rotation speed, 2000 rpm, was chosen because it is centered in the linear region of the Koutecky-Levich plot shown in Figure 8.1. The onset of the CO_2 reduction is between -0.4 and -0.5 V vs SHE. A plot of potential vs. log (current) was constructed using the CO_2 reduction data at 2000 rpm; it is shown in Figure 8.3. The Tafel slope is found to be 727 mV $decade^{-1}$.

Peak Assignments. Four significant BB-SFG peaks are observed during potential control on a platinum disk electrode in EMIM BF_4. The most prominent peak near 2050 cm^{-1}, shown in Figure 8.4, is due to the CO adsorption on platinum. [194] Here it is shown at open circuit potential following several negative potential cycles in CO_2-saturated solution with a 2.5 μJ visible beam at 800 nm and an infrared beam at 4800 nm. A peak attributed to adsorbed $\cdot CO_2^-$ is observed at 2350 cm^{-1}, when the potential is held at -0.8 V, a potential of maximum intensity, and the IR beam is at 4250 nm. One would expect to observe gaseous CO_2 at this wavenumber, but adsorbed CO_2 should be red-shifted to lower wavenumbers. [260, 261] In addition, we observe that this peak is not present initially until the electrode potential is scanned into the Tafel potential region

where CO_2 is converted to $\cdot CO_2^-$ in the ionic liquid. This correlation will be discussed further. Two peaks attributed to the ionic liquid are observed at ~1430 and ~1570 cm^{-1}, as shown in Figure 8.6, and both peaks are present in argon saturated EMIM BF_4 as well as CO_2 saturated EMIM BF_4. The peak at 1430 cm^{-1} is attributed to CH_3 bending modes, while the peak at 1570 cm^{-1} is attributed to stretching in the imidazolium ring. [262, 263]

Platinum Disk Electrochemistry and Broad-Band Sum Frequency Generation. The linear sweep voltammogram in CO_2-saturated EMIM BF_4 on platinum at 200 mV s^{-1} with a meniscus formed as compared with the same sweep in Ar-saturated liquid is shown in Figure 8.7. The reduction current slowly increases at negative potentials and then somewhat more rapidly below -0.3 V vs SHE. It then changes slope significantly below -0.5 V. Finally, a current maximum is reached at -0.95 V, at which point the reduction current decreases until it reaches -1.3 V. When multiple cycles are swept in the thin-layer cell to -1.3 V at 75 mV s^{-1}, CO gradually builds up on the surface with each cycle, as shown in the SFG spectra in Figure 8.8. When cycles are swept to much less negative potentials, CO builds up much more slowly, as shown in Table 8.1. When swept to potentials lower than -0.95 V, a very strong CO signal is observed after less than 10 cycles. At -0.94 V, it takes 18 cycles to produce a strong CO signal. However, at potentials higher than -0.94 but lower than -0.54 V, there is only a weak CO signal after 40 or more cycles. Finally, when cycled to potentials -0.54 and higher, there is very little CO signal observed. The series of spectra shown in Figure 8.9 shows the development of the peak at 2350 cm^{-1} on a clean platinum surface in CO_2-saturated EMIM BF_4. This series was taken at 4250 nm with 10 s acquisition time during a 5 mV

s^{-1} linear sweep from 0.56 V to -1.04 V in CO_2-saturated liquid. In this series, the peak appears at negative potentials and then it grows in intensity within the Tafel region. This series correlates well with the electrochemistry shown in Figure 8.7.

8.4 Discussion

Rotating Disk Electrochemistry. The Koutecky-Levich plots shown in Figure 8.1 demonstrate a linear dependence between $(\text{current})^{-1}$ and $(\text{rotation})^{-1/2}$ for a wide range of rotation rates as predicted from the Koutecky-Levich equation, which relates the current and rotation rate for an irreversible, one step, one electron reaction:

$$\frac{1}{i} = \frac{1}{i_K} + \frac{1}{0.62nFAD_o^{2/3}\omega^{1/2}\nu^{-1/6}C_o^*} \qquad (8.6)$$

where i_K is the current in the absence of mass transport effects. We find that, for two different potentials, the slope is similar, but i_K is different and also non-zero. Therefore, the electron transfer rate is the limiting factor in the measured current because mass transfer is efficient enough to keep the reactant concentration at the electrode surface equal to the concentration in the bulk. [16] Figure 8.2 shows that the practical lower potential limit of the ionic liquid is ~ -1.4 V. Therefore, EMIM BF_4 has a large enough potential window to study the electrochemical reduction of CO_2, for which we see initial stages of reduction at between -0.4 and -0.5 V.

The Tafel slope calculated from Figure 8.3 is similar to that found for carbon dioxide reduction on platinum in acetonitrile (600-700 mV dec^{-1}). [166, 167] This Tafel slope in acetonitrile is attributed to the initial electron capture by CO_2 to form $\cdot CO_2^-$, which corresponds with Equation 8.3, the rds in aprotic solvents. We find that, since the

onset for CO_2 reduction is -0.4 to -0.5 V, the Tafel region begins in this potential range and continues to ~ -0.8 V in EMIM BF_4. In acetonitrile, the Tafel region was shown to begin at ~ -1.0 V vs SHE. Therefore, the onset potential of the rds for carbon dioxide reduction in EMIM BF_4 is more positive than it is in acetonitrile. It is very likely that this is due to a stabilization of the $\cdot CO_2^-$ intermediate formed in the rds following electron capture by the carbon dioxide.

Platinum Disk Electrochemistry and Broad-Band Sum Frequency Generation. We also see features that correspond to carbon dioxide reduction in the voltammogram on a smooth platinum disk electrode (Figure 8.7). At potentials (i.e., below zero in Figure 8.7) where an electron is transferred during the rate-limiting step, conversion of CO_2 to $\cdot CO_2^-$, we observe the appearance and growth of a BB-SFG peak at 2350 cm^{-1}, as shown in Figure 8.9. [167] Therefore, we have attributed this peak to the charged anionic intermediate, $\cdot CO_2^-$, which is the product of a CO_2 molecule that captures an electron in the rate-limiting step. It is likely that this intermediate appears at much less negative potentials in the ionic liquid than in acetonitrile because it is stabilized by the ionic liquid.

The features in Figure 8.7 also correlate with the speed at which the CO molecules are formed on the surface of the platinum disk electrode as reported in Table 1. In the first region (~ -0.3 to -0.6 V vs SHE), there is a trace amount of CO formation, and the current density is less than 1 mA cm^{-2}. In the second region, where the slope is flat (~ -0.6 to -0.9 V), there is a weak signal indicating CO formation. In the final region, where

the current density increases again and approaches 2 mA cm^{-2}, the CO signal is much stronger, indicating more CO formation following the rate-determining electron transfer step that produces the charged anionic intermediate. Indeed, when several potential cycles are scanned as far negative as -1.4 V, there is rapid buildup of CO on the electrode surface; spectra from every other cycle are shown in Figure 8.

When an ionic liquid with an alkyl-methylimidazolium cation interacts with a platinum surface, its interaction can be simplified to that of a Helmholtz double layer, in which no solvation occurs (due to the lack of solvating molecules), and the charged ions shield the charged surface from the bulk liquid. [185] The imidazolium ring has its charge centered on the aromatic ring, although the charge density slightly favors the carbon bonded to both nitrogens. In the case of BMIM BF_4 adsorbed on a platinum surface, the ring lies approximately 30° from parallel with the surface when the surface is held at a potential negative of its point of zero charge (PZC) so that the positive charge on the ring can shield the negatively charged electrode surface from the bulk. [185] When the potential is scanned positive of the PZC, the ring tilts to 45° from the surface to allow the anion better access to the surface to balance the charge. Similar behavior is observed on other surfaces and is predicted from molecular simulations. [186-188] It also has been shown that a smaller alkyl chain (e.g., the ethyl chain used in our work) should further favor a parallel orientation at low potentials. [189] The PZC for EMIM BF_4 has been reported as -0.25 V vs SHE, which suggests that the ionic liquid used in our experiments should be oriented less than 45° to the platinum surface within the potential window in

which our carbon dioxide reduction takes place. [190] Future work will determine the orientation of the ionic liquid EMIM BF_4 on our platinum disk electrode.

8.5 Conclusion

We have shown via electrochemistry and spectroscopy that carbon dioxide is first reduced to its charged anionic intermediate, $\cdot CO_2^-$, at potentials more positive than previously shown for the aprotic solvent acetonitrile; this reduction is followed shortly by CO formation. We suggest that the reason for the less negative reduction potential is that the charged anionic intermediate is stabilized by ionic liquid.

8.6 Acknowledgements

This work was supported by the Army Research Office under contract W911NF-05-C-0110 and the Defense Advanced Research Projects Agency (DARPA) under grant DST 2007-0299513- 000-1. The opinions are the authors and do not reflect the findings of the Army Research Office, DARPA or the US government.

8.7 Figures and Tables

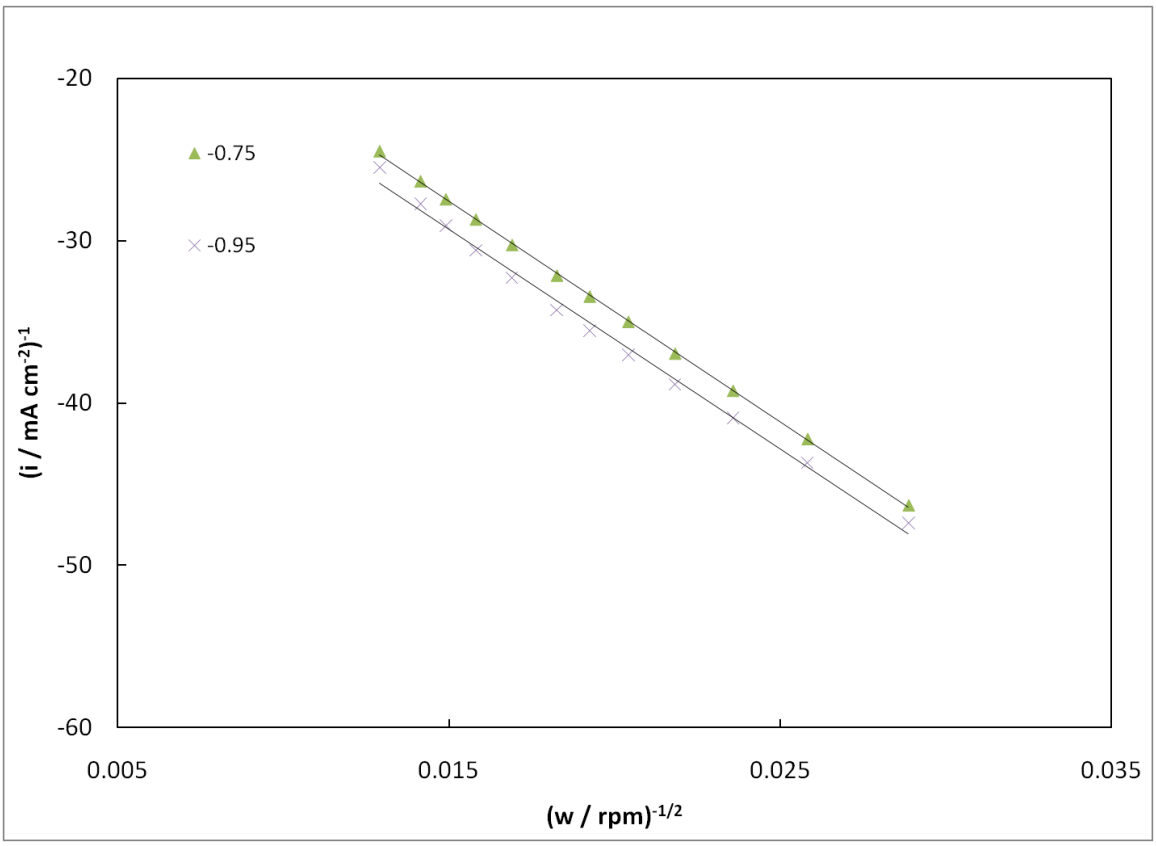

Figure 8.1. Koutechy-Levich plot for CO_2 reduction in EMIM BF_4 saturated with CO_2. The slope is approximately 1350 (mA cm^{-2} $rpm^{-1/2}$)$^{-1}$. The current at zero rotation, i_K, is -7.14 mA cm^{-2} at a potential of -0.75 V and -9.03 mA cm^{-2} at a potential of -0.95 V.

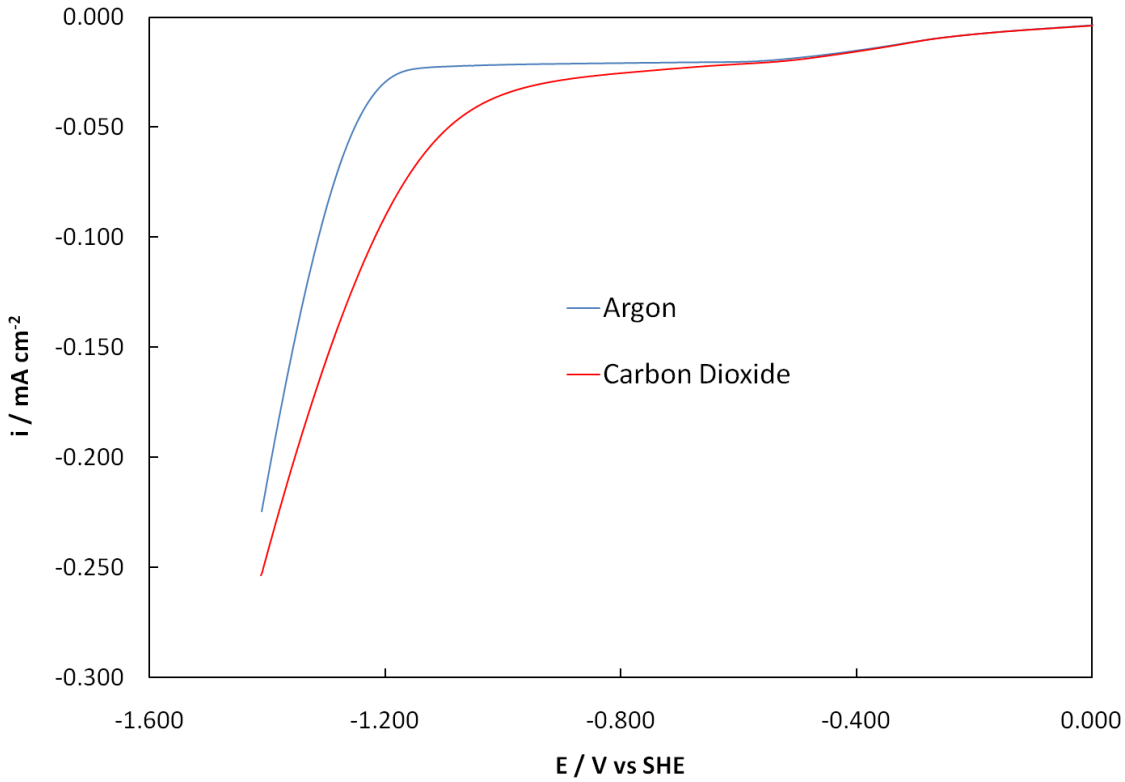

Figure 8.2. Linear sweep voltammetry shows evidence of the CO_2 reduction reaction in CO_2 saturated EMIM BF_4 on platinum black catalyst at a rotation speed of 2000 rpm, which is within the linear region of the Koutecky-Levich plot show in Figure 8.1.

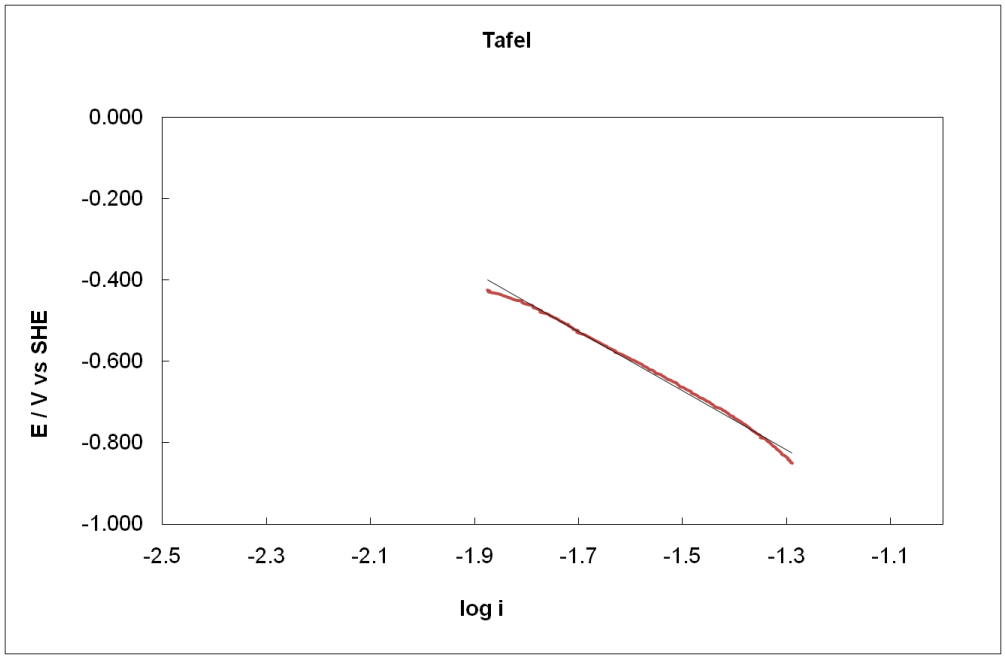

Figure 8.3. A plot of potential vs. log (current) was constructed for CO_2 reduction on platinum black catalyst in EMIM $BF_{4,}$ room temperature ionic liquid. This plot shows that the Tafel slope for this reduction is 727 mV/decade.

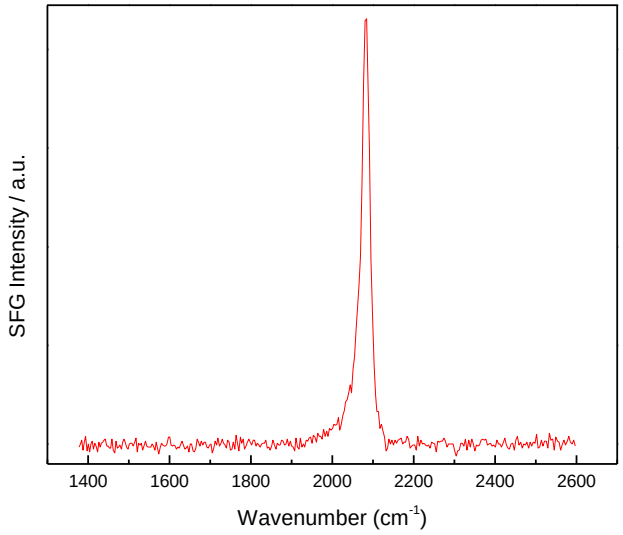

Figure 8.4. An SFG peak at ~2100 cm^{-1}, which is attributed to adsorbed CO, is shown at 0.535 V vs SHE, which is the open circuit potential following cycles in CO_2 saturated EMIM BF_4 on a platinum electrode. The spectrum was taken for 5 s with a 2.5 µJ visible beam (800 nm) and an IR beam of 4800 nm

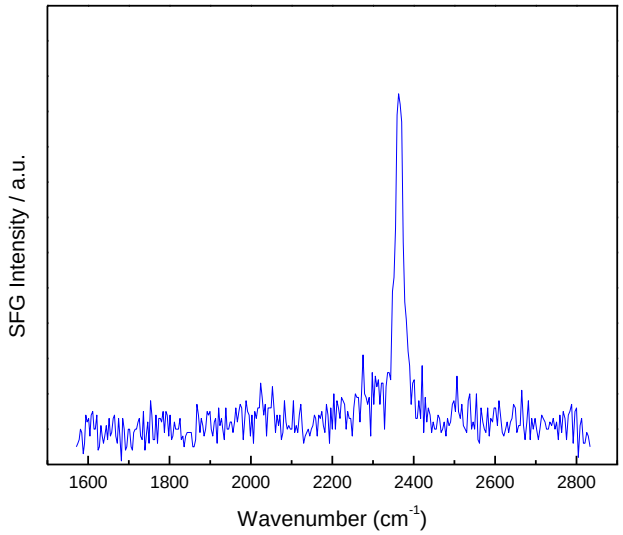

Figure 8.5. An SFG peak at ~2350 cm^{-1} attributed to $\cdot CO_2^-$ is observed at -0.8 V vs SHE, the potential where there is an intensity maximum in CO_2 saturated EMIM BF_4 on a platinum electrode. The spectrum was taken for 10 s with a 2.5 μJ visible beam (800 nm) and an IR beam of 4250 nm.

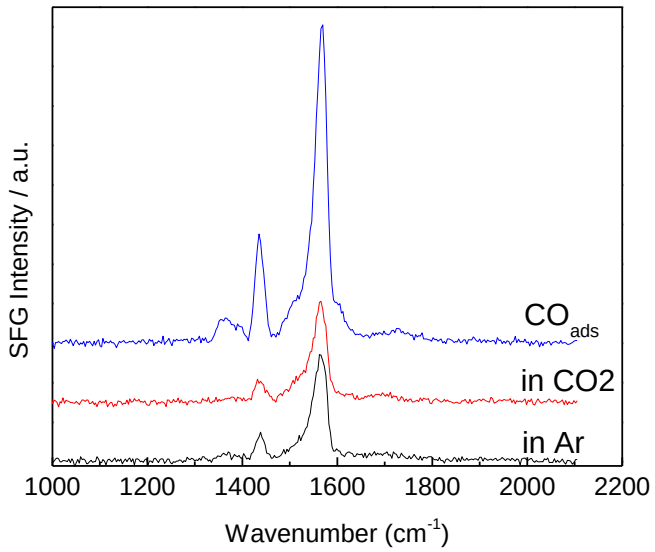

Figure 8.6. Two SFG peaks are observed in EMIM BF_4 at ~1430 (CH_3 bending) and ~1570 cm^{-1} (ring stretching). These peaks are present whether the liquid is saturated with argon or carbon dioxide, and the peaks are more intense when CO is adsorbed on the surface. The spectrum was taken for 50 s with a 4.0 μJ visible beam (800 nm) and an IR beam of 6300 nm. The spectra are offset on the y-axis to emphasize the differences.

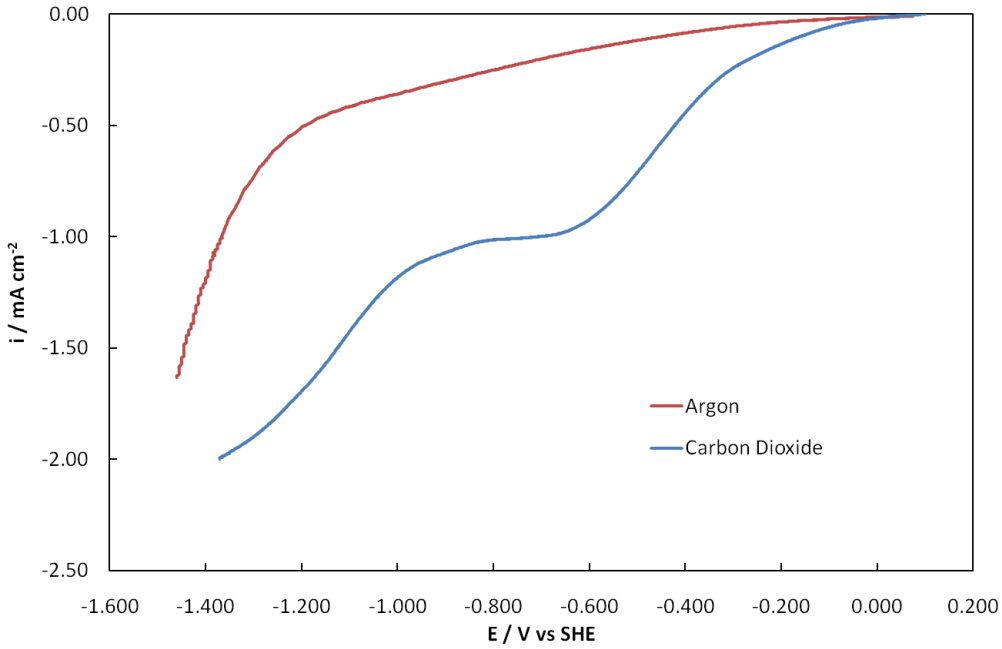

Figure 8.7. Linear sweep voltammogram with a meniscus formed between a platinum disk electrode and EMIM BF_4 at 200 mV s^{-1} in argon- and carbon dioxide-saturated liquid.

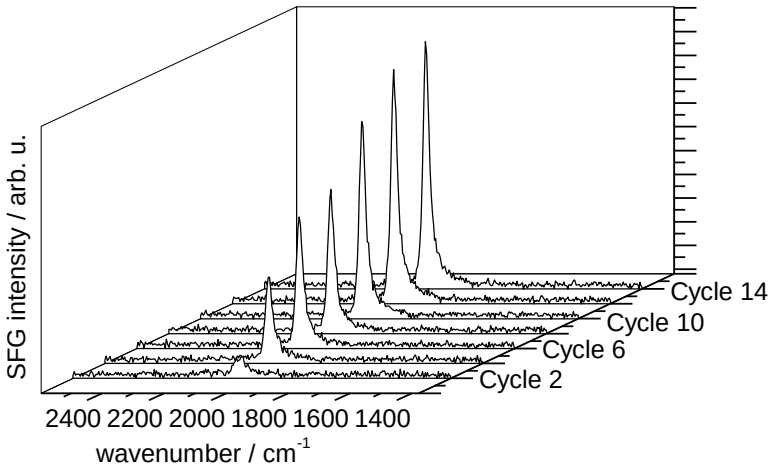

Figure 8.8. The CO signal in EMIM BF_4 increases with each potential cycle from 0.5 V to -1.4 V vs SHE. This is the CO signal at -0.2 V (open circuit potential) following each cycle.

Table 8.1. After a number of potential cycles at 75 mV s^{-1} to a certain potential minimum, a CO signal is observed. At lower potentials, the CO signal is quite strong. However, at less negative potentials, the signal is very weak.

Potential Minimum (V vs SHE)	Number of Cycles	Relative CO Signal Strength
-1.165	6	Very Strong
-1.065	8	Very Strong
-0.965	18	Strong
-0.865	40	Weak
-0.765	40	Weak
-0.665	40	Weak
-0.565	40	Trace
-0.465	40	Trace
-0.365	40	Trace
-0.265	40	Trace
-0.165	100	No Signal

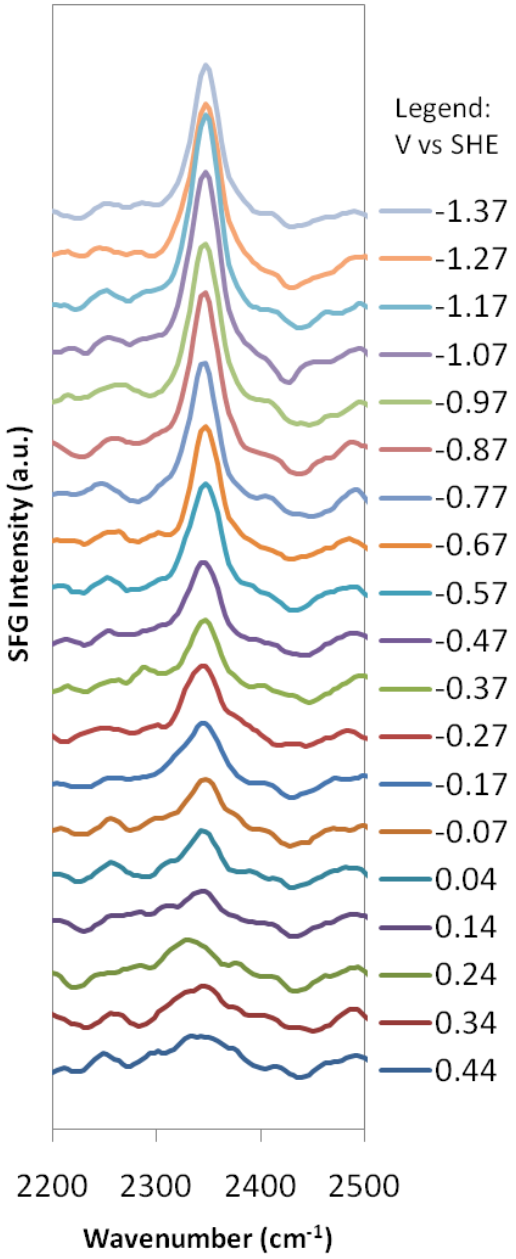

Figure 8.9. The $\cdot CO_2^-$ BB-SFG peak is observed during the first cathodic potential cycle as the potential is scanned in EMIM BF_4 at 5 mV s^{-1} on a platinum disk electrode. The acquisition time is 10 s with an 800 nm visible beam (2.5 uJ) and a 4250 nm infrared beam. As the potential is swept negative, the $\cdot CO_2^-$ peak begins to grow below at negative potentials.

Chapter 9: Conclusions and Future Work

9.1 Changes to Solution pH

It was shown that increasing the solution pH increases the rate of formic acid oxidation on both platinum and palladium nanoparticles. It was also shown that increasing the solution pH decreases the potential at which catalyst poison is oxidized; this means a lesser potential could be used to remove poison from the surface or that the poison could be removed at the same potential at which the formic acid is oxidized. This would result in substantial performance increases in the formic acid fuel cell. Work is being done now in the Masel research group by Rob Morgan that studies the effect of adding base to the binder in the catalyst ink that is used in the electrochemical cell. This work would eliminate the need to change the pH of the formic acid fuel and, therefore, eliminate the problems with membrane poisoning from the cation of the base.

9.2 Catalyst Modifications by Adatoms

Numerous catalyst formulations using palladium and some other metal were studied for their effects on the oxidation of formic acid. It was found that the irreversible adsorption of tin, antimony, or lead, on the surfaces of palladium nanoparticles promotes formic acid oxidation in an electrochemical cell and, to a lesser extent, in a fuel cell due to contributions from a steric effect and electronic effect. In this work, the hope was that the catalyst formulations might eliminate catalyst poisoning entirely. However, it was shown that substantial amounts of the catalyst poisoned over several hours in the electrochemical cell no matter which catalyst formulation was used. Work is being done now in the Masel research group by Kristin Stafford to study the effects of gold additions

to palladium, which has been suggested as a good catalyst formulation on carbon supported palladium. However, it is not likely that a new palladium-based catalyst will completely eliminate poison formation.

9.3 Carbon Dioxide Reduction

The reduction of carbon dioxide on platinum, on both nanoparticles and smooth electrodes, was shown to occur in ionic liquids at more positive potentials than previously shown in aprotic solvents. It is likely that the ionic liquid stabilizes the charged intermediate for carbon dioxide reduction because this rate-limiting step occurs at more positive potentials in the ionic liquid. Spectroscopic evidence was also shown for this charged intermediate adsorbing on the surface in this potential region. This is the beginning stage of a project involving several students in the Masel research group with the goal to convert carbon dioxide to usable fuels. Ongoing research will involve continued combination of electrochemistry and BB-SFG with single crystal surfaces of platinum. Additional work will study the electrochemistry other electrodes and other solutions in order to further optimize both carbon dioxide reduction and the formation of usable fuel products. Finally, work will be done to determine the orientation of the ionic liquid at the metal-liquid interface and its possible impact on stabilization of the charged intermediate. Preliminary data (Figures 9.1 – 9.3) shows that the BB-SFG peaks attributed to the ionic liquid in Chapter 8 are significantly different when different beam polarizations are set.

9.4 Figures

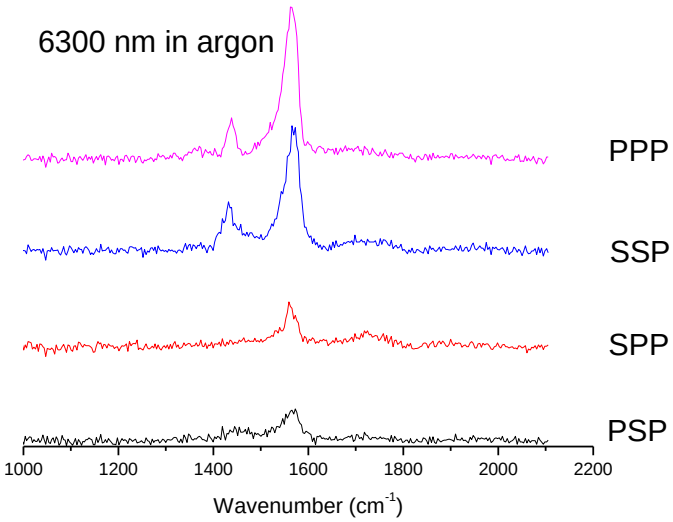

Figure 9.1. The two SFG peaks in EMIM BF_4 at ~1430 (CH_3 bending) and ~1570 cm^{-1} (ring stretching). In argon-saturated solution, the 1570 cm^{-1} peak is more intense in the PPP and SSP polarizations. However, the 1430 cm^{-1} peak that is present in the PPP and SSP polarizations disappears in the SPP and PSP polarizations. The spectra were taken for 50 s with a 4.0 μJ visible beam (800 nm) and an IR beam of 6300 nm. The spectra are offset on the y-axis to emphasize the differences.

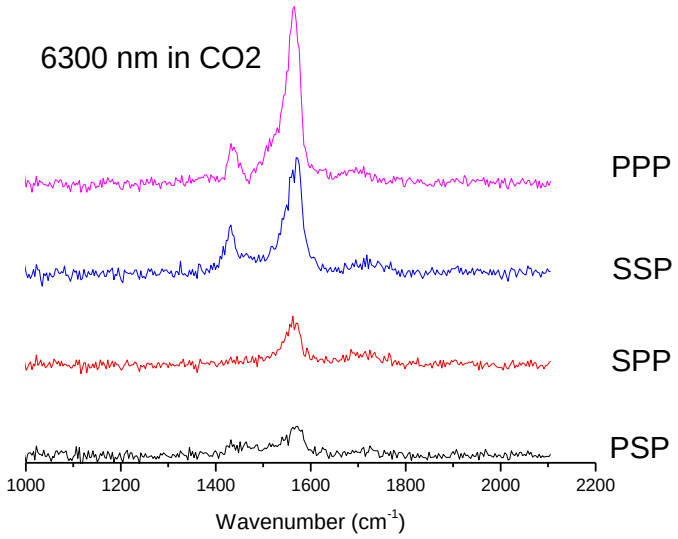

Figure 9.2 The two SFG peaks in EMIM BF_4 at ~1430 (CH_3 bending) and ~1570 cm^{-1} (ring stretching). In carbon dioxide-saturated solution, just as in argon-saturated solution, the 1570 cm^{-1} peak is more intense in the PPP and SSP polarizations. However, the 1430 cm^{-1} peak that is present in the PPP and SSP polarizations disappears in the SPP and PSP polarizations. The spectra were taken for 50 s with a 4.0 μJ visible beam (800 nm) and an IR beam of 6300 nm. The spectra are offset on the y-axis to emphasize the differences.

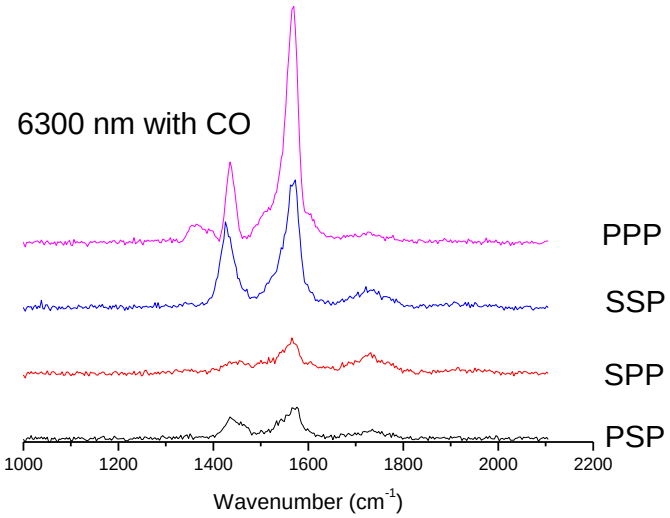

Figure 9.3. The two SFG peaks in EMIM BF_4 at ~1430 (CH_3 bending) and ~1570 cm^{-1} (ring stretching) are shown in a carbon dioxide-saturated solution following several potential cycles to adsorb significant amounts of CO at the surface. The 1570 cm^{-1} peak is most intense in the PPP. In SSP, the 1570 cm^{-1} peak is less intense, but the 1430 cm^{-1} peak is equal in intensity to the PPP polarization. In the SPP and PSP, the 1570 cm^{-1} peak is less intense, and there is a weak signal from 1430 cm^{-1} that appears in the PSP. The spectra were taken for 50 s with a 4.0 μJ visible beam (800 nm) and an IR beam of 6300 nm. The spectra are offset on the y-axis to emphasize the differences.

Appendix A: Fuel Cell Assembly Procedures

Nafion Conditioning Procedure

1. Cut Nafion® into square sheets of similar sizes.
2. Heat for 1 hour in 5% hydrogen peroxide at 80 ºC.
3. Rinse with pure water.
4. Boil in pure water for 1 hour.
5. Heat for 1 hour in 0.5 M sulfuric acid at 80 ºC.
6. Rinse with pure water.
7. Boil in pure water for 1 hour.
8. Rinse and store in pure water.

Catalyst ink preparation procedure

1. Add 50 mg of catalyst and 600 mg of Millipore water to glass vial.
2. Use platinum black catalyst for cathode; palladium black catalyst for anode.
3. Sonicate mixture for 1-2 minutes surrounded by ice bath.
4. Add 220 mg Nafion® suspension to vial.
5. Sonicate mixture for 1-2 minutes surrounded by ice bath.
6. Paint immediately, keeping ink cool in ice water bath.

Fuel cell painting procedure

1. Apply vacuum and heat (60 ºC) to the vacuum table, and let it warm up.
2. Lay conditioned Nafion® sheet on vacuum table, and cover with silicone/nylon gasket, with 2x2 cm square hole cut in it.
3. After a few minutes, Nafion® is dry and ready for painting.
4. Apply cathode catalyst ink to Nafion® surface using a short camel hair brush and multiple directions for painting. The ink should dry almost instantly when it hits the Nafion®. If it doesn't, then there is too much ink on the brush.
5. Paint in slow, even strokes, until catalyst ink is exhausted or catalyst ink begins to show signs of cracking or chipping.
6. Wait 30 minutes for ink to thoroughly dry.
7. Remove silicone sheet, and label the electrode just painted as cathode.
8. Flip membrane so unpainted membrane is facing up.
9. Paint a few strokes of remaining platinum ink off center of the anode catalyst area and let dry for 1-2 minutes
10. Cover with the silicone sheet, and paint the anode side of the Nafion® in a similar manner as the cathode side.
11. After 30 minutes of drying, the MEA is ready for fuel cell assembly.

Carbon paper painting procedure

1. Turn hot plate to 2.
2. Secure carbon paper to hot plate with tape.
3. Paint with slow brush strokes and be sure each layer dries before applying the next.
4. Paint until the ink is entirely used up.
5. Wait overnight for ink to thoroughly dry.

Fuel cell assembly

1. Place 3 bolts through the holes in the cathode flow field and gold-plated current collector.
2. Lay the cathode flow field flat with flow channels facing up. The 3 bolts should be sticking straight up, while the head of the bolts are touching the table and concealed from view.
3. Cut a piece of 20 mil silicone gasket (McMaster), and place it on top of the flow field along with the carbon cloth gas diffusion layer.
4. Place the MEA (prepared previously and hot pressed with the carbon paper at 80 C) on top of the silicone gasket and carbon cloth.
5. On top of the MEA, place a piece of 10 mil silicone gasket (McMaster) with a hole for the reference electrode.
6. Place the flow field and current collector on top of this assembly.
7. Tighten bolts and insert the remaining bolts and tighten methodically.

Appendix B: Electrochemistry Catalyst Preparation Procedures

Standard ink preparation procedure

1. Place 5.6 mg palladium catalyst into a small glass vial
2. Add 1 g water
3. Add 3 drops Nafion® suspension.
4. Sonicate for 1-2 minutes in the sonicating bath.
5. Place 12.5 uL of catalyst ink on a small electrodes (for RDE) or 50 uL of catalyst ink on the large electrodes (for other experiments)

Standard catalyst characterization procedure

1. Once electrochemical cell is clean and dried, assemble all the glassware.
2. Pour in electrolyte solution and bubble UHP argon directly into the solution for 30 minutes.
3. Clean counter electrode in hydrogen flame.
4. Place reference and counter electrodes in cell.
5. Place working electrode in cell using an adaptor or via the RDE.
6. Run several CV cycles until they are stable and judge cleanliness of the electrode surface.
7. Perform all necessary tests, CVs, CAs, modifications, etc., on the catalyst.
8. Connect catalyst as working electrode

Appendix C: XPS Catalyst Preparation Procedures

Catalyst preparation procedure

1. Place 5.6 mg palladium catalyst into a small glass vial
2. Add 1 g water
3. Sonicate for 1-2 minutes in the sonicating bath.
4. Place 50 uL of catalyst ink on a gold electrode
5. Dry catalyst
6. If catalyst fully covers the gold electrode, preparation is finished. If catalyst does not fully cover, wipe off dried catalyst and repeat from step 1 with new catalyst ink.

Electrochemical catalyst preparation

1. Setup electrochemical cells as usual (one with dilute sulfuric acid and other with adatom solution) and degas solutions for 30 minutes with argon
2. Also setup transfer flasks with pure water and degas for 30 minutes with argon
3. Attach all electrodes to prepare for experiments
4. Clean catalyst surface in sulfuric acid solution with potential cycles from ~0 to ~1.2 V vs RHE
5. Quickly transfer catalyst to adatom solution while protected with a solution droplet
6. Run a few fast scan CVs to be sure surface was not contaminated during transfer
7. Set and hold potential for several minutes in adatom solution
8. Optional: run a few CVs (until surface is stable) to be sure that only irreversibly adsorbed adatoms remain on the surface
9. Quickly transfer catalyst to transfer flask and degas five additional minutes
10. Close valves on transfer flask and carry to Materials Research Lab

Sample loading and analysis

1. Samples are carried to MRL while kept in inert transfer flask
2. Remove sample quickly and transfer to sample holder
3. Move samples into instrument chamber and pump down immediately
4. Run full spectrum scan of sample
5. Run spectra in regions of interest for carbon, palladium, and the adatom
6. Run spectra at several locations on the sample

Appendix D: Electrochemical Methods Associated with Broad-Band Sum Frequency Generation

Electrochemistry apparatus

1. Assemble the clean electrochemical cell
    a. All Kel-F and glass parts are cleaned in acid bath overnight and then dried thoroughly
    b. Care must be taken to keep all components clean during storage and also during assembly procedure
2. Clean platinum counter electrode by hydrogen flame
3. Assure that platinum electrode is clean and free of defect by visual inspection

Ionic liquid preparation

1. Place sufficient ionic liquid in a clean vacuum flask and seal
2. Place flask on heat/stir plate and turn on ~2 for heat and high value for stir
3. Leave ionic liquid under these conditions at least overnight
4. After preparation, close valve outside flask to be sure it is sealed from the atmosphere
5. If liquid sits more than a few days following preparation, repeat procedure beginning at step 1 to ensure well-prepared ionic liquid for experiments.

Electrochemical methods

1. Prior to placing electrochemical cell in the BB-SFG chamber, run a few full scan potential cycles at 200 mV s^{-1} from -1.5 V to +1.5 V followed by 40-100 potential cycles at 200 mV s^{-1} from 0.5 V to -1 V in an argon-saturated ionic liquid
    a. When cycles stabilize, check for evidence of water and surface impurities
    b. If neither is present, it is safe to move on to next step
    c. If water is present in the ionic liquid, it must be removed from the electrochemical cell and replaced with dry, freshly prepared ionic liquid (therefore, it is always good to have some backup liquid already prepared before beginning spectroscopy experiments)
    d. If surface impurities are evident on the platinum crystal, it must be removed and polished and/or flame annealed.
2. Place electrochemical cell in BB-SFG chamber and begin bubbling carbon dioxide in the ionic liquid for 30 minutes
3. Scan fifteen potential cycles at 200 mV s^{-1} from ~0.5 to -1 V vs SHE to adsorb enough CO to observe a strong BB-SFG peak
4. Once the laser is aligned a variety of experiments can be performed
    a. CO can be stripped from the electrode surface by scanning the potential out to +1.5 V vs SHE (or by setting that potential for a few seconds)
    b. TLE can be performed at slow scan rates, such as 5 mV s^{-1} in order to combine spectroscopy with electrochemistry

Preventing laser-assisted desorption

1. The adsorbed CO exhibits strong laser assisted desorption, so the visible beam should be reduced to 2.5 μJ when probing CO to prevent this
2. The IR beam intensity can also be lowered if necessary
3. To determine the amount of laser-assisted desorption, align the laser and hold the electrode at open circuit potential
    a. If the signal decreases while held in one spot, the CO is probably desorbing
    b. If the signal regains intensity when the laser beam is moved and then decreases again, the CO is certainly desorbing
4. When probing other peaks, such as ionic liquid peaks, the visible power can be increased to 4.0 μJ without any laser assisted desorption

References

1. Weart, S.R., *The Discovery of the Risk of Global Warming.* Physics Today, 1997. **50**(1): p. 34-40.
2. Roy, S.C., et al., *Toward Solar Fuels: Photocatalytic Conversion of Carbon Dioxide to Hydrocarbons*. ACS Nano, 2010.
3. Scheffer, M. and S.R. Carpenter, *Catastrophic regime shifts in ecosystems: linking theory to observation.* Trends in Ecology & Evolution, 2003. **18**(12): p. 648-656.
4. Webpage. [cited 2010 March]; Available from: http://mdgs.un.org.
5. Rao, A.B. and E.S. Rubin, *A Technical, Economic, and Environmental Assessment of Amine-Based CO2 Capture Technology for Power Plant Greenhouse Gas Control*. Environmental Science & Technology, 2002. **36**(20): p. 4467-4475.
6. Delacourt, C., et al., *Design of an electrochemical cell making syngas (CO+H-2) from CO2 and H2O reduction at room temperature.* Journal of The Electrochemical Society, 2008. **155**(1): p. B42-B49.
7. Webpage. *Carbon dioxide emissions, by country*. [cited 2010 March]; Available from: http://mdgs.un.org.
8. Webpage. *Global carbon dioxide concentration*. [cited 2010 March]; Available from: http://www.environment.gov.au.
9. Laraminie, J. and A. Dicks, *Fuel Cell Systems Explained*. 2003, West Sussex, England: John Wiley & Sons, Inc.
10. Kreuer, K.-D., *Proton Conductivity: Materials and Applications.* Chemistry of Materials, 1996. **8**(3): p. 610-641.
11. van Grotthuss, C.J.D., Ann. Chim., 1806. **58**: p. 54.
12. Agmon, N., *The Grotthuss mechanism.* Chemical Physics Letters, 1995. **244**(5-6): p. 456-462.
13. Klaus-Dieter Kreuer, A.R.W.W., *Vehicle Mechanism, A New Model for the Interpretation of the Conductivity of Fast Proton Conductors.* Angewandte Chemie International Edition in English, 1982. **21**(3): p. 208-209.
14. Y. Sone, P.E., and D. Simonsson, J. Electrochem. Soc, 1996. **143**: p. 1254.
15. O'Hayre, R., et al., *Fuel Cell Fundamentals*. 1 ed. 2006, Hoboken, NJ: John Wiley & Sons Inc.
16. Bard, A.J. and L.R. Faulkner, *Electrochemical Methods: Fundamentals and Applications*. 2001, Hoboken, NJ: John Wiley & Sons, Inc.
17. Larminie, J. and A. Dicks, *Fuel Cell Systems Explained*. Second ed. 2003, West Sussex, England: John Wiley & Sons Ltd.
18. Moghaddam, S., et al., *Millimeter-Scale Fuel Cell With Onboard Fuel and Passive Control System.* Microelectromechanical Systems, Journal of, 2008. **17**(6): p. 1388-1395.
19. Qi, Z. and A. Kaufman, *Open circuit voltage and methanol crossover in DMFCs.* Journal of Power Sources, 2002. **110**(1): p. 177-185.

20. Goodenough, J.B., et al., *Methanol oxidation on unsupported and carbon supported Pt + Ru anodes.* Journal of Electroanalytical Chemistry, 1988. **240**(1-2): p. 133-145.
21. Herrero, E., et al., *Poison formation reaction from formic acid and methanol on Pt(111) electrodes modified by irreversibly adsorbed Bi and As.* Journal of Electroanalytical Chemistry, 1993. **350**(1-2): p. 73-88.
22. Swathirajan, S. and S. Bruckenstein, *Thermodynamics and kinetics of underpotential deposition of metal monolayers on polycrystalline substrates.* Electrochimica Acta, 1983. **28**(7): p. 865-877.
23. Wieckowski, A.a.S., J., *Comparative study of adsorption and oxidation of formic acid and methanol on platinized electrodes in acidic solution.* Electroanal. Chem, 1975. **63**: p. 365-377.
24. Rice, C., et al., *Direct formic acid fuel cells.* Journal of Power Sources, 2002. **111**(1): p. 83-89.
25. Larsen, R., et al., *Unusually active palladium-based catalysts for the electrooxidation of formic acid.* Journal of Power Sources, 2006. **157**(1): p. 78-84.
26. Wilde, C.P., Zhang, M., *Profiles of adsorption during the oxidation of small organic molecules: oxidation of formic acid at polycrystalline Pt in acid solutions.* J. Chem. Soc., Faraday Trans., 1994. **90**: p. 1233-1240.
27. Matsumoto, F., et al., *Electrocatalytic activity of ordered intermetallic PtPb nanoparticles prepared by borohydride reduction toward formic acid oxidation.* Journal of The Electrochemical Society, 2008. **155**(2): p. B148-B154.
28. Ha, S., B. Adams, and R.I. Masel, *A miniature air breathing direct formic acid fuel cell.* Journal of Power Sources, 2004. **128**(2): p. 119-124.
29. Wang, X., J.M. Hu, and I.M. Hsing, *Electrochemical investigation of formic acid electro-oxidation and its crossover through a Nafion (R) membrane.* Journal of Electroanalytical Chemistry, 2004. **562**(1): p. 73-80.
30. Zhu, Y., S.Y. Ha, and R.I. Masel, *High power density direct formic acid fuel cells.* Journal of Power Sources, 2004. **130**(1-2): p. 8-14.
31. Ha, S., Z. Dunbar, and R.I. Masel, *Characterization of a high performing passive direct formic acid fuel cell.* Journal of Power Sources, 2006. **158**(1): p. 129-136.
32. Li, X. and A.A. Gewirth, *Oxygen Electroreduction through a Superoxide Intermediate on Bi-Modified Au Surfaces.* Journal of the American Chemical Society, 2005. **127**(14): p. 5252-5260.
33. Haan, J.L., et al., *Performance of the direct formic acid fuel cell with electrochemically modified palladium-antimony anode catalyst.* Electrochimica Acta, 2010. **55**(7): p. 2477-2481.
34. Uhm, S., H.J. Lee, and J. Lee, *Understanding underlying processes in formic acid fuel cells.* Physical Chemistry Chemical Physics, 2009. **11**(41): p. 9326-9336.
35. Jeon, M.K., et al., *Combinatorial Search for Quaternary Methanol Tolerant Oxygen Electro-Reduction Catalyst.* Fuel Cells, 2010. **10**(1): p. 93-98.
36. Angerstein-Kozlowska, H., *Comprehensive Treatise on Electrochemistry*, ed. E. Yeager. Vol. 9. 1984, New York: Plenum Press.
37. Waszczuk, P., et al., *A nanoparticle catalyst with superior activity for electrooxidation of formic acid (vol 4, pg 599, 2002).* Electrochemistry Communications, 2002. **4**(9): p. 732-732.

38. Waszczuk, P., et al., *Methanol electrooxidation on platinum/ruthenium nanoparticle catalysts.* Journal of Catalysis, 2001. **203**(1): p. 1-6.
39. Biegler, T., D.A.J. Rand, and R. Woods, *Limiting oxygen coverage on platinized platinum; Relevance to determination of real platinum area by hydrogen adsorption.* Journal of Electroanalytical Chemistry, 1971. **29**(2): p. 269-277.
40. Sogaard, M., M. Odgaard, and E.M. Skou, *An improved method for the determination of the electrochemical active area of porous composite platinum electrodes.* Solid State Ionics, 2001. **145**(1-4): p. 31-35.
41. Takasu, Y., et al., *Effects of the surface area of carbon support on the characteristics of highly-dispersed Pt---Ru particles as catalysts for methanol oxidation.* Electrochimica Acta, 2003. **48**(25-26): p. 3861-3868.
42. Xia, X.H. and T. Iwasita, *Influence of Underpotential Deposited Lead upon the Oxidation of HCOOH in HClO[sub 4] at Platinum Electrodes.* Journal of The Electrochemical Society, 1993. **140**(9): p. 2559-2565.
43. Sun, S.G., J. Clavilier, and A. Bewick, *The Mechanism of Electrocatalytic Oxidation of Formic-Acid on Pt (100) and Pt (111) in Sulfuric-Acid Solution - an Emirs Study.* Journal of Electroanalytical Chemistry, 1988. **240**(1-2): p. 147-159.
44. Gasteiger, H.A., N.M. Markovic, and P.N. Ross, *H2 and CO Electrooxidation on Well-Characterized Pt, Ru, and Pt-Ru. 1. Rotating Disk Electrode Studies of the Pure Gases Including Temperature Effects.* J. Phys. Chem., 1995. **99**(20): p. 8290-8301.
45. Parsons, R. and T. VanderNoot, *The oxidation of small organic molecules : A survey of recent fuel cell related research.* Journal of Electroanalytical Chemistry, 1988. **257**(1-2): p. 9-45.
46. Capon, D. and R. Parsons, *The oxidation of formic acid on noble metal electrodes a comparison of the behaviour of pure electrodes.* Electroanalytical Chemistry and Interfacial Electrochemistry, 1973. **44**: p. 239-254.
47. Wieckowski, A. and J. Sobkowski, *Copmarative study of adsorption and oxidation of formic acid and methanol on platinized electrodes in acidic solution.* Journal of Electroanalytical Chemistry, 1975. **63**: p. 365-377.
48. Clavilier, J., et al., *Formic-Acid Oxidation on Single-Crystal Platinum-Electrodes - Comparison with Polycrystalline Platinum.* Journal of Electroanalytical Chemistry, 1981. **124**(1-2): p. 321-326.
49. Capon, A. and R. Parsons, *The oxidation of formic acid on noble metal electrodes: II. A comparison of the behaviour of pure electrodes.* Journal of Electroanalytical Chemistry, 1973. **44**(2): p. 239-254.
50. Capon, A. and R. Parsons, *The oxidation of formic acid at noble metal electrodes Part III. Intermediates and mechanism on platinum electrodes.* Journal of Electroanalytical Chemistry, 1973. **45**(2): p. 205-231.
51. Wieckowski, A., J. Sobkowski, and A. Jablonska, *Adsorption and oxidation of formic acid on platinized electrode. Test of validity of the radiometric method.* Journal of Electroanalytical Chemistry and Interfacial Electrochemistry, 1974. **55**(3): p. 383-9.
52. Capon, A. and R. Parson, *The oxidation of formic acid at noble metal electrodes: I. Review of previous work.* Journal of Electroanalytical Chemistry, 1973. **44**(1): p. 1-7.

53. Markovic, N.M. and P.N. Ross, *Surface science studies of model fuel cell electrocatalysts.* Surface Science Reports, 2002. **45**(4-6): p. 117-229.
54. Rice, C., et al., *Catalysts for direct formic acid fuel cells.* Journal of Power Sources, 2003. **115**(2): p. 229-235.
55. Waszczuk, P., et al., *A nanoparticle catalyst with superior activity for electrooxidation of formic acid.* Electrochemistry Communications, 2002. **4**(7): p. 599-603.
56. Vidal, F., et al., *SFG study of methanol dissociative adsorption at Pt(100), Pt(100) and Pt(111) electrodes surfaces.* Surface Science, 2002. **502**: p. 485-489.
57. Watanabe, M. and S. Motoo, *Electrocatalysis by Ad-atoms .3. Enhancement of the Oxidation of Carbon Monoxide on Platinum by Ruthenium Ad-atoms.* Electroanalytical Chemistry and Interfacial Electrochemistry, 1975. **60**: p. 275-283.
58. Lu, G.Q., A. Crown, and A. Wieckowski, *Formic acid decomposition on polycrystalline platinum and palladized platinum electrodes.* Journal of Physical Chemistry B, 1999. **103**(44): p. 9700-9711.
59. Chen, Y.X., et al., *Bridge-Bonded Formate: Active Intermediate or Spectator Species in Formic Acid Oxidation on a Pt Film Electrode?* Langmuir, 2006. **22**(25): p. 10399-10408.
60. Larsen, R. and R.I. Masel, *Kinetic Study of CO Tolerance during Electro-oxidation of Formic Acid on Spontaneously Deposited Pt/Pd and Pt/Ru Nanoparticles.* Electrochemical and Solid-State Letters, 2004. **7**(6): p. A148-A150.
61. Zhao, M., et al., *Kinetic Study of Electro-oxidation of Formic Acid on Spontaneously-Deposited Pt/Pd Nanoparticles.* Journal of The Electrochemical Society, 2004. **151**(1): p. A131-A136.
62. Yu, X. and P.G. Pickup, *Recent advances in direct formic acid fuel cells (DFAFC).* Journal of Power Sources, 2008. **182**(1): p. 124-132.
63. Zhu, Y., Z. Khan, and R.I. Masel, *The behavior of palladium catalysts in direct formic acid fuel cells.* Journal of Power Sources, 2005. **139**(1-2): p. 15-20.
64. Zhang, R., et al., *Micro-energy re-activating method to recover proton exchange membrane fuel cell performance*. 2007: US Patent Application 2007154743.
65. Masel, R.I., et al., *Low contaminant formic acid fuel for direct liquid fuel cell* 2006: US Patent Application 2006059769.
66. Gates, B.C. and G.M. Schwab, *The dehydration of formic acid catalyzed by polystyrene sulfonic acid.* Journal of Catalysis, 1969. **15**(4): p. 430-434.
67. Shi, A.C., et al., *Perspective on the use of gas adsorption for particle-shape control in supported metal catalysis.* Mater. Res. Soc. Symp. Proc., 1988. **111**(Microstruct. Prop. Catal.): p. 59-64.
68. Shi, A.C. and R.I. Masel, *Effects of gas adsorption on particle shapes in supported platinum catalysts.* J. Catal., 1989. **120**(2): p. 421-31.
69. Wang, J. and R.I. Masel, *Methanol adsorption and decomposition on (1 x 1)platinum(110) and (2 x 1)platinum(110): identification of the active site for carbon-oxygen bond scission during alcohol decomposition on platinum.* J. Catal., 1990. **126**(2): p. 519-31.

70. Wang, J. and R.I. Masel, *Carbon-oxygen bond scission during methanol decomposition on (1*1)platinum(110).* J. Am. Chem. Soc., 1991. **113**(15): p. 5850-6.
71. Wang, J. and R.I. Masel, *Methanol adsorption and decomposition on (2*1) platinum(110): enhanced stability of the methoxy intermediate on a stepped surface.* Surf. Sci., 1991. **243**(1-3): p. 199-209.
72. Law, W.L., et al., *Effect of organic impurities on the performance of direct formic acid fuel cells.* Journal of The Electrochemical Society, 2009. **156**(5).
73. Adzic, R.R., et al., *Electrocatalysis by foreign metal monolayers: Oxidation of formic acid on platinum.* Journal of Electroanalytical Chemistry, 1975. **65**(2, Part 2): p. 587-601.
74. Adzic, R.R., et al., *Electrochemical oxidation of formic acid at noble metals: Catalytic effects of foreign metal monolayers.* Journal of Electroanalytical Chemistry, 1977. **80**(1): p. 81-99.
75. Adzic, R.R., et al., *Catalytic effects of monolayers of metals deposited at underpotentials: Oxidation of formic acid on platinum.* Journal of Electroanalytical Chemistry, 1975. **61**(1): p. 117-120.
76. Gerischer, H., D.M. Kolb, and M. Przasnyski, *Chemisorption of metal atoms on metal surfaces in correlation to work function differences.* Surface Science, 1974. **43**(2): p. 662-666.
77. Kolb, D.M., Przasnys.M, and Gerische.H, *UNDERPOTENTIAL DEPOSITION OF METALS AND WORK FUNCTION DIFFERENCES.* Journal of Electroanalytical Chemistry, 1974. **54**(1): p. 25-38.
78. Jung, G., H. Park, and C.K. Rhee, *Contrasting electrochemical behavior of irreversibly adsorbed Sb monolayer on Pt(100) and Pt(111) single crystal electrode surfaces.* Journal of Electroanalytical Chemistry, 1998. **453**(1-2): p. 243-247.
79. Zhao, J., C. Jung, and C.K. Rhee, *Adlayers of Sb Irreversibly Adsorbed on Pt(111): An Electrochemical Scanning Tunneling Microscopy Study.* J. Phys. Chem. B, 2006. **110**(22): p. 10814-10821.
80. Wang, H., et al., *Electrocatalytic mechanism and kinetics of SOMs oxidation on ordered PtPb and PtBi intermetallic compounds: DEMS and FTIRS study.* Physical Chemistry Chemical Physics, 2008. **10**(25): p. 3739-3751.
81. Kang, S., et al., *Influence of Bi Modification of Pt Anode Catalyst in Direct Formic Acid Fuel Cells.* J. Phys. Chem. B, 2006. **110**(14): p. 7270-7274.
82. Uhm, S., S.T. Chung, and J. Lee, *Activity of Pt anode catalyst modified by underpotential deposited Pb in a direct formic acid fuel cell.* Electrochemistry Communications, 2007. **9**(8): p. 2027-2031.
83. Lee, J.K., et al., *Influence of underpotentially deposited Sb onto Pt anode surface on the performance of direct formic acid fuel cells.* Electrochimica Acta, 2008. **53**(21): p. 6089-6092.
84. Fonseca, I.T.E., A.C. Marin, and D. Pletcher, *The influence of Cu adatoms on a Pt electrode on the oxidation of formic acid.* Journal of Electroanalytical Chemistry, 1987. **218**(1-2): p. 327-329.
85. Watanabe, M., M. Horiuchi, and S. Motoo, *Electrocatalysis by ad-atoms : Part XXIII. Design of platinum ad-electrodes for formic acid fuel cells with ad-atoms*

of the IVth and the Vth groups. Journal of Electroanalytical Chemistry, 1988. **250**(1): p. 117-125.
86. Adzic, R.R., et al., *Catalytic effects of monolayers of metals deposited at underpotentials: Oxidation of formic acid on platinum.* Journal of Electroanalytical Chemistry, 1975. **61**(1): p. 117-120.
87. Adzic, R.R., M.D. Spasojevic, and A.R. Despic, *Electrocatalysis by foreign metal monolayers: Oxidation of formic acid on palladium.* Journal of Electroanalytical Chemistry, 1978. **92**(1): p. 31-43.
88. Clavilier, J., et al., *Heterogeneous electrocatalysis on well-defined platinum surfaces modified by controlled amounts of irreversibly adsorbed adatoms : Part III. Formic acid oxidation on the Pt (100)-Bi system.* Journal of Electroanalytical Chemistry, 1989. **261**(1): p. 113-125.
89. Koljadko, J., et al., *The formation and behavior of Ag adsorbates at Pd electrodes and their influence on electrocatalytic oxidation of formic acid at Pd.* Journal of Electroanalytical Chemistry, 1982. **137**(1): p. 117-125.
90. Watanabe, M. and S. Motoo, *Electrocatalysis by ad-atoms: Part I. Enhancement of the oxidation of methanol on platinum and palladium by gold ad-atoms.* Journal of Electroanalytical Chemistry, 1975. **60**(3): p. 259-266.
91. Watanabe, M. and S. Motoo, *Electrocatalysis by ad-atoms: Part III. Enhancement of the oxidation of carbon monoxide on platinum by ruthenium ad-atoms.* Journal of Electroanalytical Chemistry, 1975. **60**(3): p. 275-283.
92. Motoo, S. and M. Watanabe, *Electrocatalysis by Sn and Ge AD-atoms.* Journal of Electroanalytical Chemistry, 1976. **69**(3): p. 429-431.
93. Fonseca, I., J. Lin-Cai, and D. Pletcher, *A Potential Step Study of the Influence of Metal Adatoms and Solution pH on the Rate of Formic Acid Oxidation at Pt Electrodes.* Journal of The Electrochemical Society, 1983. **130**(11): p. 2187-2192.
94. Hamm, U.W., et al., *On the valence state of bismuth adsorbed on a Pt(111) electrode: an electrochemistry, LEED and XPS study.* Electrochimica Acta, 1998. **43**(19-20): p. 2969-2978.
95. Wang, X., et al., *Carbon-supported Pd-Ir catalyst as anodic catalyst in direct formic acid fuel cell.* Journal of Power Sources, 2008. **175**(2): p. 784-788.
96. Chen, W., et al., *Study of carbon-supported Au catalyst as the cathodic catalyst in a direct formic acid fuel cell prepared using a polyvinyl alcohol protection method.* Journal of Power Sources, 2007. **167**(2): p. 315-318.
97. Zhang, L., et al., *A carbon-supported Pd-P catalyst as the anodic catalyst in a direct formic acid fuel cell.* Journal of Power Sources, 2006. **162**(1): p. 177-179.
98. Zhang, L., et al., *Preparation method of an ultrafine carbon supported Pd catalyst as an anodic catalyst in a direct formic acid fuel cell.* Electrochemistry Communications, 2006. **8**(10): p. 1625-1627.
99. Gold, S., et al., *Acid loaded porous silicon as a proton exchange membrane for micro-fuel cells.* Journal of Power Sources, 2004. **135**(1-2): p. 198-203.
100. Hammer, B. and J.K. Norskov, *Theoretical surface science and catalysis--calculations and concepts Advances in Catalysis*, in *Impact of Surface Science on Catalysis*, B.C.G.a.H. Knozinger, Editor. 2000, Academic Press. p. 71-129.
101. Norskov, J.K., et al., *Universality in Heterogeneous Catalysis.* Journal of Catalysis, 2002. **209**(2): p. 275-278.

102. Greeley, J., J.K. Norskov, and M. Mavrikakis, *Electronic structure and catalysis on metal surfaces.* Annual Review of Physical Chemistry, 2002. **53**: p. 319-348.
103. Stamenkovic, V.R., et al., *Improved Oxygen Reduction Activity on Pt3Ni(111) via Increased Surface Site Availability 10.1126/science.1135941*. Science, 2007. **315**(5811): p. 493-497.
104. Rodriguez, J.A. and D.W. Goodman, *The Nature of the Metal Metal Bond in Bimetallic Surfaces.* Science, 1992. **257**(5072): p. 897-903.
105. Zhou, W.P., et al., *Size Effects in Electronic and Catalytic Properties of Unsupported Palladium Nanoparticles in Electrooxidation of Formic Acid.* J. Phys. Chem. B, 2006. **110**(27): p. 13393-13398.
106. Zhou, W. and J.Y. Lee, *Particle Size Effects in Pd-Catalyzed Electrooxidation of Formic Acid.* The Journal of Physical Chemistry C, 2008. **112**(10): p. 3789-3793.
107. Yang, G., et al., *Preparation of carbon supported Pd-P catalyst with high content of element phosphorus and its electrocatalytic performance for formic acid oxidation.* Electrochemistry Communications, 2010. **12**(3): p. 492-495.
108. Oloman, C. and H. Li, *Electrochemical processing of carbon dioxide.* ChemSusChem, 2008. **1**(5): p. 385-391.
109. Hori, Y., *Electrochemical CO2 reduction on metal electrodes.* Modern Aspects of Electrochemistry, 2008. **42**: p. 89-189.
110. Kaneco, S., et al., *Electrochemical reduction of high pressure carbon dioxide at a Cu electrode in cold methanol with CsOH supporting salt.* Chemical Engineering Journal, 2007. **128**(1): p. 47-50.
111. Gattrell, M., N. Gupta, and A. Co, *Electrochemical reduction of CO2 to hydrocarbons to store renewable electrical energy and upgrade biogas.* Energy Conversion and Management, 2007. **48**(4): p. 1255-1265.
112. Raebiger, J.W., et al., *Electrochemical Reduction of CO2 to CO Catalyzed by a Bimetallic Palladium Complex.* Organometallics, 2006. **25**(14): p. 3345-3351.
113. Kaneco, S., et al., *Electrochemical reduction of CO2 in copper particle-suspended methanol.* Chemical Engineering Journal, 2006. **119**(2-3): p. 107-112.
114. Kaneco, S., et al., *Electrochemical reduction of carbon dioxide to ethylene at a copper electrode in methanol using potassium hydroxide and rubidium hydroxide supporting electrolytes.* Electrochimica Acta, 2006. **51**(16): p. 3316-3321.
115. Kaneco, S., et al., *Electrochemical reduction of CO2 to methane at the Cu electrode in methanol with sodium supporting salts and its comparison with other alkaline salts.* Energy & Fuels, 2006. **20**(1): p. 409-414.
116. Kaneco, S., et al., *Effect of sodium cation on the electrochemical reduction of CO2 at a copper electrode in methanol.* Journal of Solid State Electrochemistry, 2006. **11**(4): p. 490-495.
117. Kaneco, S., et al., *Electrochemical reduction of high pressure CO2 at a Cu electrode in cold methanol.* Electrochimica Acta, 2006. **51**(23): p. 4880-4885.
118. Gupta, N., M. Gattrell, and B. MacDougall, *Calculation for the cathode surface concentrations in the electrochemical reduction of CO2 in KHCO3 solutions.* Journal of Applied Electrochemistry, 2006. **36**(2): p. 161-172.
119. Gattrell, M., N. Gupta, and A. Co, *A review of the aqueous electrochemical reduction of CO2 to hydrocarbons at copper.* Journal of Electroanalytical Chemistry, 2006. **594**(1): p. 1-19.

120. DuBois, D.L., *Carbon. Electrochemical reactions of carbon dioxide.* Encyclopedia of Electrochemistry, 2006. **7a**: p. 202-225.
121. Smolinka, T., et al., *CO2 reduction on Pt electrocatalysts and its impact on H2 oxidation in CO2 containing fuel cell feed gas - A combined in situ infrared spectroscopy, mass spectrometry and fuel cell performance study.* Electrochimica Acta, 2005. **50**(25-26): p. 5189-5199.
122. Qu, J.P., et al., *Electrochemical reduction of CO2 on RuO2/TiO2 nanotubes composite modified Pt electrode.* Electrochimica Acta, 2005. **50**(16-17): p. 3576-3580.
123. Park, J.-Y. and E.D. Wachsman, *Lower Temperature Electrolytic Reduction of CO2 to O2 and CO with High-Conductivity Solid Oxide Bilayer Electrolytes.* Journal of The Electrochemical Society, 2005. **152**(8): p. A1654-A1659.
124. Hori, Y., et al., *"Deactivation of copper electrode" in electrochemical reduction of CO2.* Electrochimica Acta, 2005. **50**(27): p. 5354-5369.
125. Zhao, G.Y., et al., *Electrochemical reduction of supercritical carbon dioxide in ionic liquid 1-n-butyl-3-methylimidazolium hexafluorophosphate.* Journal of Supercritical Fluids, 2004. **32**(1-3): p. 287-291.
126. Yano, H., et al., *Selective electrochemical reduction of CO2 to ethylene at a three-phase interface on copper(I) halide-confined Cu-mesh electrodes in acidic solutions of potassium halides.* Journal of Electroanalytical Chemistry, 2004. **565**(2): p. 287-293.
127. Scibioh, M.A. and B. Viswanathan, *Electrochemical reduction of carbon dioxide: a status report.* Proceedings of the Indian National Science Academy, Part A: Physical Sciences, 2004. **70**(3): p. 407-462.
128. Kaneco, S., et al., *Electrochemical reduction of CO2 at alloy electrode in methanol.* Studies in Surface Science and Catalysis, 2004. **153**(Carbon Dioxide Utilization for Global Sustainability): p. 277-282.
129. Akahori, Y., et al., *New electrochemical process for CO2 reduction to from formic acid from combustion flue gases.* Electrochemistry (Tokyo, Japan), 2004. **72**(4): p. 266-270.
130. Spataru, N., et al., *Electrochemical reduction of carbon dioxide at ruthenium dioxide deposited on boron-doped diamond.* Journal of Applied Electrochemistry, 2003. **33**(12): p. 1205-1210.
131. Riquelme, M.A., et al., *Electrocatalytic reduction of carbon dioxide at polymeric cobalt tetra (3-amino (phenyl) porphyrin glassy carbon-modified electrodes.* Journal of the Chilean Chemical Society, 2003. **48**(2): p. 89-92.
132. Ogura, K., *Electrochemical and selective conversion of CO2 to ethylene.* Electrochemistry, 2003. **71**(8): p. 676-680.
133. Koleli, F., et al., *Electrochemical reduction of CO2 at Pb- and Sn-electrodes in a fixed-bed reactor in aqueous K2CO3 and KHCO3 media.* Journal of Applied Electrochemistry, 2003. **33**(5): p. 447-450.
134. Kaneco, S., et al., *Electrochemical reduction of CO2 on Cu electrode in methanol at low temperature.* ACS Symposium Series, 2003. **852**(Utilization of Greenhouse Gases): p. 169-182.

135. Yano, H., et al., *Electrochemical reduction of CO2 at three-phase (gas|liquid|solid) and two-phase (liquid|solid) interfaces on Ag electrodes.* Journal of Electroanalytical Chemistry, 2002. **533**(1-2): p. 113-118.
136. Takahashi, I., et al., *Electrochemical reduction of CO2 at copper single crystal Cu(S)-[n(111)*(111)] and Cu(S)-[n(110)*(100)] electrodes.* Journal of Electroanalytical Chemistry, 2002. **533**(1-2): p. 135-143.
137. Stevens, G.B., T. Reda, and B. Raguse, *Energy storage by the electrochemical reduction of CO2 to CO at a porous Au film.* Journal of Electroanalytical Chemistry, 2002. **526**(1-2): p. 125-133.
138. Scibioh, M.A., et al., *Electrochemical reduction of CO2 at hanging mercury drop electrode by nickel (II) macrocyclic complex of 1,3,6,8,12,15-hexaazatricyclo [13.3.1.1] eicosane.* Bulletin of Electrochemistry, 2002. **18**(2): p. 57-61.
139. Schrebler, R., et al., *Study of the electrochemical reduction of CO2 on a polypyrrole electrode modified by rhenium and copper-rhenium microalloy in methanol media.* Journal of Electroanalytical Chemistry, 2002. **533**(1-2): p. 167-175.
140. Momose, Y., K. Sato, and O. Ohno, *Electrochemical reduction of CO2 at copper electrodes and its relationship to the metal surface characteristics.* Surface and Interface Analysis, 2002. **34**(1): p. 615-618.
141. Magdesieva, T.V., et al., *Electrochemical reduction of CO2 with transition metal phthalocyanine and porphyrin complexes supported on activated carbon fibers.* Journal of The Electrochemical Society, 2002. **149**(6): p. D89-D95.
142. Koleli, F., T. Atilan, and N. Palamut, *Electrochemical reduction of CO2 on granule electrodes in a fixed-bed reactor in aqueous medium.* Fresenius Environmental Bulletin, 2002. **11**(6): p. 278-283.
143. Kaneco, S., et al., *Electrochemical conversion of carbon dioxide to methane in aqueous NaHCO3 solution at less than 273 K.* Electrochimica Acta, 2002. **48**(1): p. 51-55.
144. Hori, Y., et al., *Selective formation of C2 compounds from electrochemical reduction of CO2 at a series of copper single crystal electrodes.* Journal of Physical Chemistry B, 2002. **106**(1): p. 15-17.
145. Aydin, R. and F. Koleli, *Electrochemical reduction of CO2 on a polyaniline electrode under ambient conditions and at high pressure in methanol.* Journal of Electroanalytical Chemistry, 2002. **535**(1-2): p. 107-112.
146. Tryk, D.A., et al., *Recent developments in electrochemical and photoelectrochemical CO2 reduction: involvement of the (CO2)2.- dimer radical anion.* Applied Organometallic Chemistry, 2001. **15**(2): p. 113-120.
147. Schrebler, R., et al., *Study of the electrochemical reduction of CO2 on electrodeposited rhenium electrodes in methanol media.* Journal of Electroanalytical Chemistry, 2001. **516**(1-2): p. 23-30.
148. Kaneco, S., et al., *Electrochemical reduction of carbon dioxide using aqueous LiClO4 solution at less than 273 K.* ITE Letters on Batteries, New Technologies & Medicine, 2001. **2**(1): p. 83-87.
149. Yamamoto, T., et al., *Electrochemical reduction of CO2 in the micropores of activated carbon fibers.* Journal of The Electrochemical Society, 2000. **147**(9): p. 3393-3400.

150. Tomita, Y., et al., *Electrochemical Reduction of Carbon Dioxide at a Platinum Electrode in Acetonitrile-Water Mixtures.* Journal of The Electrochemical Society, 2000. **147**(11): p. 4164-4167.
151. Scihioh, M.A. and V.R. Vijayaraghavan, *Electrochemical reduction of carbon dioxide using nickel (II) macrocyclic complex of 1,8-diethyl-1,3,6,8,10,13-hexaazacyclotetradecane at hmde in water.* Bulletin of Electrochemistry, 2000. **16**(8): p. 376-381.
152. Ohta, K., et al., *Electrochemical reduction of carbon dioxide at Cu electrode under ultrasonic irradiation.* Journal of the Electrochemical Society, 2000. **147**(1): p. 233-237.
153. Ogura, K., H. Yano, and M. Nakayama, *Electrochemical reduction of CO2 with gas-diffusion electrodes fabricated using metal, alloy and polymer-confined nets.* Preprints - American Chemical Society, Division of Petroleum Chemistry, 2000. **45**(1): p. 89-91.
154. Kaneco, S., et al., *Reduction of carbon dioxide to petrochemical intermediates.* Energy Sources, 2000. **22**(2): p. 127-135.
155. Ishimaru, S., R. Shiratsuchi, and G. Nogami, *Pulsed electroreduction of CO2 on Cu-Ag alloy electrodes.* Journal of The Electrochemical Society, 2000. **147**(5): p. 1864-1867.
156. Ikeda, S., et al., *Electrochemical reduction behavior of carbon dioxide on sintered zinc oxide electrode in aqueous solution.* Electrochemistry, 2000. **68**(4): p. 257-261.
157. Hoshi, N. and Y. Hori, *Electrochemical reduction of carbon dioxide at a series of platinum single crystal electrodes.* Electrochimica Acta, 2000. **45**(25-26): p. 4263-4270.
158. Halmann, M.M. and M. Steinberg, *Greenhouse Gas Carbon Dioxide Mitigation*. 1999, Boca Raton, Florida: Lewis Publishers.
159. Sanchez-Sanchez, C.M., et al., *Electrochemical approaches to alleviation of the problem of carbon dioxide accumulation.* Pure and Applied Chemistry, 2001. **73**(12): p. 1917-1927.
160. Lukaszewski, M., H. Siwek, and A. Czerwinski, *Electrosorption of carbon dioxide on platinum group metals and alloys-a review.* Journal of Solid State Electrochemistry, 2009. **13**(6): p. 813-827.
161. Ikeda, S., T. Takagi, and K. Ito, *Selective formation of formic acid, oxalic acid, and carbon monoxide by electrochemical reduction of carbon dioxide.* Bulletin of the Chemical Society of Japan, 1987. **60**(7): p. 2517-22.
162. Bockris, J.O.M. and J.C. Wass, *The photoelectrocatalytic reduction of carbon dioxide.* Journal of the Electrochemical Society, 1989. **136**(9): p. 2521-8.
163. Chandrasekaran, K. and J.O.M. Bockris, *In-situ spectroscopic investigation of adsorbed intermediate radicals in electrochemical reactions: carbon dioxide(1-) (CO2-) on platinum.* Surface Science, 1987. **185**(3): p. 495-514.
164. Gennaro, A., et al., *Mechanism of the electrochemical reduction of carbon dioxide at inert electrodes in media of low proton availability.* Journal of the Chemical Society, Faraday Transactions, 1996. **92**(20): p. 3963-3968.
165. Bockris, J.O. and K. Chandrasekaran, *Fourier transform infrared spectroscopic investigation of adsorbed intermediates in electrochemical reactions.* ACS

Symposium Series, 1988. **378**(Electrochem. Surf. Sci.: Mol. Phenom. Electrode Surf.): p. 351-68.
166. Maiorova, N.A., O.A. Khazova, and Y.B. Vasil'ev, *Electroreduction of carbon dioxide in aprotic solvents.* Elektrokhimiya, 1986. **22**(9): p. 1196-204.
167. Vassil'ev, Y.B., et al., *Electroreduction of carbon dioxide. Part II. The mechanism of reduction in aprotic solvents.* Journal of Electroanalytical Chemistry and Interfacial Electrochemistry, 1985. **189**(2): p. 295-309.
168. Barnes, A.S., et al., *Unusual Voltammetry of the Reduction of O2 in [C4dmim][N(Tf)2] Reveals a Strong Interaction of O2•− with the [C4dmim]+ Cation.* The Journal of Physical Chemistry C, 2008. **112**(35): p. 13709-13715.
169. Islam, M.M. and T. Ohsaka, *Roles of Ion Pairing on Electroreduction of Dioxygen in Imidazolium-Cation-Based Room-Temperature Ionic Liquid.* The Journal of Physical Chemistry C, 2008. **112**(4): p. 1269-1275.
170. Chen, Y., et al., *Solubility of CO2 in imidazolium-based tetrafluoroborate ionic liquids.* Thermochimica Acta, 2006. **441**(1): p. 42-44.
171. Gutowski, K.E. and E.J. Maginn, *Amine-Functionalized Task-Specific Ionic Liquids: A Mechanistic Explanation for the Dramatic Increase in Viscosity upon Complexation with CO2 from Molecular Simulation.* Journal of the American Chemical Society, 2008. **130**(44): p. 14690-14704.
172. Schneider, W.F. and E. Mindrup, *First-principles evaluation of CO2 complexation in functionalized ionic liquids.* Abstracts of Papers, 236th ACS National Meeting, Philadelphia, PA, United States, August 17-21, 2008, 2008: p. IEC-165.
173. Anderson, J.L., J.K. Dixon, and J.F. Brennecke, *Solubility of CO2, CH4, C2H6, C2H4, O2, and N2 in 1-Hexyl-3-methylpyridinium Bis(trifluoromethylsulfonyl)imide: Comparison to Other Ionic Liquids.* Accounts of Chemical Research, 2007. **40**(11): p. 1208-1216.
174. Yokozeki, A., et al., *Physical and chemical absorptions of carbon dioxide in room-temperature ionic liquids.* The journal of physical chemistry. B, 2008. **112**(51): p. 16654-63.
175. Kroon, M.C., et al., *High-Pressure Phase Behavior of Systems with Ionic Liquids: Part V. The Binary System Carbon Dioxide + 1-Butyl-3-methylimidazolium Tetrafluoroborate.* Journal of Chemical and Engineering Data, 2005. **50**(1): p. 173-176.
176. Shariati, A. and C.J. Peters, *High-pressure phase behavior of systems with ionic liquids: II. The binary system carbon dioxide+1-ethyl-3-methylimidazolium hexafluorophosphate.* Journal of Supercritical Fluids, 2004. **29**(1-2): p. 43-48.
177. Bara, J.E., et al., *Room-Temperature Ionic Liquids and Composite Materials: Platform Technologies for CO2 Capture.* Accounts of Chemical Research, 2010. **43**(1): p. 152-159.
178. Buzzeo, M.C., C. Hardacre, and R.G. Compton, *Extended Electrochemical Windows Made Accessible by Room Temperature Ionic Liquid/Organic Solvent Electrolyte Systems.* ChemPhysChem, 2006. **7**(1): p. 176-180.

179. Buzzeo, M.C., R.G. Evans, and R.G. Compton, *Non-Haloaluminate Room-Temperature Ionic Liquids in Electrochemistry - A Review.* ChemPhysChem, 2004. **5**(8): p. 1106-1120.
180. Fuller, J., et al., *Structure of 1 -Ethyl-3-methylimidazolium Hexafluorophosphate: Model for Room Temperature Molten Salts.* Journal of the Chemical Society, Chemical Communications, 1994: p. 299.
181. Shiflett, M.B. and A. Yokozeki, *Solubilities and Diffusivities of Carbon Dioxide in Ionic Liquids: [bmim][PF6] and [bmim][BF4].* Industrial & Engineering Chemistry Research, 2005. **44**(12): p. 4453-4464.
182. Snook, G.A., et al., *Evaluation of a Ag|Ag+ reference electrode for use in room temperature ionic liquids.* Electrochemistry Communications, 2006. **8**(9): p. 1405-1411.
183. Saheb, A., J. Janata, and M. Josowicz, *Reference Electrode for Ionic Liquids.* Electroanalysis, 2006. **18**(4): p. 405-409.
184. Rogers, E.I., et al., *Voltammetric Characterization of the Ferrocene|Ferrocenium and Cobaltocenium|Cobaltocene Redox Couples in RTILs.* The Journal of Physical Chemistry C, 2008. **112**(7): p. 2729-2735.
185. Rivera-Rubero, S. and S. Baldelli, *Surface Spectroscopy of Room-temperature Ionic Liquids on a Platinum Electrode: A Sum Frequency Generation Study.* The Journal of Physical Chemistry B, 2004. **108**(39): p. 15133-15140.
186. Atkin, R., et al., *AFM and STM Studies on the Surface Interaction of [BMP]TFSA and [EMIm]TFSA Ionic Liquids with Au(111).* The Journal of Physical Chemistry C, 2009. **113**(30): p. 13266-13272.
187. Borisenko, N., S. Zein El Abedin, and F. Endres, *In Situ STM Investigation of Gold Reconstruction and of Silicon Electrodeposition on Au(111) in the Room Temperature Ionic Liquid 1-Butyl-1-methylpyrrolidinium Bis(trifluoromethylsulfonyl)imide.* The Journal of Physical Chemistry B, 2006. **110**(12): p. 6250-6256.
188. Lin, L.G., et al., *An in situ STM study on the long-range surface restructuring of Au(1 1 1) in a non-chloroaluminumated ionic liquid.* Electrochemistry Communications, 2003. **5**(12): p. 995-999.
189. Rollins, J.B., B.D. Fitchett, and J.C. Conboy, *Structure and Orientation of the Imidazolium Cation at the Room-Temperature Ionic Liquid/SiO2 Interface Measured by Sum-Frequency Vibrational Spectroscopyâ€* The Journal of Physical Chemistry B, 2007. **111**(18): p. 4990-4999.
190. Nanjundiah, C., S.F. McDevitt, and V.R. Koch, *Differential Capacitance Measurements in Solvent-Free Ionic Liquids at Hg and C Interfaces.* Journal of The Electrochemical Society, 1997. **144**(10): p. 3392-3397.
191. Shen, Y.R., *Surface properties probed by second-harmonic and sum-frequency generation.* Nature, 1989. **337**(6207): p. 519-525.
192. Richmond, G.L., *Molecular Bonding and Interactions at Aqueous Surfaces as Probed by Vibrational Sum Frequency Spectroscopy.* Chemical Reviews, 2002. **102**(8): p. 2693-2724.
193. Vidal, F. and A. Tadjeddine, *Sum-firequency generation spectroscopy of interfaces.* Reports on Progress in Physics, 2005. **68**(5): p. 1095-1127.

194. Behrens, R.L., et al., *Broad-band sum frequency generation study of formic acid chemisorption on a Pt (1 0 0) electrode.* Journal of Electroanalytical Chemistry, 2010. **In Press, Corrected Proof**.
195. Lagutchev, A., et al., *Vibrational sum frequency generation studies of the (2Ã—2) â†' (âˆš19Ã—âˆš19) phase transition of CO on Pt(111) electrodes.* Journal of Chemical Physics, 2006. **125**(15).
196. Lu, G.Q., et al., *Quantitative vibrational sum-frequency generation spectroscopy of thin layer electrochemistry: CO on a Pt electrode.* Surface Science, 2005. **585**(1-2): p. 3-16.
197. Website. [cited 2010 March]; Available from: http://www.ncbi.nlm.nih.gov.
198. Website. *Nafion structure*. [cited 2010 April]; Available from: en.wikipedia.org.
199. Webpage. *Sum of frequencies*. [cited 2010 March]; Available from: www.chem.queensu.ca.
200. Wilson, M.S. and S. Gottesfeld, *Thin-film catalyst layers for polymer electrolyte fuel cell electrodes.* Journal of Applied Electrochemistry, 1992. **22**.
201. Zhang, J. and A.M. Bond, *Practical considerations associated with voltammetric studies in room temperature ionic liquids.* The Analyst, 2005. **130**(8): p. 1132-1147.
202. Pavlishchuk, V.V. and A.W. Addison, *Conversion constants for redox potentials measured versus different reference electrodes in acetonitrile solutions at 25°C.* Inorganica Chimica Acta, 2000. **298**(1): p. 97-102.
203. Barrosse-Antle, L.E., et al., *Voltammetry in Room Temperature Ionic Liquids: Comparisons and Contrasts with Conventional Electrochemical Solvents.* Chemistry - An Asian Journal, 2009. **5**(2): p. 202-230.
204. Haan, J.L. and R.I. Masel, *The influence of solution pH on rates of an electrocatalytic reaction: Formic acid electrooxidation on platinum and palladium.* Electrochimica Acta, 2009. **54**(16): p. 4073-4078.
205. Miesse, C.M., et al., *Direct formic acid fuel cell portable power system for the operation of a laptop computer.* Journal of Power Sources, 2006. **162**(1): p. 532-540.
206. Larsen, R., J. Zakzeski, and R.I. Masel, *Unexpected activity of palladium on vanadia catalysts for formic acid electro-oxidation.* Electrochemical and Solid-State Letters, 2005. **8**(6): p. 291-3.
207. Chen, W., et al., *Composition effects of FePt alloy nanoparticles on the electro-oxidation of formic acid.* Langmuir, 2007. **23**(22): p. 11303-11310.
208. Cheng, T.T. and E.L. Gyenge, *Efficient Anodes for Direct Methanol and Formic Acid Fuel Cells: the Synergy Between Catalyst and Three-Dimensional Support.* Journal of the Electrochemical Society, 2008. **155**(8): p. B819-B828.
209. Chetty, R. and K. Scott, *Characterisation of thermally deposited platinum and palladium catalysts for direct formic acid fuel cells.* Journal of New Materials for Electrochemical Systems, 2007. **10**(3): p. 135-142.
210. Chu, K.-L., M.A. Shannon, and R.I. Masel, *Porous silicon fuel cells for micro power generation.* Journal of Micromechanics and Microengineering, 2007. **17**(9): p. S243-S249.

211. Ge, J., et al., *Controllable Synthesis of Pd Nanocatalysts for Direct Formic Acid Fuel Cell (DFAFC) Application: From Pd Hollow Nanospheres to Pd Nanoparticles.* Journal of Physical Chemistry C, 2007. **111**(46): p. 17305-17310.
212. Guo, Y., Y. Zheng, and M. Huang, *Enhanced activity of PtSn/C anodic electrocatalyst prepared by formic acid reduction for direct ethanol fuel cells.* Electrochimica Acta, 2008. **53**(7): p. 3102-3108.
213. Liu, Z., et al., *Nanostructured Pt/C and Pd/C catalysts for direct formic acid fuel cells.* Journal of Power Sources, 2006. **161**(2): p. 831-835.
214. Qiao, H., H. Shiroishi, and T. Okada, *Passive micro tubular direct formic acid fuel cells (DFAFCs) with chemically assembled Pd anode nano-catalysts on polymer electrolytes.* Electrochimica Acta, 2007. **53**(1): p. 59-65.
215. Uhm, S., S.T. Chung, and J. Lee, *Characterization of direct formic acid fuel cells by Impedance Studies: In comparison of direct methanol fuel cells.* Journal of Power Sources, 2008. **178**(1): p. 34-43.
216. Uhm, S., et al., *Highly effective anode structure in a direct formic acid fuel cell.* Electrochimica Acta, 2008. **53**(16): p. 5162-5168.
217. Wang, R., S. Liao, and S. Ji, *High performance Pd-based catalysts for oxidation of formic acid.* Journal of Power Sources, 2008. **180**(1): p. 205-208.
218. Yeom, J., et al., *Passive direct formic acid microfabricated fuel cells.* Journal of Power Sources, 2006. **160**(2): p. 1058-1064.
219. Zhang, L.J., Z.Y. Wang, and D.G. Xia, *Bimetallic PtPb for formic acid electro-oxidation.* Journal of Alloys and Compounds, 2006. **426**(1-2): p. 268-271.
220. Iordache, C., et al., *Electrochemical oxidation of formic acid using a noble metal based catalyst with admetals*. 2008: WO Patent Application 2008080227.
221. Iordache, C., et al., *Catalysts including metal oxide for organic fuel cells*. 2008: WO Patent Application 2008006210.
222. Kim, H., et al., *Liquid feed fuel cell with orientation-independent fuel delivery capability*. 2007: US Patent Application 2007184329.
223. Masel, R.I., Y. Zhu, and Z. Kahn, *Fuel For A Fuel Cell* 2005: British Patent GB2,424,650B.
224. Masel, R.I., Y. Zhu, and R.T. Larsen, *Fuel cells using palladium-based electrocatalysts*. 2005: US Patent Application 2005136309.
225. Masel, R.I., Y. Zhu, and R.T. Larsen, *Improved palladium-based electrocatalysts and fuel cells employing such electrocatalysts*. 2005: WO Patent Application 2005048379.
226. Masel, R.I., et al., *Fuel cells and fuel cells catalysts*. 2006: US Patent US7,132,188, British Patent, GB2,401,987.
227. Masel, R.I. and C.A. Rice, *Solids supporting mass transfer for fuel cells and other applications and solutions and methods for forming* 2006: US Patent US7,108,773.
228. Masel, R.I., R.T. Larsen, and S. Ha, *Formic Acid Fuel Cells and Catalysts*. 2006: British Patent GB2,422,048.
229. Masel, R.I., S. Ha, and B. Adams, *Organic passive direct fuel cells*. 2007: US Patent US7,282,282, British Patent GB2,419,135A.
230. Gottlieb, M.H., *Anodic Oxidation of Formic Acid at Platinum Electrodes.* Journal of The Electrochemical Society, 1964. **111**(4): p. 465-472.

231. Marcus, R.A., *On the Theory of Oxidation-Reduction Reactions Involving Electron Transfer. I.* The Journal of Chemical Physics, 1956. **24**(5): p. 966-978.
232. Marcus, R.A., *Chemical and Electrochemical Electron-Transfer Theory.* Annual Review of Physical Chemistry, 1964. **15**(1): p. 155-196.
233. Marcus, R.A., *On the Theory of Electron-Transfer Reactions. VI. Unified Treatment for Homogeneous and Electrode Reactions.* The Journal of Chemical Physics, 1965. **43**(2): p. 679-701.
234. Marcus, R.A., *Electron transfer at electrodes and in solution: Comparison of theory and experiment.* Electrochimica Acta, 1968. **13**(5): p. 995-1004.
235. Adzic, R.R., M.I. Hofman, and D.M. Drazic, *Oxidation of formates on a platinum electrode in neutral solutions.* Journal of Electroanalytical Chemistry, 1980. **110**(1-3): p. 361-368.
236. Ines, F., L.-C. Jiang, and P. Derek, *A Potential Step Study of the Influence of Metal Adatoms and Solution pH on the Rate of Formic Acid Oxidation at Pt Electrodes.* Journal of The Electrochemical Society, 1983. **130**(11): p. 2187-2192.
237. Kita, H., T. Katagiri, and K. Kunimatsu, *Electrochemical oxidation of HCOONa on Pt in acidic solutions.* Journal of Electroanalytical Chemistry, 1987. **220**(1): p. 125-138.
238. Rosenbaum, M., U. Schröder, and F. Scholz, *Investigation of the electrocatalytic oxidation of formate and ethanol at platinum black under microbial fuel cell conditions.* Journal of Solid State Electrochemistry, 2006. **10**(10): p. 872-878.
239. Ferrer, J.E. and L. Victori, *Electro-oxidation of formic acid on the iridium electrode as a function of pH.* Electrochimica Acta, 1993. **38**(12): p. 1631-1636.
240. Leung, L.W.H. and M.J. Weaver, *Influence of adsorbed carbon monoxide on electrocatalytic oxidation of simple organic molecules at platinum and palladium electrodes in acidic solution: a survey using real-time FTIR spectroscopy.* Langmuir, 1990. **6**(2): p. 323-333.
241. Lu, G.Q., A. Crown, and A. Wieckowski, *Formic Acid Decomposition on Polycrystalline Platinum and Palladized Platinum Electrodes.* J. Phys. Chem. B, 1999. **103**(44): p. 9700-9711.
242. Kita, H., K. Shimazu, and K. Kunimatsu, *Electrochemical oxidation of CO on Pt in acidic and alkaline solutions : Part I. voltammetric study on the adsorbed species and effects of aging and Sn(IV) pretreatment.* Journal of Electroanalytical Chemistry, 1988. **241**(1-2): p. 163-179.
243. Spendelow, J.S., et al., *Mechanism of CO Oxidation on Pt(111) in Alkaline Media.* J. Phys. Chem. B, 2006. **110**(19): p. 9545-9555.
244. Chen, N., P. Blowers, and R.I. Masel, *Formation of hydronium and water-hydronium complexes during coadsorption of hydrogen and water on (2x1)Pt(110).* Surface Science, 1999. **419**(2-3): p. 150-157.
245. Blowers, P. and R.I. Masel, *An Extension of the Marcus Equation for Atom Transfer Reactions.* J. Phys. Chem. A, 1999. **103**(35): p. 7047-7054.
246. Masel, R.I., *Chemical Kinetics and Catalysis*. 2001, New Jersey: John Wiley & Sons, Inc.
247. Ha, S., Z.W. Dunbar, and R.I. Masel, *Characterization of A High Performing Passive Direct Formic Acid Fuel Cell.* Journal of Power Sources, 2006. **To appear**.

248. Ha, S., et al., *Direct formic acid fuel cells with 600 mA.cm-2 at 0.4 V and 22 DegC.* Fuel Cells (Weinheim, Germany), 2004. **4**(4): p. 337-343.
249. Haan, J.L. and R.I. Masel, *Recent Progress in Improving the Oxidation of Formic Acid on High Surface Area Platinum and Palladium Catalysts: Surface Alloying and pH Effects.* ECS Transactions, 2008. **16**(2): p. 627-638.
250. Lorenz, W.J., et al., *The Formation of Monolayer Metal Films on Electrodes.* Journal of The Electrochemical Society, 1974. **121**(9): p. 1167-1177.
251. Szabo, S., *Investigations of copper, silver and bismuth deposition on palladium in perchloric acid media.* Journal of Electroanalytical Chemistry, 1977. **77**(2): p. 193-203.
252. Lim, D.-H., et al., *A new synthesis of a highly dispersed and CO tolerant PtSn/C electrocatalyst for low-temperature fuel cell; its electrocatalytic activity and long-term durability.* Applied Catalysis B: Environmental, 2009. **89**(3-4): p. 484-493.
253. Xia, X.H., *New insights into the influence of upd Sn on the oxidation of formic acid on platinum in acidic solution.* Electrochimica Acta, 1999. **45**(7): p. 1057-1066.
254. Bakos, I. and S. Szabo, *Electrochemical adsorption of tin on palladium.* Electrochimica Acta, 2001. **46**(16): p. 2507-2513.
255. Waszczuk, P., et al., *Adsorption of CO poison on fuel cell nanoparticle electrodes from methanol solutions: a radioactive labeling study.* Journal of Electroanalytical Chemistry, 2001. **511**(1-2): p. 55-64.
256. Wang, Y., et al., *Application of normal pulse voltammetry to the kinetic study of formic acid oxidation on a carbon supported Pd electrocatalyst.* Journal of Power Sources, 2009. **189**(2): p. 1020-1022.
257. Schmidt, T.J., et al., *Bi adsorption on Pt(111) in perchloric acid solution: A rotating ring-disk electrode and XPS study.* Physical Chemistry Chemical Physics, 2000. **2**(19): p. 4379-4386.
258. Morgan, R.D., J.L. Haan, and R.I. Masel, *Effects of Nafion Loading in Anode Catalyst Inks on the Miniature Direct Formic Acid Fuel Cell.* Journal of Power Sources, 2010. **Accepted Manuscript**.
259. Pourbaix, M., *Atlas of Electrochemical Equilibria in Aqueous Solutions*. 1966, London, England: Pergamon Press Ltd.
260. Iwasita, T., A. Rodes, and E. Pastor, *Vibrational spectroscopy of carbonate adsorbed on Pt(111) and Pt(110) single-crystal electrodes.* Journal of Electroanalytical Chemistry, 1995. **383**(1-2): p. 181-189.
261. Rodes, A., E. Pastor, and T. Iwasita, *Structural efects on CO2 reduction at Pt single-crystal electrodes: Part 2. Pt(111) and vicinal surfaces in the [01] zone.* Journal of Electroanalytical Chemistry, 1994. **373**(1-2): p. 167-175.
262. Hofft, O., S. Bahr, and V. Kempter, *Investigations with Infrared Spectroscopy on Films of the Ionic Liquid [EMIM]Tf2N.* Langmuir, 2008. **24**(20): p. 11562-11566.
263. Sergey , A.K., et al., *Molecular Structure, Vibrational Spectra, and Hydrogen Bonding of the Ionic Liquid 1-Ethyl-3-methyl-1<I>H</I>-imidazolium Tetrafluoroborate.* Helvetica Chimica Acta, 2004. **87**(10): p. 2556-2565.

Author's Biography

John Haan was born and raised in Summit, IL. His first college degree was a B.S. in Materials Science and Engineering from the University of Wisconsin – Madison in 1999. He then went to work for 2 years as a process engineer at SSI Technologies in Janesville, WI. He then moved back to UW to become a faculty teaching assistant for 2 years; here he decided he wanted to be a college chemistry professor, with an emphasis on teaching. He went to the University of Florida in 2003 to earn an M.S. in chemistry education, where he and his wife, Joanna, who also enrolled for this degree, rewrote a general chemistry laboratory course that is now taken by 3,000 students per year at UF. John then enrolled in the chemistry doctoral program at the University of Illinois at Urbana-Champaign in 2005. Upon completion of his PhD studying energy chemistry, John will begin work as an Assistant Professor of Chemistry at Towson University in Maryland beginning in Summer 2010.